Design And Development of Mobile Image Overlay System For Image-Guided Interventions

by

Manjunath Anand

A thesis submitted to the
Department of Mechanical and Materials Engineering
in conformity with the requirements for
the degree of Master of Applied Science

Queen's University
Kingston, Ontario, Canada
June 2014

Abstract

Numerous studies have demonstrated the potential efficacy of percutaneous image-guided interventions over open surgical interventions. The conventional image-guided procedures are limited by the freehand technique, requiring mental 3D registration and hand-eye coordination for needle placement. The outcomes of these procedures are associated with longer duration and increased patient discomfort with high radiation exposure. Previously, a static image overlay system was proposed for aiding needle interventions. Certain drawbacks associated with the static system limited the clinical translation.

To overcome the ergonomic issues and longer calibration duration associated with static system, an adjustable image overlay system was proposed. The system consisted of monitor and semi-transparent mirror, attached together to an articulated mobile arm. The 90-degree mirror-monitor configuration was proposed to improve the physician access around the patient. MicronTracker was integrated for dynamic tracking of the patient and device. A novel method for auto-direct calibration of the virtual image overlay plane was proposed. Due to large mechanical structure, the precise movement was limited and consumed useful space in the procedure room. A mobile image overlay system with reduced system weight and smaller dimensions was proposed to eliminate the need for mechanical structure. A tablet computer and

beamsplitter were used as the display device and mirror respectively. An image overlay visualization module of the 3D Slicer was developed to project the correct image slice upon the tablet device.

The system weight was reduced to 1 kg and the image overlay plane tracking precision (0.11mm STD=0.05) was similar to the printed physical markers. The auto-calibration of the image overlay plane can be done in two simple steps, away from the patient table and without additional phantom. Based on the successful pre-clinical testing of the previous static system, the mobile image overlay system with reduced weight, increased tracking precision and easier maneuverability, can be possibly hand-held by the physician to explore the image volume over the patient and be used for a wide range of procedures. The mobile image overlay system shall be classified as Class II device as per FDA regulations, do not require extensive verification and validation efforts and further improves the commercialization opportunities.

Acknowledgments

I would like to express my gratitude to my supervisor, Dr. Gabor Fichtinger, whose expertise, understanding, and patience, added considerably to my graduate experience. I am very fortunate to have an opportunity to work under his leadership who cared so much about my learning experience and professional growth. I thoroughly enjoyed working for my thesis project which gave me an in-depth understanding of the challenges associated with medical device development and the clinical deployment. I attribute the level of my Master's degree to his encouragement and effort and without him this thesis, too, would not have been completed or written. One simply could not wish for a better or friendlier supervisor.

To Dr. Genevieve Dumas, Dr. Keyvan Hashtrudi-Zaad and Dr. J. Timothy Bryant, my committee members during the oral defense of my thesis, I am very much grateful for the knowledge you have imparted for the improvement of this thesis. Your insights and comments are very much appreciated.

In my daily work I have been blessed with a friendly and cheerful group of fellow students and colleagues. I am especially grateful to Dr. Andras Lasso and Dr. Tamas Ungi for their guidance throughout the project. Franklin King was particularly helpful in developing the prototype software and patiently teaching the image processing tools. I would like to thank Matthew Holden, Paweena U-Thainual, Ryan Anderson,

and all my other colleagues at Perk Lab who, in one way or another, have been part of the completion of this thesis work. I am greatly indebted to my collaborators Dr. John Rudan, Dr. Jagadeesan Jayender, Dr. Jan Fritz, Dr. John A. Carrino and Dr. Ferenc A. Jolesz for their time spent on polishing my publications. I am grateful to the staff at the Department of Mechanical and Materials Engineering, the School of Computing and the International Center, for assisting me in many different ways. Jane Davies, Amie Bello, Gabrielle Whan, Ita Mcconnell, Susan Anderson, Julia Blackstock, and Michael Vanberkel, deserve special mention.

I would also like to thank my family for the support they provided me through my entire life. Many friends have helped me stay sane through these difficult years. Their support and care helped me overcome setbacks and stay focused on my graduate study. I greatly value their friendship and I deeply appreciate their belief in me. In particular, I must acknowledge my friends Flavia Occhini, Shanmukha Ayyappa, and Siddharth Vikal, without whose encouragement, I would not have finished this thesis.

In conclusion, I recognize that this research would not have been possible without the financial assistance of the following agencies. Cancer Care Ontario through Applied Cancer Research Unit and Research Chair in Cancer Imaging grants; the Discovery Grant of NSERC, Canada; National Center for Research Resources and National Institute of Biomedical Imaging and Bioengineering of the NIH USA, through grant numbers P41EB015898, P41RR019703 and R01 CA118371, and express my gratitude to those agencies. Dr. Fichtinger was funded as Cancer Care Ontario Research Chair.

"At the end, thanks to you, the reader. If you are reading this line after the others, you at least read one page of my thesis. Thank You."

Manjunath Anand

Contents

List of Tables

List of Figures

Chapter 1

Introduction

1.1 Image-guided interventions

Image-guided interventions are the medical procedures that use computer-based systems to provide virtual images to help the physician precisely visualize and target the surgical site [28]. Ultrasound (US), Fluoroscopy, Computed Tomography (CT) and Magnetic Resonance (MR) imaging are some of the enabling imaging modalities. Every intervention starts with the visualization of the target using the scanned image volume pre-operatively (CT/MR) or intra-operatively (US/fluoroscopy) and planning the path to reach the chosen target. The evidence supports the pre-operative procedures (such as needle biopsies) as the superior method as compared with the open surgical procedures performed in the operating room [29] [30] [31] for diagnosis of tumors. The use of image guidance is likely to reduce the complications and increase the likelihood of specimen adequacy and procedural success [32]. Open procedures carry the potential disadvantages of increased patient discomfort, higher rates of wound complications, and prolonged recovery compared with percutaneous procedures [33] [34]. The image-guided interventions performed pre-operatively have the advantages

of potentially avoiding surgery when the samples are benign and providing a preoperative diagnosis to facilitate multidisciplinary planning when samples are positive for malignancy. The imaging modalities are precise and accurate; surgeons can plan the tool placement path to the targeted area avoiding healthy tissues before an incision is made. The other medical procedures that are performed percutaneously (i.e., across the skin) with image guidance are spine injection, needle based aspirations and local ablation therapies [20]. In 2005, the image-guided interventions market in the US, which encompassed systems used for neurosurgery, spine, and orthopedic procedures, was valued at over $115 million according to the Millenium Research Group. In the following section, each imaging modalities are briefly discussed.

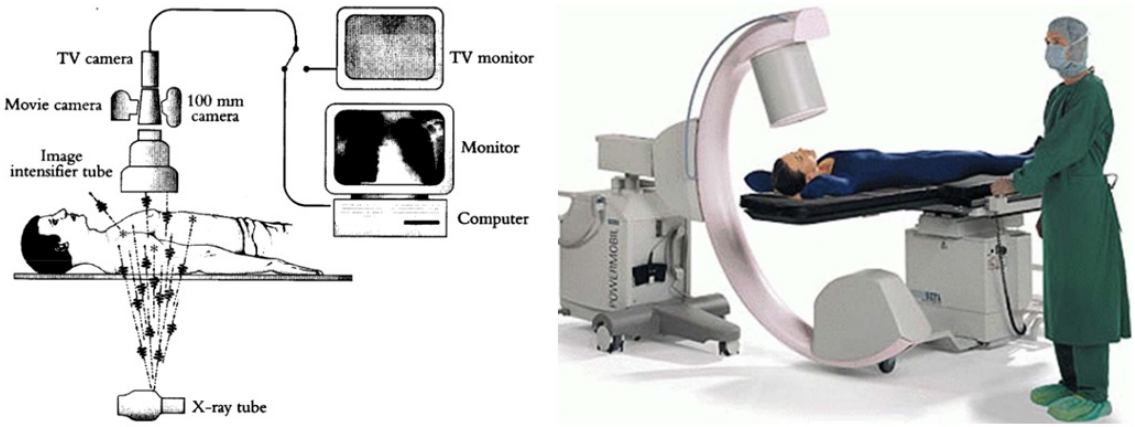

Figure 1.1: Fluoroscopic C-arm device: Left). Schematic representation of the working principle of a fluoroscopic C-arm device [1]. Right). Image intensifier C-arm *(Siemens Healthcare)*.

1.1.1 Fluoroscopy-guided interventions

Fluoroscopy is an imaging technique that uses X-rays to obtain real-time image of the internal structures of a patient through the use of fluoroscope. The fluoroscopic device shown in Figure 1.1 consists of an X-ray generator and an image intensifier or a

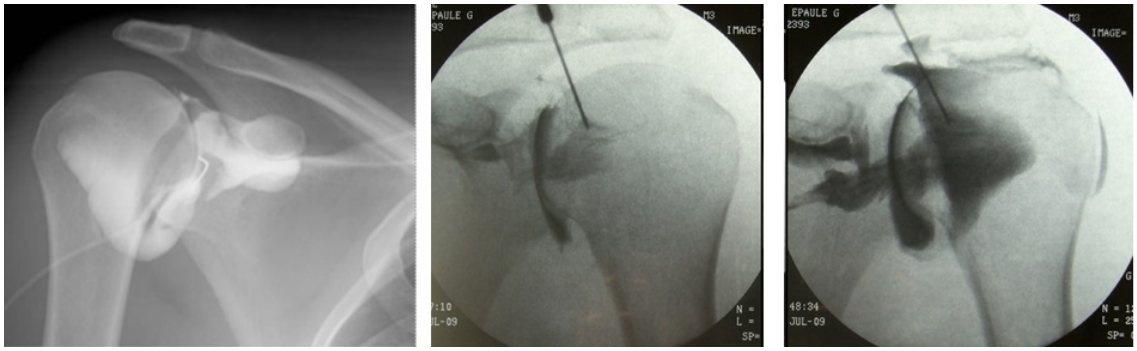

Figure 1.2: Fluoroscopic images Left). Shoulder arthrography [2]. Middle). Needle inserted using fluoroscopic image-guidance *(wikipedia.com)* and Right). Injection of contrast *(wikipedia.com)*.

flat panel detector. The X-rays produced by the generator passes through the patient body and the attenuated X-rays are detected by the image intensifier or flat panel detector to form a digital image. Fluoroscopy in combination with iodine contrast medium application is regarded as the gold standard for vascular interventions. The fluoroscopy provides real-time images of the region of interest along with the tools such as needle and hence it is also used for guiding needles for musculoskeletal procedures like arthrography [2] as shown in Figure 1.2.

The fluoroscopic devices are mobile, generate real-time images of the internal structures, have good bone contrast and are inexpensive as compared to other ionizing imaging modalities. However, the wider applications of the fluoroscopy is limited due to low intrinsic soft tissue contrast, increased radiation exposure to the physican and the patient, and the lack of three-dimensional information in the projection images.

1.1.2 Ultrasound-guided interventions

Ultrasound imaging modality uses high-frequency sound waves to produce diagnostic images of the soft tissues such as muscles and internal organs. The device (Figure

1.3 a) consists of a transducer which produces high frequency sound waves that are either reflected and / or attenuated by the internal body structures. The reflected sound waves are converted into electrical signals by the transducers producing an image that is displayed upon the monitor. The image is based on the frequency and strength (amplitude) of the sound signal and the time it takes to return from the internal organs to the transducer.

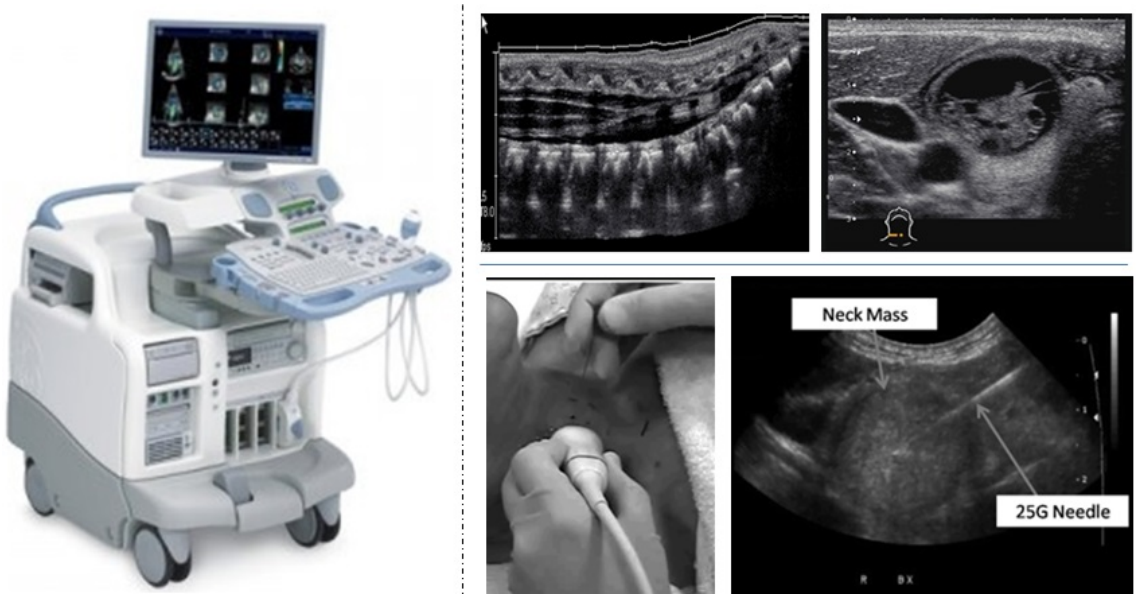

Figure 1.3: Ultrasound image-guided interventions: Starting from left A). Ultrasound imaging system *(GE Healthcare)*. B). Anatomical images of pediatric spine and adult liver using Ultrasound imaging system *(Oregon Institute of Technology)*. C). Ultrasound-guided Fine-Needle Capillary with corresponding sonogram of a needle positioned for biopsy of a large neck mass [3].

The ultrasound device is hand-held and provides wider flexibility in positioning upon the patient. Some of the ultrasound-guided interventions include biopsies of the breast, lung, spleen, soft tissues and bone; pain management (spine injection - Figure 1.3 b); and tumor ablations [35]. In addition, the contrast agents can be

applied to improve image contrast or to acquire dynamic perfusion information [36] [37]. The ultrasound imaging is non-ionizing, real-time, less expensive compared to any other imaging modalities and do not have the same risks as x-rays or other types of ionizing radiations. However, the field of view is limited, image quality deteriorates with depth, bone and air may impair the visualization of the target as they prevent ultrasound penetration, and the surgical instruments such as needles generates imaging artifacts.

1.1.3 Computed tomography (CT) -guided interventions

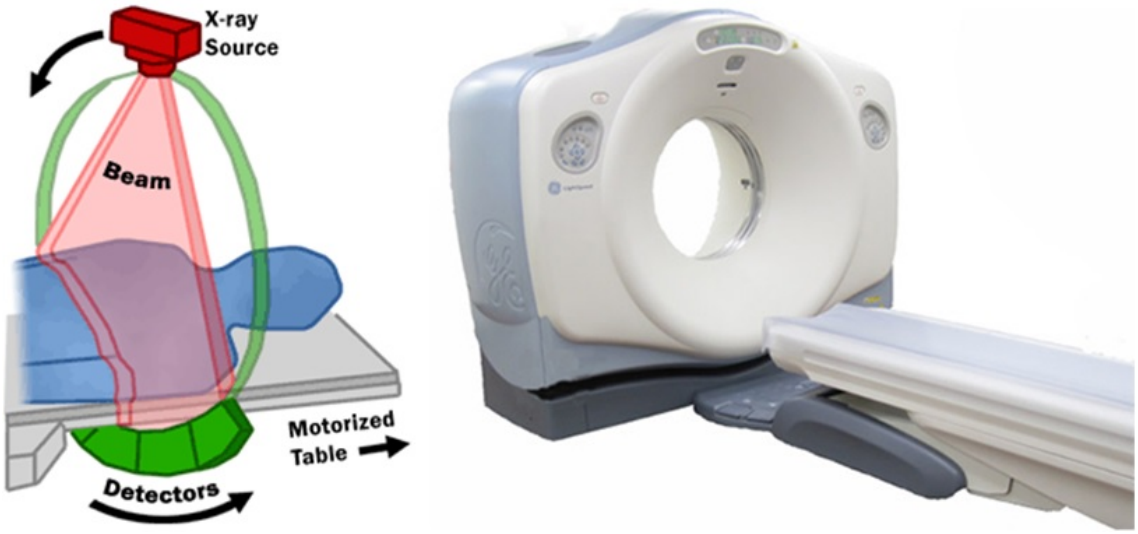

Figure 1.4: Computed Tomography machines: A). Working principle *(fda.gov)* .B). CT machine *(GE Healthcare)*.

Computed tomography (CT) is a noninvasive imaging modality that uses specialized X-ray equipment to produce cross-sectional images of the patient body. Typical CT machine (Figure 1.4 b) consists of an X-ray source and digital detectors attached to high speed rotating ring. During rotation, the X-ray source produces a narrow, fan-shaped beam of X-rays (Figure 1.4 a) that passes through a section of the patient's

body and the attenuated X-rays are detected by the digital detectors creating a digital 3D image volume. The current state-of-the-art technology scanners are equipped with spiral continuous rotation with dual-source and dual-energy X-ray sources and iterative reconstruction techniques [38].

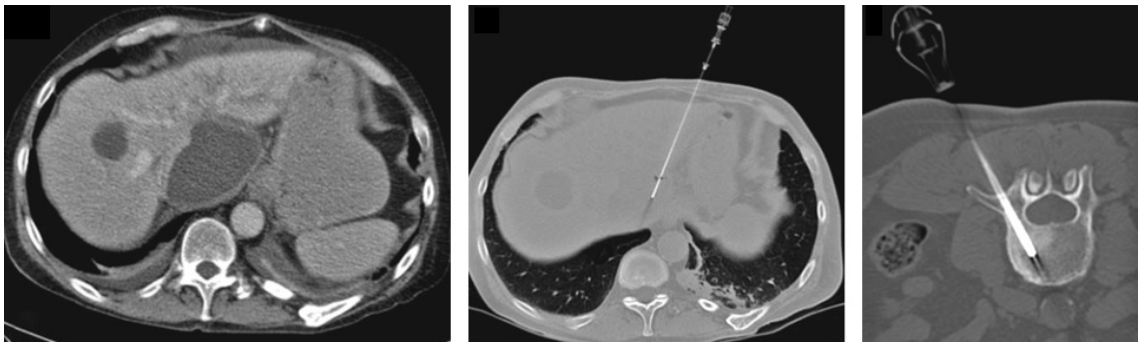

Figure 1.5: CT-guided interventions: A and B). A fine-needle aspiration of a liquid structure behind the left liver lobe after liver surgery [2]. C). drill biopsy of a bone metastasis in a vertebral body (L3) [2].

The CT images of the internal organs (Figure 1.5 a and b), bones (Figure 1.5 c), soft tissues, and blood vessels provide greater clarity and more details than the conventional X-ray images or the ultrasound images. The CT image-guided interventions are widely practiced since it provides detailed information to diagnose, plan treatment and evaluate many conditions eliminating the need for exploratory surgery. The shorter duration of the scans has enabled many CT-guided interventions performed under near real-time. Repeated scans can result in increased radiation exposure to the patient and the interventionalist. It has poor contrast for soft tissues; however, the improvements in image quality (contrast) come only at a cost of increased radiation dose [39].

1.1.4 Magnetic resonance (MR) -guided interventions

Magnetic resonance imaging (MRI) shown in Figure 1.6 uses strong magnetic fields and radio waves to produce cross-sectional images of organs and internal structures in the body. It is an excellent imaging modality for the detection and characterization of soft tissues. The signal detected depends upon the water content and local magnetic properties. The superior tissue contrast allows for accurate differentiation of the pathologic and surrounding normal structures and helps to avoid critical structures in the puncture route [40].

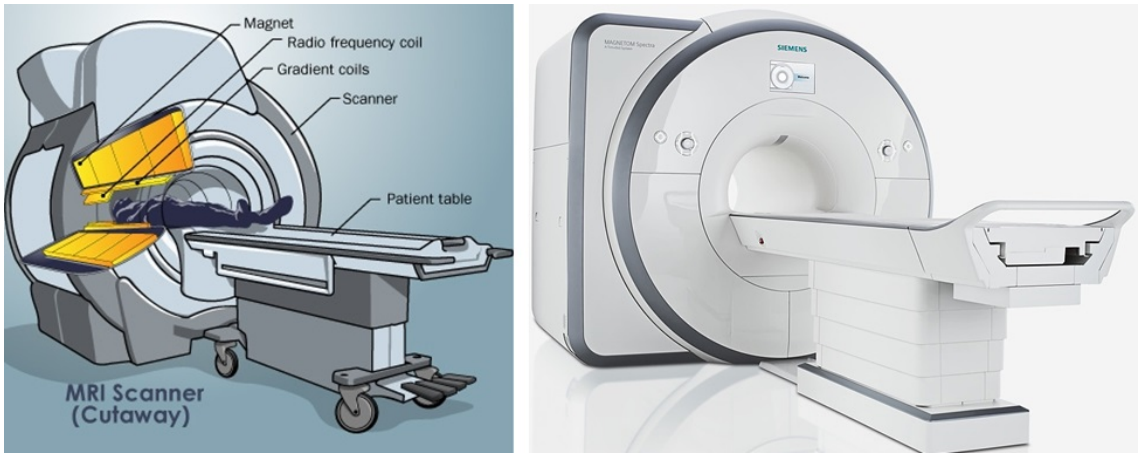

Figure 1.6: Magnetic Resonance machines: A). Working principle *(howstuffworks.com)* .B). MR machine *(Siemens Healthcare)*.

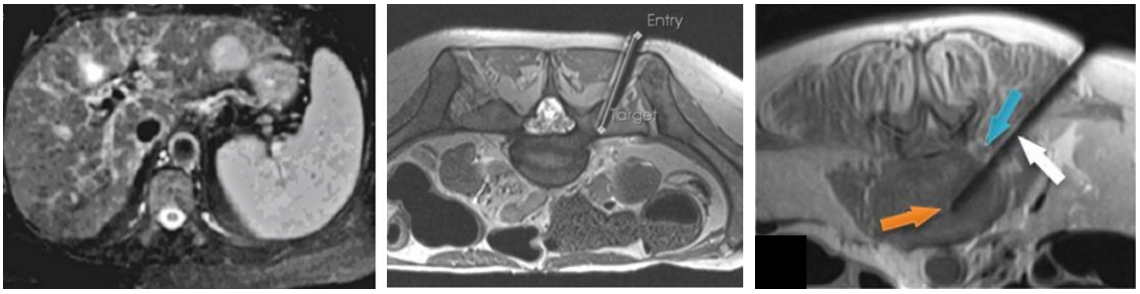

Figure 1.7: MR-guided interventions: Left). Liver tumor clearly visualized on the T2-weighted MR image [2]. Middle). MR-guided biopsy of a right sacral osseous lesion [4]. Right). Axial spine image following needle placement demonstrates the tip of the needle (white arrows) in the nucleus pulposus of the disk (orange arrow). The blue arrow indicates the spared L4 nerve root [5].

Minimally invasive diagnostic and therapeutic image based interventions have been performed under near real-time MR guidance [41]. A wide variety of interventional procedures (Figure 1.7 B) from open brain surgeries to noninvasive focused ultrasound ablations have been guided with MR [39]. There are no potential hazards associated with the technology; however the imaging scan is longer and expensive compared to other imaging methods. The magnet may cause malfunctioning of the implanted medical devices and may cause damage or injury due to presence of metal objects inside the body [42]. The biopsies under MR are limited due to short tunnel and the presence of magnet limits the use of surgical (metallic) tools for real-time MR-guided interventions.

1.2 Freehand image-guided needle interventions

There is mounting evidence of CT (Computed Tomography)-guided percutaneous needle interventions applied for wide range of procedures. Over one million CT-guided needle insertions are performed each year in the United States. The conventional

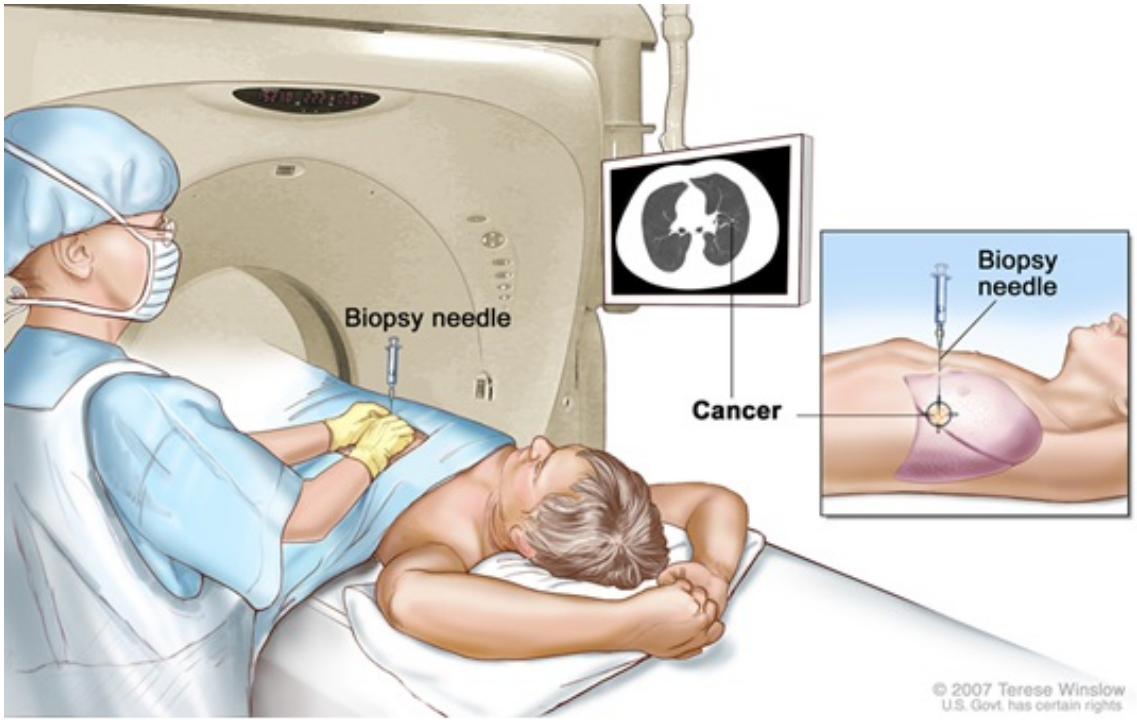

Figure 1.8: Conventional image-guided needle insertion procedure (Biopsy) (*Translational Research Informatics Center, Japan).*

image-guided needle placement procedure which is freehand and unassisted is shown in Figure 1.8. The patient and image volume are decoupled from each other. For about 80% of the procedures which are simple, the physician effectively bridges the patient and the image volume together. For the remaining 20% of the complex procedures, the physician spends longer duration in the procedure room and the patient is subjected to multiple punctures and repeated radiation exposure.

The typical work-flow of the conventional image-guided needle insertion procedure is shown in Figure 1.9. The physician browses the scanned image volume displayed upon the procedure room monitor, the target and needle entry points are identified. Through a series of mental 3D registration and hand-eye coordination, the physician transfers the information of needle placement location and orientation upon the

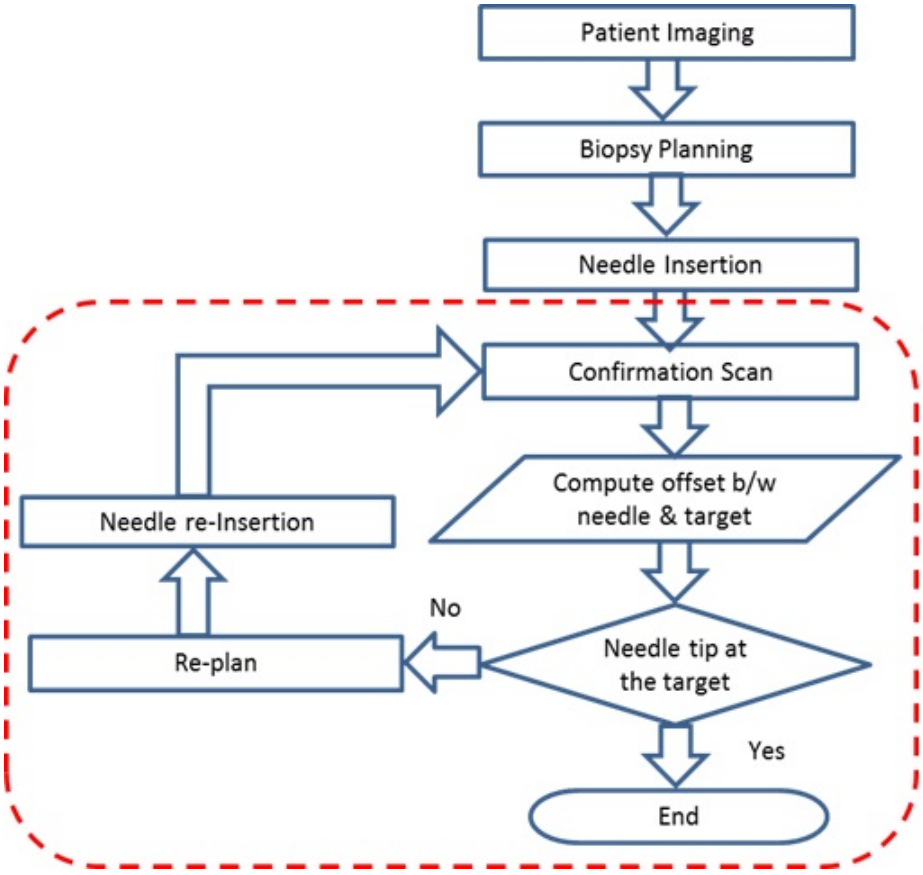

Figure 1.9: Flow chart representing the typical work-flow of conventional image-guided freehand needle interventions.

patient. In order to confirm the needle tip at the intended target location, a confirmation imaging scan of the patient along with needle is performed. The offset between the needle tip and the target inside the patient body are measured using the newly scanned image volume. Depending upon the offset measured, the needle placement is re-planned and this iteration process of needle reinsertion and confirmation CT scan is continued until the needle tip is at the desired target location.

The outcome of the freehand image-guided needle interventions are usually measured by the accuracy of needle placement. The errors associated with needle misplacement in percutaneous procedures are due to human errors [43], imaging limitations, target uncertainty [44], tissue deformation and needle deflection [45]. The human and target uncertainty may be related to poor techniques, insufficient physician skills or geometry related problems. The tissue deformation and needle deflection are inevitable and there is a limited opportunity and technological advancements to minimize the error due to tissue deformation and needle deflection.

Human errors stem from the task itself; it is an intensely manual procedure which depends on the skill of the physician to effectively transform the information from the 'virtual' world displayed upon the monitor to the patient inhabited 'real world'. The physician must remember the insertion plan and associated image and then insert the needle using precise hand-eye coordination. Additional confirmation imaging scan is required to ensure the needle tip is within the defined limits (or measure offset error). Depending upon the offset error measured, the needle reinsertion followed by the confirmation scan continues until the needle tip is within the desired tolerance limits. There is no defined tolerance for the accuracy of needle insertion in clinical practice and in general, insertions with less needle misplacement result in more effective treatment or increase the precision of diagnosis [46]. Each correction; however, increases the radiation exposure with increased number of punctures causing the risk of post-procedure complication and discomfort to the patient. On the other hand, the precious procedure time of the physician is also lost due to longer duration spent (up to 40 minutes) for simpler procedures (average 15 minutes). Therefore reducing the needle misplacement error due to human error is a logical imperative.

1.3 Thesis contributions

The main objective of this thesis project is to design and develop a system aiding the physician to perform image-guided freehand needle insertion using augmented reality image overlay concept. The limitations associated with the previous systems inhibiting the clinical translation of the image overlay concept are analyzed in detail.

An adjustable image overlay system was design and the prototype was developed to overcome the ergonomic issues of the previous static image overlay system. Workspace analysis was conducted to explore a optimal configuration between the mirror and monitor. The study was conducted between the earlier 60-degree design and the newly proposed 90-degree design.Feasibility of using different tracking devices were analyzed and MicronTracker was integrated successfully to provide dynamic tracking of the system and the patient during the procedure. A novel virtual image overlay plane calibration technique was proposed. In this technique, the MicronTracker camera can actually to "see-through" the mirror and determine the pose of the virtual planar markers and calculate the transform between the virtual and physical markers for real-time tracking. Improved laser plane alignment procedure was proposed to align the laser plane with the virtual image overlay plane. Due to mechanical instability associated with the adjustable system, the mobile image overlay system was proposed.

The mobile image overlay system using tablet display device and beamsplitter mirror was designed and the prototype was developed. The use of tablet display device and the beamsplitter reduced the system weight with smaller device dimensions and improved the virtual plane image quality and the tracking precision. The image overlay module of 3D Slicer was developed to display the correct image slice in the

virtual plane at the correct 3D location determined by optical tracking system. An optical tracker aided laser alignment method was developed and a high power output laser diode was used to improve the laser line visibility under normal lighting conditions. The validation phantom design and the steps involved in system accuracy validation are discussed in detail.

Following are the contributions made as part of the thesis project.

1. Design and prototype development of adjustable image overlay system
2. Workspace analysis study done to determine the optimal workspace configuration
3. Novel calibration technique proposed using MicronTracker
4. Method for dynamic tracking of the patient and the device proposed
5. Design and prototype development of mobile image overlay system
6. Use of tablet computer as the display device and beamsplitter as the mirror
7. Laser plane alignment method proposed using laser alignment tool and 3D Slicer
8. Validation phantom design and developed; Image overlay module of 3D Slicer developed

The development of the mobile image overlay system represents the technological advancements to completely mobilize the 2D image overlay concept and enable the clinical translation.

1.4 Thesis outline

The thesis is composed of two main parts, corresponding to two different systems developed for image-guided interventions and is organized as follows:

Chapter 1 presents the background of image-guided interventions and the limitations associated with freehand needle placement.

Chapter 2 reports a literature review of different image-guided needle interventions and augmented reality systems. The 2D image overlay concept and limitations associated with the previous systems motivating the development of the proposed new concept are discussed. The potential clinical applications for the proposed system are discussed in detail.

Chapter 3 presents the conceptual design and prototype development of the adjustable image overlay system. The workspace analysis resulting in the introduction of newly proposed 90-degree mirror-monitor configuration, integration of optical tracking system for dynamic tracking and the auto-calibration of the virtual image overlay plane are discussed. The limitations due to mechanical instability of the adjustable system motivating the design of the mobile image overlay system are presented.

Chapter 4 presents the conceptual design and prototype development of the mobile image overlay system. The workspace analysis, selection of viewbox components, development of 3D Slicer image overlay module, validation phantom design, laser alignment method and system accuracy validation method are discussed.

Finally, *Chapter 5* presents the experiments and results of the workspace analysis, mechanical improvements, image overlay plane accuracy and cost analysis. The

outcomes and achievements of the thesis contributions are summarized. The future work required for effective translation of the mobile system into clinical space is presented.

Chapter 2

Augmented Reality Image Overlay Systems

It follows from the previous chapter, it is imperative to minimize human induced needle placement error in order to lower the radiation exposure, reduce procedure duration and minimize the post-procedure complications. For biopsies, the needle misplacement leads to faulty diagnosis of the tumor. There is an even greater need for precise and consistent aiming of the needle delivery for spine injections. Needle misplacement during spine injection may result in over pushing the needle causing sharp pain to the patient and must be avoided at all cost. Percutaneous nephrolithotomy (PCNL) on the other hand is associated with increased radiation exposure due to multiple fluoroscopic images required to guide the wire into the kidney [47]. Parathyroidectomy procedure is associated with visible scar and post-procedure complications due to the longer incision that is required to explore the diseased parathyroid gland. The driving clinical applications for the proposed solution are discussed in detail later in section 2.5.

A variety of technical solutions such as medical robots, tracked navigation systems, hand-held guides and augmented reality systems have been proposed to aid the accurate needle placement and assist the physician to perform image-guided minimally

invasive procedures more effectively. All these solutions were aimed at minimizing the procedure duration with lower radiation exposure, followed by reducing the post-procedure complications. The key objectives of these solutions were to minimize the role of physician's hand-eye coordination and need for additional imaging guidance such as fluoroscopy or ultrasound to aid the needle placement.

2.1 Tracked navigation systems

Figure 2.1: Left) Optical navigation system (*BrainLab AG.*). Right) A) Electromagnetic tracking system - NDI Aurora *NDI Medical Inc.*. B) Tracking sensor 0.5 mm dia [6].

The position of the surgical tools, patient and other devices are continuously tracked in real-time by surgical navigation systems such as optical and electromagnetic tracking systems. The main advantage of the tracked navigation systems is that the procedure can be pre-planned with the patient image volume taken previously and spatially register with the physical location of the patient using surgical navigators [48]. The position of the tracked surgical tool can be displayed in real time with respect to the image volume upon the computer screen providing image guidance for navigating the surgical tool into the patient body. The optical tracking system (Figure 2.1) uses active and passive markers which are continuously tracked by the

sensors to determine the pose in real-time. The electromagnetic (Figure 2.1) trackers uses spiral coils in X, Y and Z direction and the electromagnetic field to the coils in real-time to determine the pose. The optical trackers uses stereoscopic camera or infrared sensors to track the marked or reflective objects in real-time to report the pose.

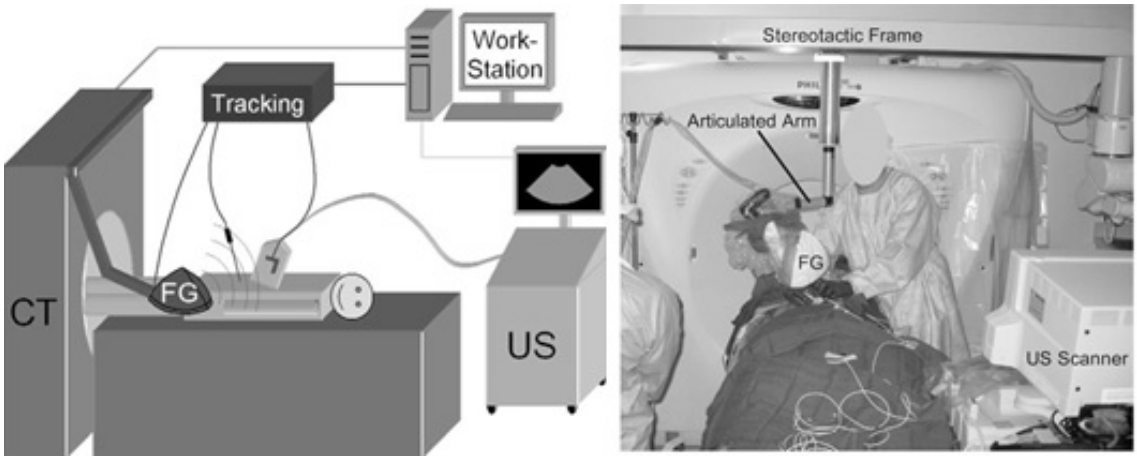

Figure 2.2: Electromagnetic tracking system for needle guidance [7]: Left) System concept design. Right) System in use.

The tracked navigations systems further enhance the freehand needle insertion by providing real-time feedback of the instrument position with respect to patient image volume. Numerous clinical studies have been conducted using tracked navigations systems for applications such as neurosurgery [49], biopsies [50] [6] [52] [51] [7], endovascular [6], radio-frequency ablation [51], and thermal ablation [7]. The technical success rate of 85% and above was achieved with the first pass [51] [7], while the second pass reported a 97% [7] and above achievement rate for electromagnetic tracked under ultrasound guidance for biopsies and radio-frequency ablation procedures. The system setup for electromagnetic tracker with ultrasound image guidance is shown in Figure 2.2.

The greatest advantage of the electromagnetic tracker is not requiring the clear line-of-sight between the field generator and sensors mounted upon the target. The sensing coils can be placed close to the tip of tracked instrument, and thus closer to the point of surgical interest, tracking inside the human body with a flexible instrument is possible. The distance between the sensor and the field generator, and presence of metallic objects in the field have an influence upon the accuracy of the pose measured. Recently, miniaturization of the sensor coils has lowered the effect on the accuracy due to presence of metals in the field of generator [53]. It has been reported that the electromagnetic tracking systems encounter problems when metallic objects are within the operating area [53] [54] [55]. This has somewhat hampered the widespread use of electromagnetic tracking systems in surgical procedures. Also the need for a wired connection of the trackers and field generator to the module box further limits the wider adoption of this tracking modality [56] [53] [54] [57].

The optical navigation systems have the advantage of being light weight, wireless, and accurate over the whole operating area [58] [59] [56] [53] [54]. The main disadvantage of the optical system is the requirement of clear line-of-sight between camera and optical trackers has limited its applications [56] [57]. Kral *et al.* [60] reported the accuracy of optical tracking was near the resolution of the camera system, whereas the accuracy of electromagnetic tracking was lower. Only optical tracking allowed for an application accuracy of considerably less than 1mm in high-resolution datasets [60]. The reliability of the optical tracking system was better than the electromagnetic tracking [61].

2.2 Robot-assisted systems

Medical robots have demonstrated the potential for improving the precision and capabilities of the physicians. The robot-assisted biopsy using CT guidance was proposed by Kettenbach *et al.* [62] and the graphical representation of the concept is shown in Figure 2.3. The system consists of a 4-DOF (degrees of freedom) robotic arm that uses three linear axes and one rotational axis for gross positioning of the needle positioning unit. At the end of the robotic arm, a 3-DOF needle positioning unit is mounted for fine positioning. The robot and the CT coordinates are registered together using the fiducial registration method defined by Detmer *et al.* [8]. Biopsy procedures were performed (Figure 2.4) using the custom-made phantom consisting of beans. With single needle pass, all biopsy specimens were targeted with accuracy of 1.2 ± 0.9 mm and 0.6 ± 0.4 mm in X and Z axes respectively [62].

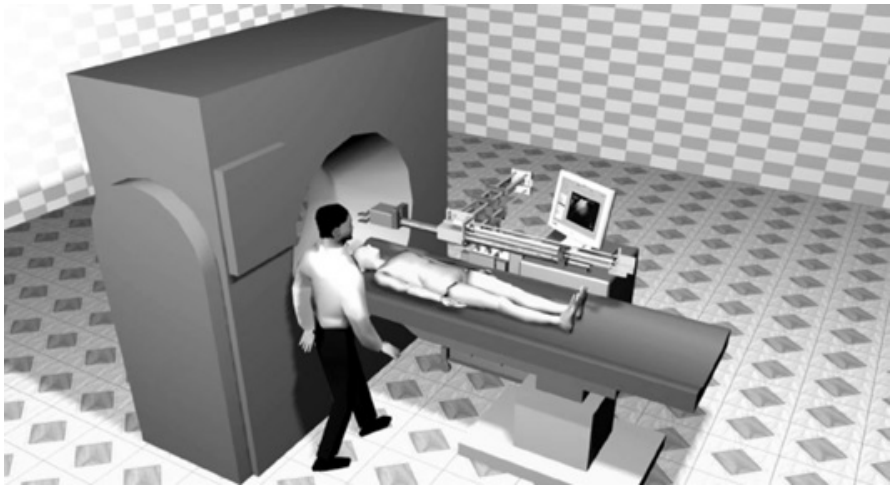

Figure 2.3: Graphical representation of the robot for CT-guided interventions. The robot, user-interface and input devices are located along the CT table [8].

A variety of many other surgical robots have been investigated [63] [64] for assisting image-guided needle interventions. Although the high accuracy of needle insertion

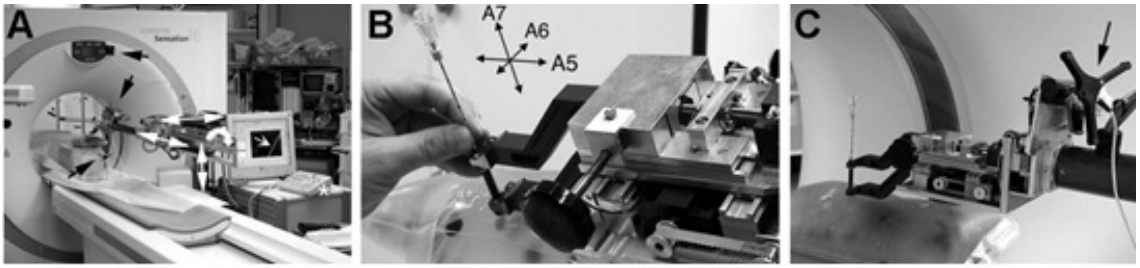

Figure 2.4: CT-guided needle insertion [8] : A) Gel phantom with the robot arm. B) Needle position unit. C) Needle inserted into gel phantom.

and concept feasibility were demonstrated with the robot-assisted systems, large scale commercial deployment into clinical space has been limited as the systems are expensive, prohibitively complex with longer duration for initial setup and requirement of highly skilled personnel to operate the system.

2.3 Augmented reality (AR) systems

Augmented reality (AR) systems superimpose computer-generated images onto the user's vision of the real world, giving the user the additional information generated from the computer model. Using an AR system, the user's view of the real world is enhanced. In medical applications, the computer generated tomographic (CT) image or virtual organ is superimposed onto the physician's view of the patient providing "X-ray vision". During interventional procedures, preoperative computed tomography, magnetic resonance imaging, ultrasonography, or other imaging methods are used to obtain information for surgical planning. The preoperative image volume is registered to the physical location of the patient through landmark or fiducial registration. A variety of methods have been developed to superimpose the virtual image upon to the user's vision of the real world and some of them are discussed in the following sections.

Video AR systems

Video-based AR systems overlays the scanned image volume with stereoscopic real-time image of the region of interest. The video-based AR concept has been explored widely for laparoscopic procedures where video endoscope is used to view the region of interest. Reittner *et al.* [9] demonstrated CT-guided endoscopic sinus surgery with electromagnetic tracking of the tool. The patient physical location and the tool are registered together with the image volume and continuously tracked using the electromagnetic tracking system. As the tool is navigated into the patient, the correct location of the tool tip with respect to CT volume is displayed upon the monitor along with the real-time endoscope image (Figure 2.5).

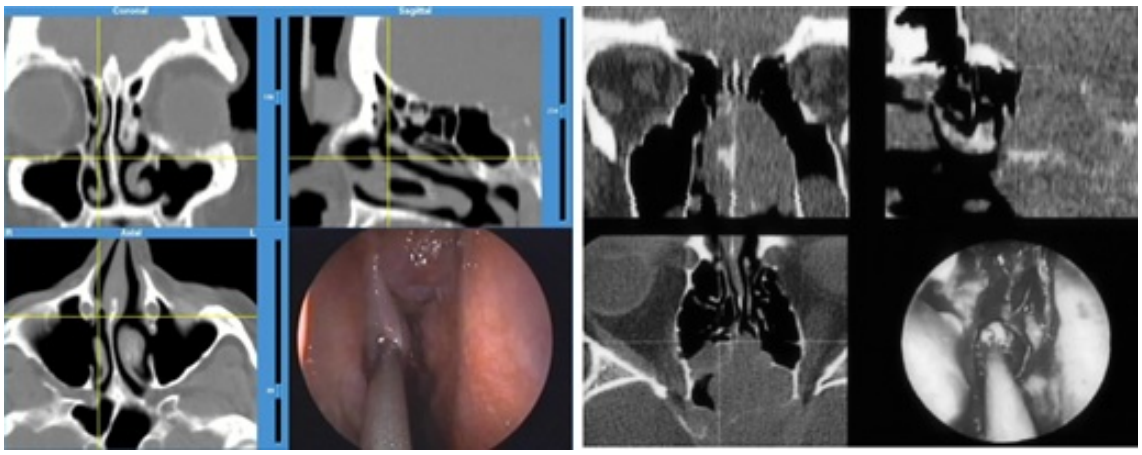

Figure 2.5: Video-based AR systems: Left) CT image superimposed with endoscope image, cross-hairs indicate exactly where the probe is on each of the coronal, sagittal and axial views (*sinuses.com*). Right) Crosshairs accurately localize the probe tip at the anterior wall of the sphenoid sinus [9].

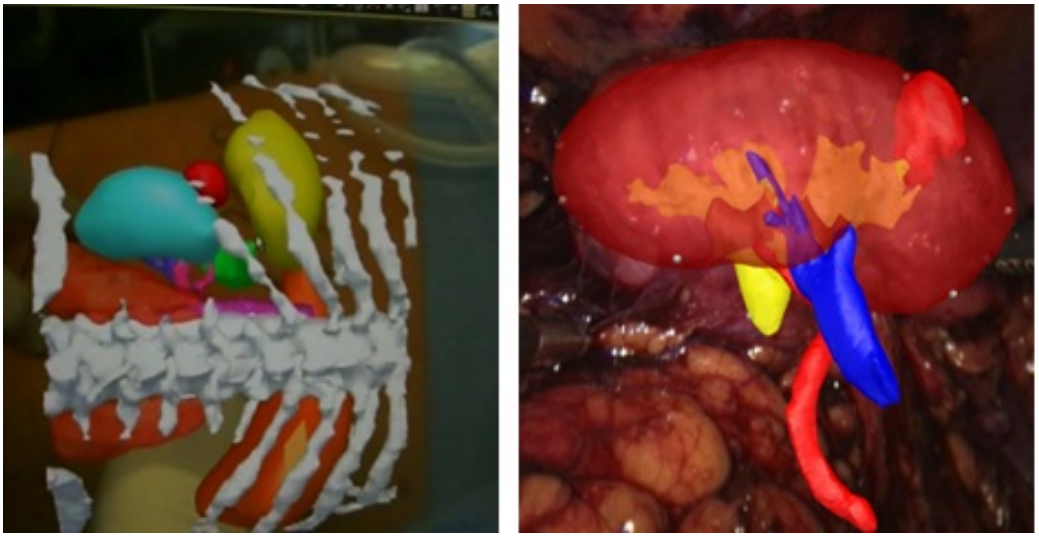

Figure 2.6: Video AR system [10] : Left) Overlay of augmented reality image for ideal port placement. Right) Renal tumors were identified through the surrounding fat.

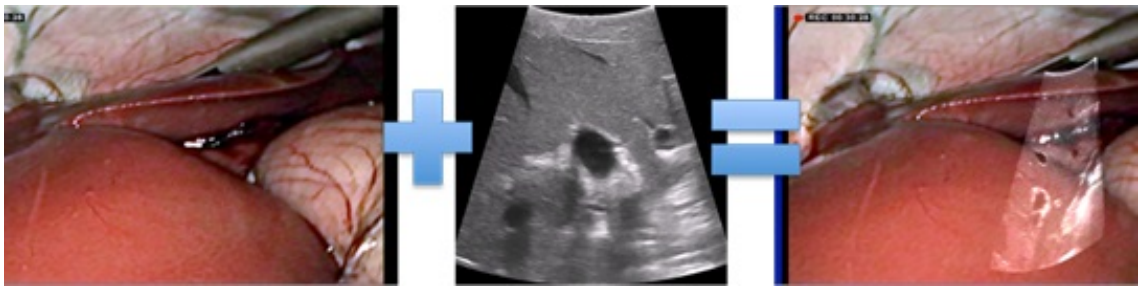

Figure 2.7: Laparoscopic ultrasound system (LUS) [10]: Left) Original 3D laparoscopic image. Middle) Laparoscopic ultrasound image. Right) Stereoscopic video AR image.

Recent technological advancements including 3D video endoscope with high resolution and high quality video imaging has enabled 3D visualization. This has created more interest for research groups to explore the augmented reality concepts enabling more accurate and faster procedure outcomes. Dogu *et al.* [65] demonstrated the concept of overlaying fluoroscopic image over the 3D video endoscopy image and displayed upon the monitor giving the physician "X-ray vision"

together with high definition 3D image of the organ of interest. Figure 2.6 shows the use of video AR system to aid the port placement and identification of renal tumors surrounded by fat. Xin *et al.* [10] developed a real-time stereoscopic augmented-reality (AR) system for laparoscopic surgery by merging live laparoscopic ultrasound (LUS) with stereoscopic video, as shown in Figure 2.7. This system enhances the visualization of surgical anatomy by overlaying the real-time laparoscopic ultrasound images of the organ which otherwise would have been challenging with depth constraint for ultrasound image quality when done from the external surface of the patient. The video-based AR system are limited to laparoscopic procedures as it requires the physician to look at the monitor for the 3D images. Mounting the pre- or intraoperative imaging properties onto the real-time video endoscopic images in a real-time manner will simplify and increase the precision of laparoscopic procedures [10] [65].

Head-mounted video displays

These devices effectively display the superimposed image upon the display device mounted on the physician's head. It consists of a stereo camera and the display device. During the procedure, the real-time stereoscopic video is merged with the real-time ultrasound images or pre-operative MRI / CT images and projected upon the head-mounted display systems providing the augmented reality vision for the physician, as shown in Figure 2.8. Sauer *et al.* [66] proposed a head-mounted display system for aiding ultrasound-guided needle biopsies and similar systems were proposed by Birkfellner *et al.* [67] and Gao *et al.* [13] for overlaying the preoperative CT/MRI images. These systems require expensive display systems and require the continuous tracking of the physician's head with respect to patient.

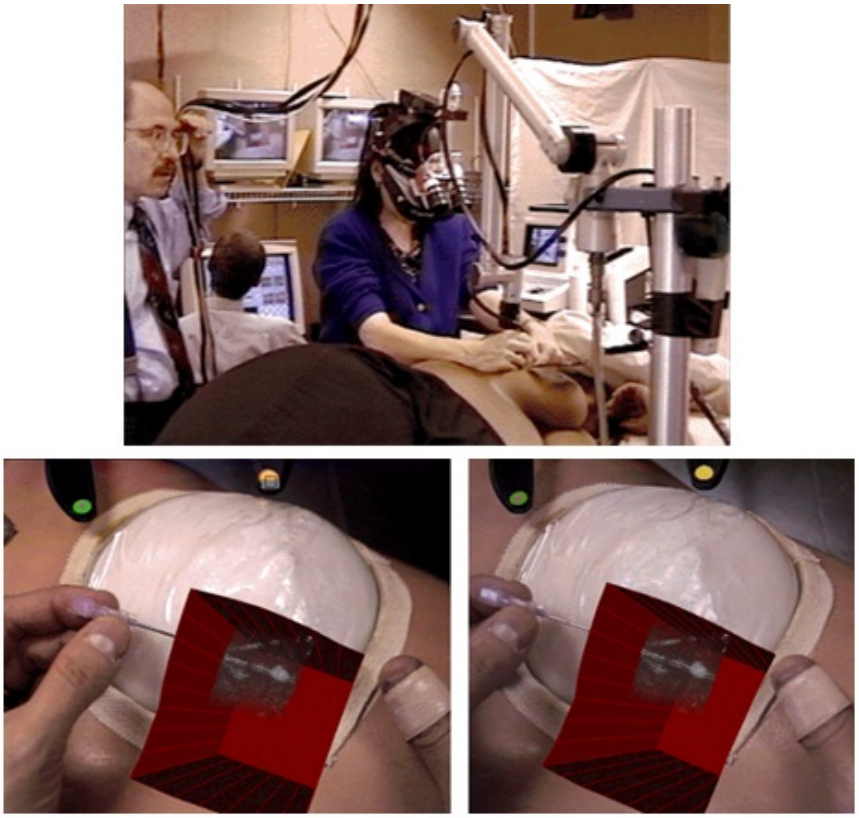

Figure 2.8: Head-mounted projector displays [11]: Top) Physician wearing augmented reality head-mounted display. Bottom) Real-time stereo head mount display view with ultrasound volume display.

Head-mounted projector displays

The expensive display systems can be replaced by a projector and semi-transparent mirror system. Head-mounted projector display systems display the AR image upon the real object by using the projector and projecting the virtual image upon the half-silvered mirror. The schematic representation of head-mounted projector display is shown in Figure 2.9. The physician can simultaneously see the reflected virtual image and the real object through the mirror providing AR vision, as shown in Figure 2.9. Gao *et al.* [13] developed Varioscope AR, an ultra-light and compact design head-mounted projective display, as shown in Figure 2.9. Hua *et*

al. [68] and Argotti *et al.* [69] have also investigated the use of this technique in some of their systems.

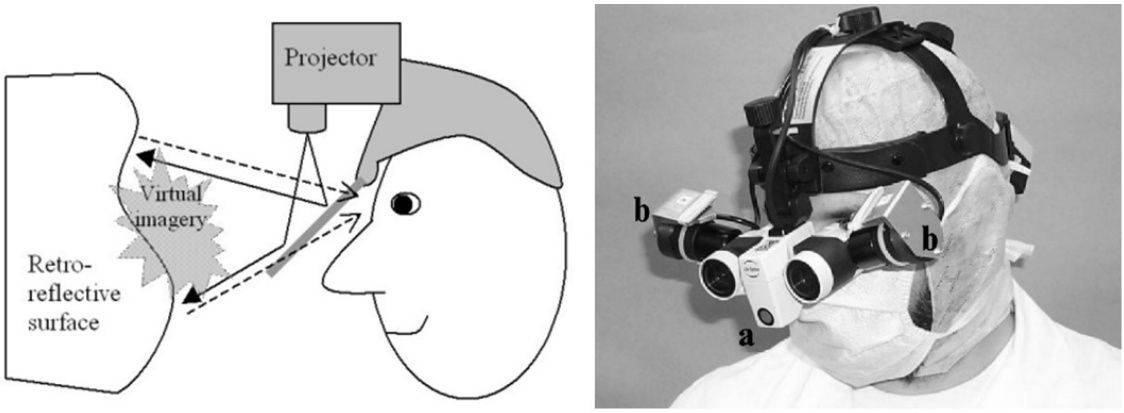

Figure 2.9: Head-mounted project displays: Left) schematic representation [12] and (right) prototype of the Varioscope AR [13]. (a) base instrument and (b) housing for the projection optics with the miniature displays

In general, the physician's head and hand-held instrument requires continuous tracking during the procedure. The registration of patient, image volume, head mount device with stereo camera and display system are very tedious. Only one person can view the AR image at a time. The user must focus on the display which is very close to the eye causing *"VR sickness"*. These limitations have inhibited the large scale clinical deployment of the head-mounted projector displays.

Volumetric image overlay systems

The primary limitation of head-mounted displays is the *"VR sickness"* [70]. The volumetric image overlay systems presents an effort to move the virtual image far away from the user's eye to just above the patient. A two-dimensional coronal image overlay concept was proposed to overlay coronal image over the patient, as shown in Figure 2.10 and the prototype developed for pelvis screw fixation [15] is shown in Figure 2.11. The mirror and monitor are configured together so that the

reflected image from the display monitor is floating over the object of interest when "seen through" the mirror. Further enhancement utilizing stereoscopic technique was implemented to produce 3D images [71] [14]. This was achieved by projecting slightly different images the eye would see as if looking at 3D image, as shown in Figure 2.10. The Intelligente Analyse und Informationssyteme (IAIS) group at *Fraunhofer Institute* developed *ARSyS-Tricoder*, as shown in Figure 2.12 to project the 3D planning and surgical path upon the patient. The proposed system eliminated the need of head-mounted displays but was feasible only for coronary images, required continuous tracking of the physician's head to project the right 3D image upon the mirror and limited only for port or tool entry guidance as the information about depth was missing.

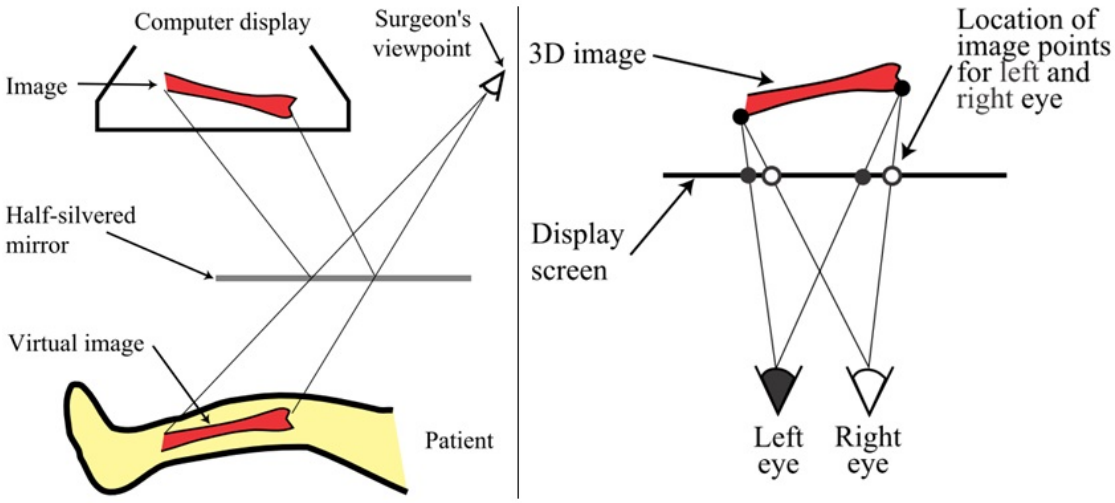

Figure 2.10: Volumetric image overlay concept [14]: Left) Using a half-silvered mirror to create a semi-transparent 'virtual' effect. Right) Location of image points on display for each eye to produce stereoscopic effect.

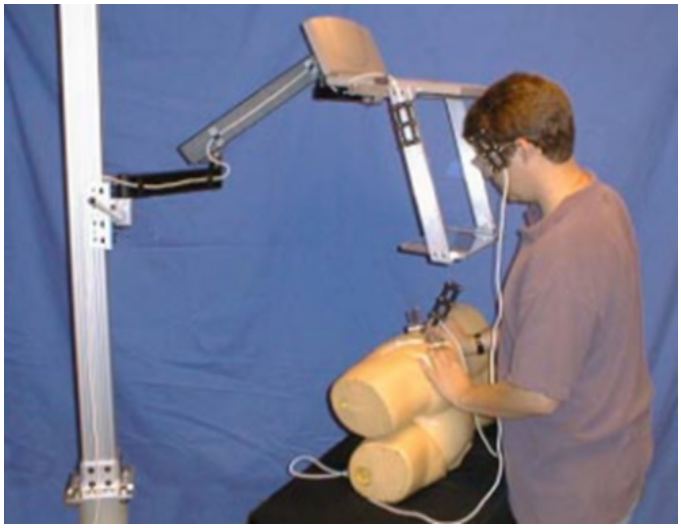

Figure 2.11: Volumetric image overlay prototype used for pelvic screw fixation simulation [15]. The physician's head is continuously tracked.

Figure 2.12: ARSyS-Tricorder : Image overlay system with a large screen for interventional image guidance (*Fraunhofer Institut Intelligente Analyse und Informationssyteme (IAIS), Sankt Augustin, Germany)*

Camera-projector system

This system represents an effort to eliminate the need for display-mirror configuration and need for tracking the physicians head location by projecting the preoperative 3D model of the patient onto the external anatomy (skin) of the

patient using industrial camera-projector systems. Wu *et al.* [16] proposed an Augmented Reality Computer Assisted Spine Surgery (ARCASS), as shown in Figure 2.13 to provide entry-point guidance for the vertebroplasty spinal surgery.

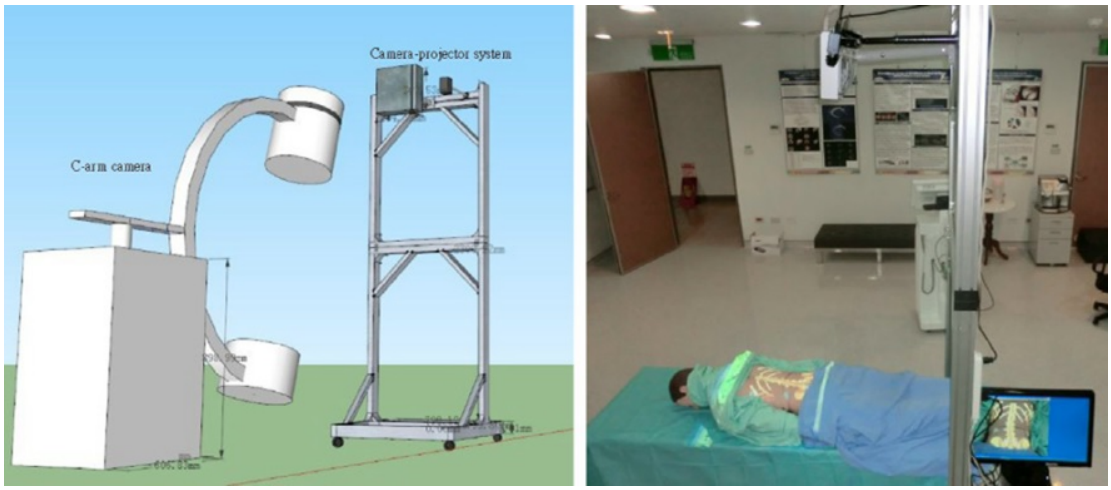

Figure 2.13: ARCASS system developed by IRCAD, France: Left) System concept. Right) Prototype developed [16].

A patient specific 3D model was constructed from pre-operative CT image volume using "Visible-Patient" *(visiblepatient.eu)* tool developed by the *Research Institute against Digestive Cancer (IRCAD)*, France. The camera-projector system was calibrated together using a chessboard pattern method as proposed by Park *et al.* [72]. The patient and image volume are fused together using the marker based automatic registration method. A set of markers are mounted upon the patient so that it is visible for the camera and also appears in the CT image volume. The patient 3D model is automatically aligned with the physical location of the patient by aligning the markers in CT volume with actual markers seen by the camera. With the help of the patient 3D model overlaid upon the patient, the entry and target points are determined and indicated over the patient, as shown

in Figure 2.14. The needle insertion is performed by placing the needle tip upon the entry point and orienting towards the target.

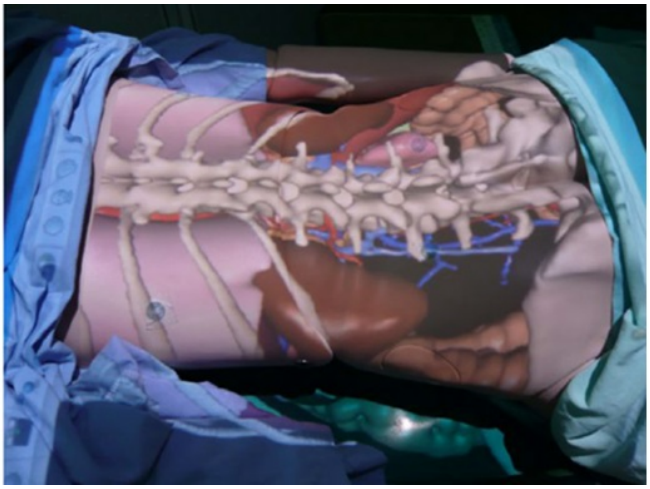

Figure 2.14: Overlay of image (patient model) upon the dummy patient model using ARCASS system [16].

The camera-projector system reduced the procedure duration by 70% compared to conventional C-arm assisted method and decreased intra-operative radiation exposure [16]. Some limitations of the camera-projector system are i.) only able to project the coronal image, ii.) the instrusion of physician into the line of sight of the projected image area, iii.) limited range of projection (150 - 200 cm) between the projector and patient, and iv.) insufficient information for needle orientation.

Image overlay systems

The tracked navigation systems and surgical robots are prohibitively complex and/or expensive for routine clinical use. Video AR systems, Head-mounted systems, camera-projector system and volumetric image overlay systems require

elaborate calibration, registration, and spatial tracking of all actors and components. In the pursuit of simpler augmented reality systems, Stetten *et al.* [17] [73] and our research group [20] had proposed 2D image overlay system consisting of mirror-monitor configuration attached together so that the virtual image formed due to reflection through the mirror is floating inside the patient (augmented reality effect) at the correct 3D location. This technique provides the physician the "X-ray" vision of the patient when "seen through" mirror. This technique provided an optically stable 2D reflection image without the need for physician's head tracking and allows multiple users to view the same image simultaneously.

Ultrasound real-time tomographic overlay

Stetten *et al.* [17] [73] proposed an image overlay concept to overlay real-time ultrasound images upon the patient. The display-mirror setup is attached upon the ultrasound probe so that the reflected virtual image through semi-transparent mirror is aligned with ultrasound plane from the probe and appears floating inside the patient when "seen through" the mirror.

The Sonic Flashlight [17] shown in Figure 2.15 was developed by Via Lab *(vialab.org)* for direct visualization of ultrasound images using real-time tomographic reflection method. The system has been extensively validated for vascular access and has been found to be beneficial compared to conventional ultrasound guidance system [73].

CT/MR-guided image overlay systems

Similar to ultrasound real-time tomographic overlay system developed by Stetten *et al.* [17], a static image overlay system (Figure 2.21) was proposed by our research group [20] [21] at Johns Hopkins University and Queen's University to

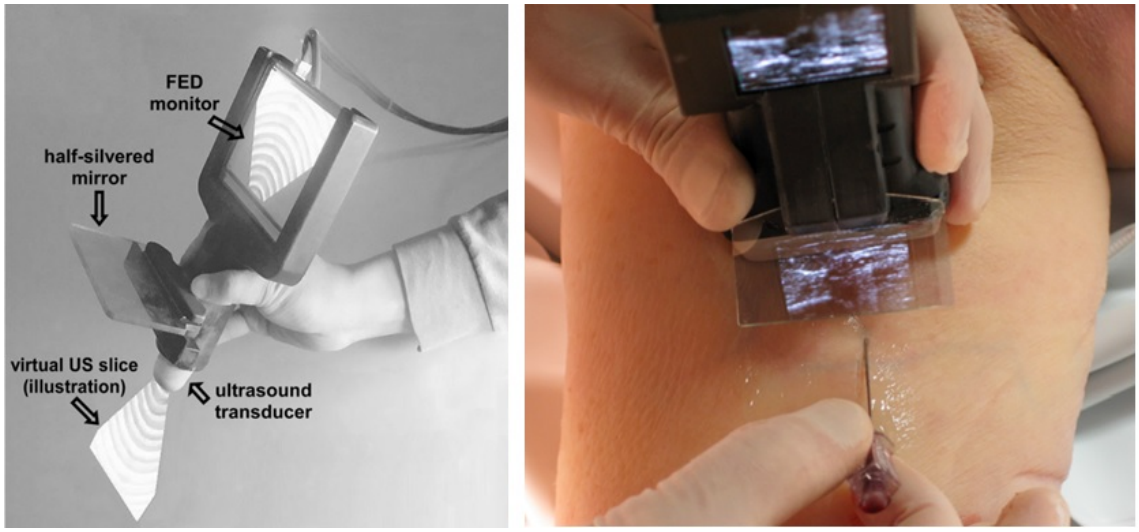

Figure 2.15: Sonic Flashlight [17]: A) Concept demonstration using mock-up prototype. B) Engineering prototype developed.

aid CT/MR-guided needle placement procedures. The system consisted of display monitor and mirror attached together at angle 60° between each other. It provided accurate transverse image guidance for musculoskeletal interventions of the shoulder, hip and spine [74] [22]. The static system developed earlier [20] [21] was associated with mechanical and ergonomic issues limiting its translation into clinical applications. These limitations are discussed in detail later and this thesis project is aimed at improving the ergonomic design and overcoming the mechanical issues enabling the translation of 2D image overlay concept into clinical applications.

Perk Station

Motivated by the successful pre-clinical trials of earlier systems [20] [21], augmented reality surgical navigation training suite (Perk Station) shown in Figure 2.16 was developed by our research group [75] [76] to assist the augmented reality needle placement training to the physicians and hone their skills in variety of

clinical applications (Figure 2.17). The development of the "Perk Station" was inexpensive, simple and easily replicated; it was used for teaching computer assisted surgery at all levels in a standard 'dry' laboratory conditions. The training conducted using the Perk Station has demonstrated the improvement of needle placement accuracy for several clinical procedures [18] [77].

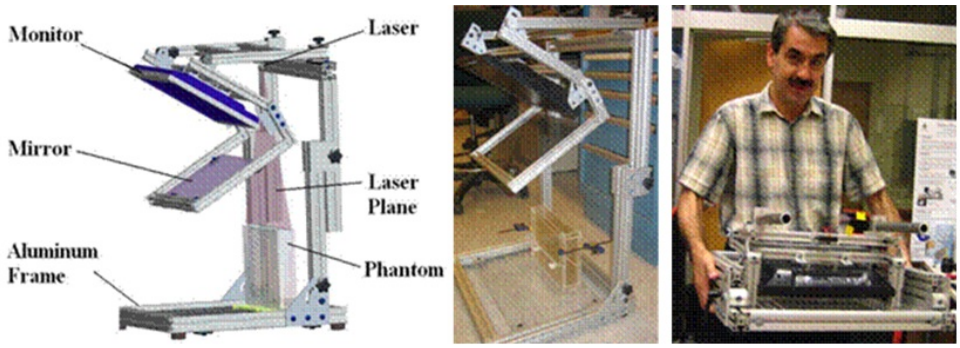

Figure 2.16: Perk Station: Left) System CAD design. Middle) Prototype assembled. Right) System folded for transportation *(perk.cs.queensu.ca)*.

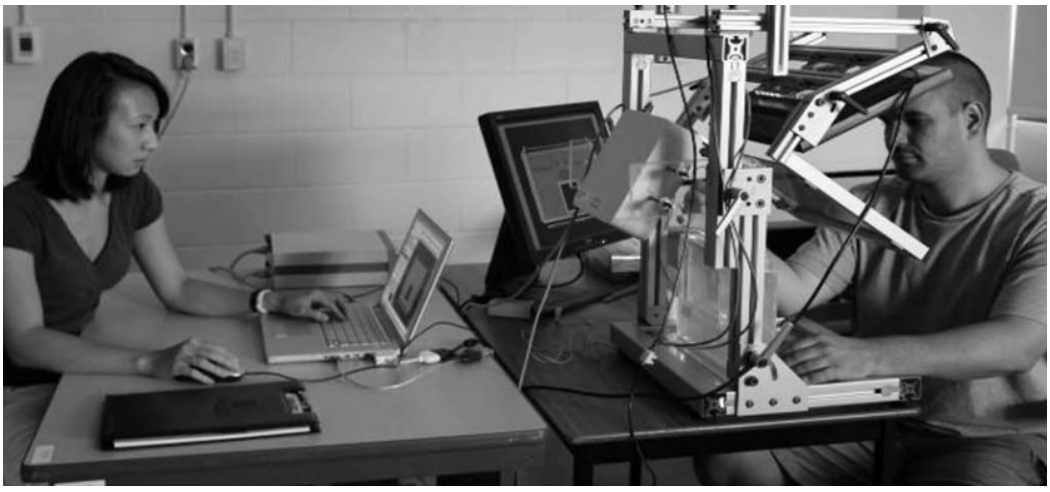

Figure 2.17: Perk Station [18]: The observer (left) sits opposite the trainee (right) and monitors the needle insertion visually. The side of the phantom facing the trainee is covered to prevent the trainee from direct visual access to the target.

2.4 2D image overlay system

A 2D image overlay system works based upon the optical properties of semi-transparent mirror to allow seeing through the mirror while reflecting the monitor image, as shown in Figure 2.18. The system consisted of a display monitor and a semi-transparent mirror attached together so that the virtual image formed due to reflection through the mirror is actually floating inside the patient at the correct 3D location. The display monitor used was either a normal LCD (liquid crystal display) display for CT-guided systems or a MR compatible monitors for MR-guided systems. The semi-transparent mirror is made of polycarbonate sheet with a transparent thin coating of aluminium on one side which forms the reflective surface of the mirror. The monitor and mirror are attached at angle $\theta_1 = 60^\circ$ and the reflected image is formed at angle $\theta_2 = 60^\circ$ with respect to the mirror ($\theta_1 = \theta_2$). The physical location of the virtual image overlay plane upon the patient is indicated by a laser plane (Figure 2.18).

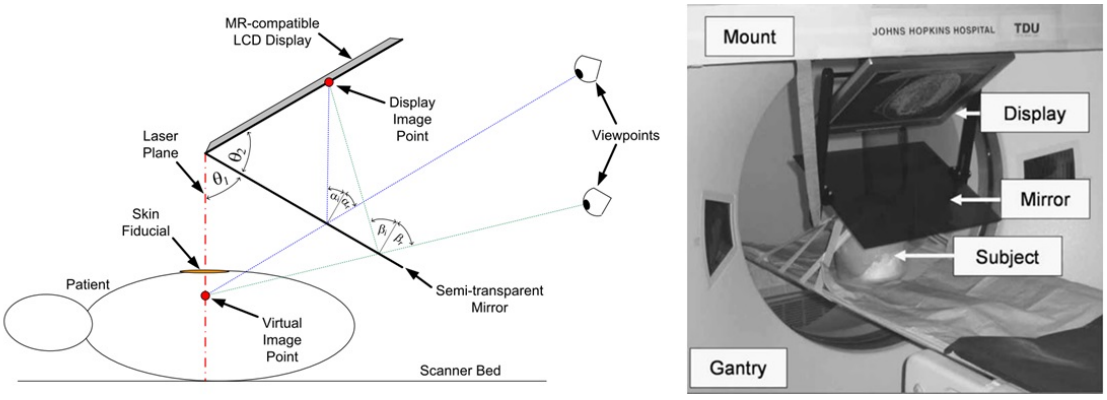

Figure 2.18: 2D image overlay concept: Left) Graphical representation of the working principle [19]. Right) First prototype developed with mirror-monitor setup mounted upon the scanner [20].

The first prototype developed by our research group at Johns Hopkins University to demonstrate the 2D image overlay concept is shown in Figure 2.18. The mirror-monitor setup was attached to the scanner machine so that the reflected virtual image is aligned with the scanner transverse plane. The laser plane was manually aligned with the scanner inner laser plane and the virtual image overlay plane was manually calibrated to the scanner coordinate system using Z-frame registration method (Figure 2.18) proposed by Lee *et al.* [78]. Further a stereotactic calibration method (Figure 2.19) was developed to reduce the role of human judgment and parallax error [20].

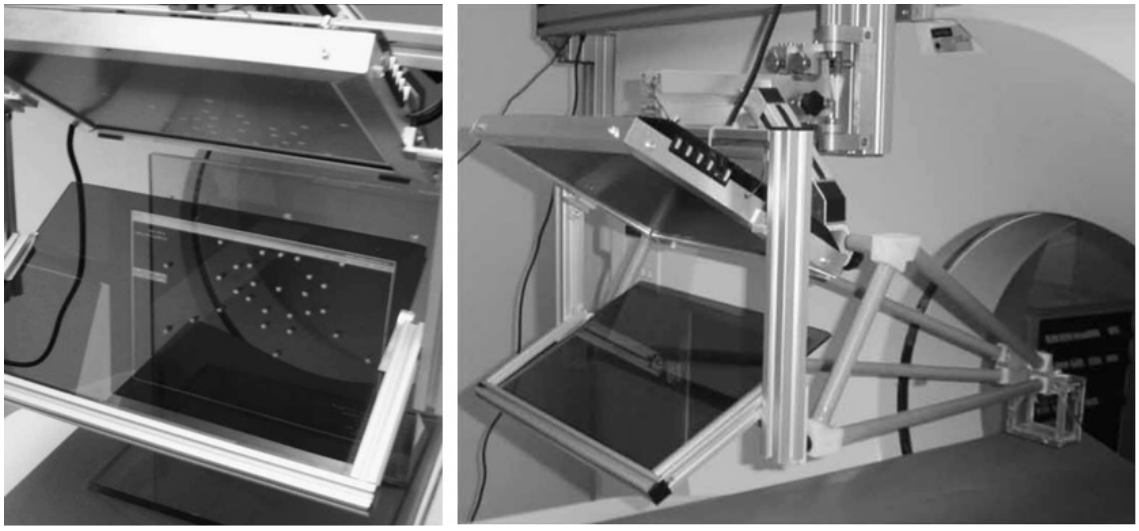

Figure 2.19: Image overlay plane calibration [20]: Left) Z-frame registration method. Right) Stereotactic calibration method.

Upon successful alignment of laser plane and calibration of virtual image overlay plane, a correct image was displayed in virtual plane depending upon the system position with respect to the patient [20]. The patient table is moved along the longitudinal axis to browse the image volume (transverse plane) over the patient until the right image slice with the target is seen. The insertion target and needle entry points are indicated in the software and the virtual needle insertion path is drawn

by the software. The length of needle insertion is also indicated by the software. For procedures which required needle insertion along the oblique plane, the entire scanner machine along with the image overlay device is rotated, as shown in Figure 2.20 and the virtual image overlay plane oblique rotation was limited by the scanner rotation limits (less than 10°).

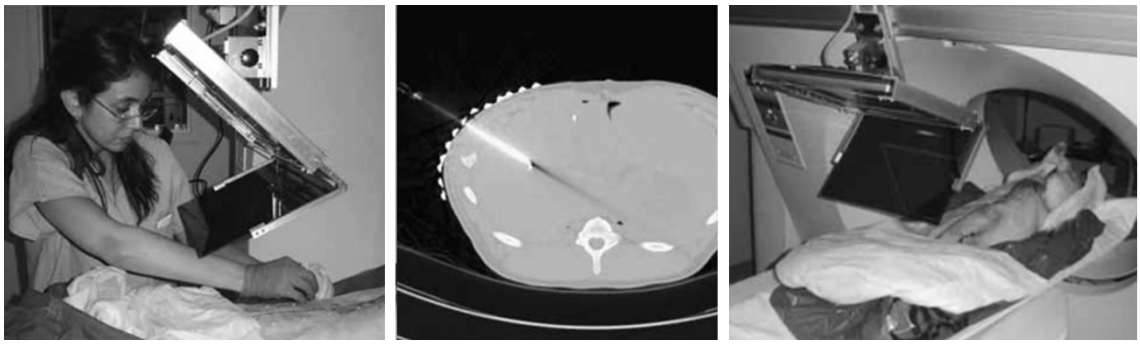

Figure 2.20: Cadaveric experiments [20]: Left) Needle insertion in the liver of a ventilated pig cadaver with straight gantry. Middle) Confirmation CT image. Right) Scanner tilted for oblique image.

The steps required for the needle insertion using augmented reality image guidance are as below:

1. Place the needle tip at the intersection of laser line upon the patient (or phantom) and needle insertion path displayed in the virtual plane
2. Orient the needle so that the laser line cuts through the center of needle head
3. Align the needle along the needle insertion path displayed in the virtual plane
4. Push the needle into the patient or phantom until the mark indicating the depth of needle insertion

The first prototype developed was mounted inside the scanner bore to align the virtual plane with the scanner inner laser plane. This limited the physician's workspace around the patient, often restricted and several targets were not accessible thereby limiting the number of possible clinical applications.

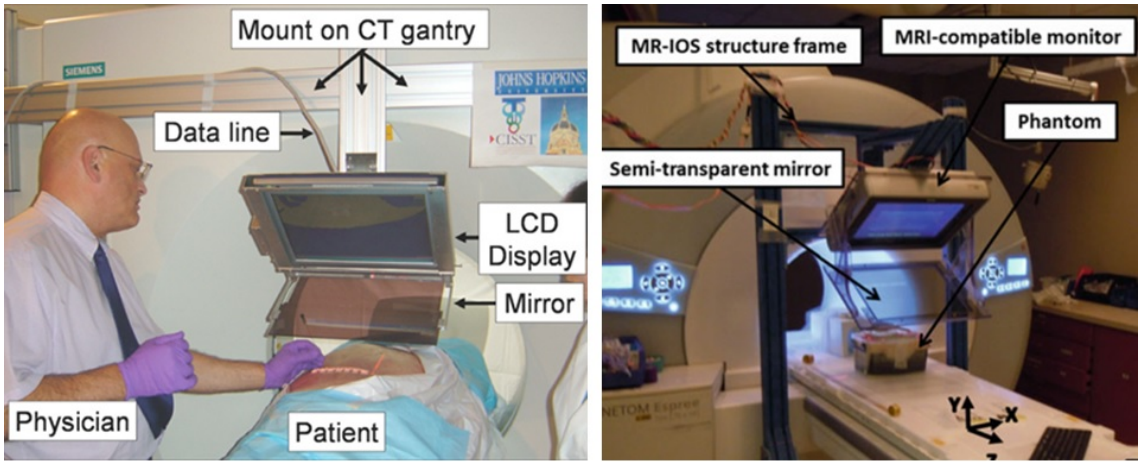

Figure 2.21: Previous static image overlay systems developed: Left) Overlay mounted on scanner (CT) [21]. Right) Overlay on floor mount (MRI) [22].

An improved version of the static image overlay system [21] shown in Figure 2.21 was developed to increase the workspace around the physician. The system improved the workspace accessibility, but not sufficient enough to allow many clinical procedures. The laser plane alignment was further more challenging as the laser plane was moved away from the scanner inner laser plane. The new scanners developed were no more rectangular in shape and hence the image overlay system was required to be independent of the scanner mounting. The design was further enhanced [21] by mounting the mirror-monitor setup upon a frame over the patient table, as shown in Figure 2.20. Several pre-clinical studies (Figure 2.22) were conducted for applications such as lumbar spine procedures [23]; shoulder and hip arthrography [22]; spine injection [5] and bone biopsy [4]. The results of these studies have been published in

the top Radiology Journals [73] [23] [5] [4] clearly indicating the clinical importance of the 2D image overlay concept.

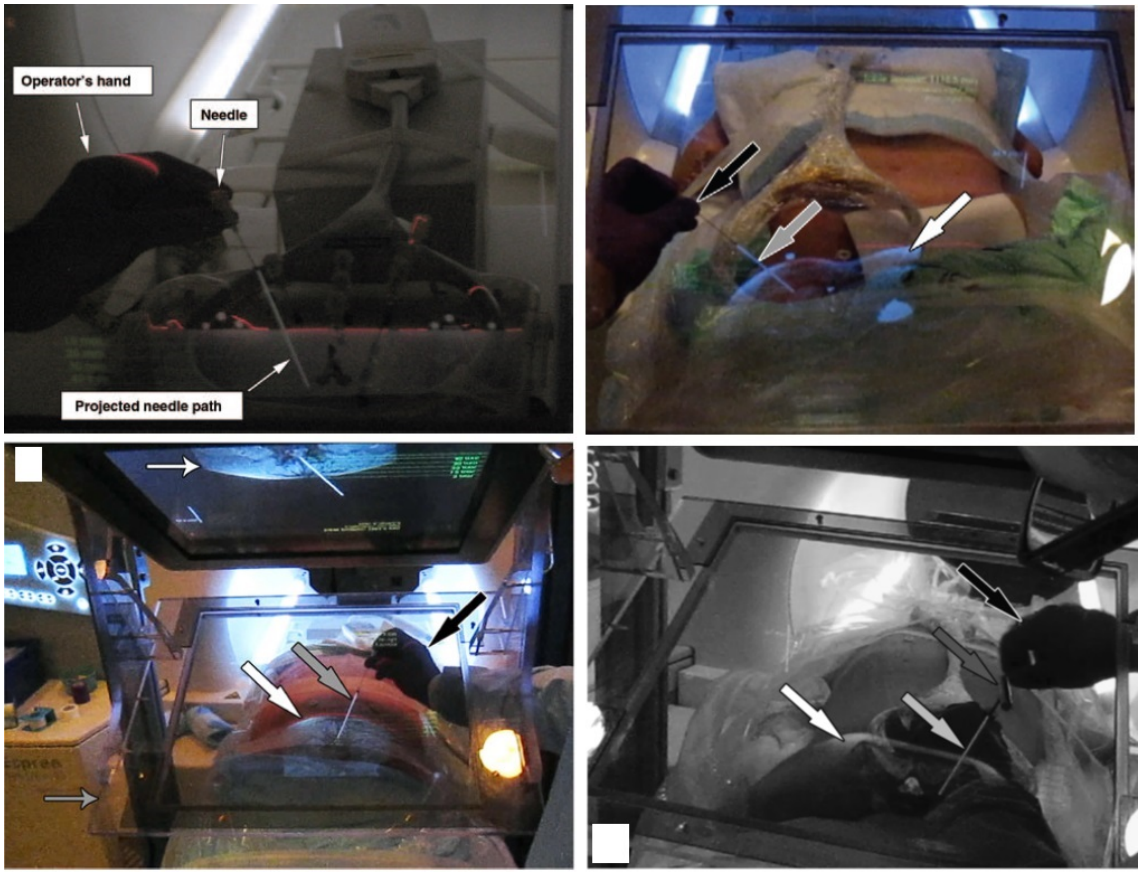

Figure 2.22: Pre-clinical trials performed with static image overlay system: *Clockwise* A). Lumbar spine procedures [23]. B) Shoulder and hip arthrography [22]. C) Spine injection [5]. D). Bone biopsy [4].

2.5 Driving clinical applications

The previously proposed static image overlay system has been extensively used for musculoskeletal procedures.The current thesis project is aimed at developing an image overlay system to assist image-guided percutaneous interventions for musculoskeletal procedures, parathyroidectomy, and percutaneous nephrolithotomy. The parathyroidectomy and percutaneous nephrolithotomy procedures are considered as the potential clinical applications since the 2D image overlay concept could provide significant benefits to the physician and the patient compared to conventional methods. In the following sections, the details of the procedures shall be explained and the problems associated using the conventional methods are discussed.

2.5.1 Musculoskeletal procedures

The interventional procedures in musculoskeletal (MSK) region are, in effect, minimally invasive procedures of surgical nature. These procedures have been performed under the imaging modalities such as ultrasound, computed tomography and magnetic resonance. Due to large number of procedures performed annually and the associated economic interests, there has been significant demand for technological advancements because the interventional team must perform the procedures in a very short duration with minimal post-operative complications and reduced hospital stay eventually reducing the overall associated cost. Based on the successful outcomes with the previous systems, we propose the following MSK procedures: biopsies and spinal injection, as the potential applications for the proposed solution.

Musculoskeletal Biopsy

Skeletal tumors are the common causes of bone destruction in the adult patients.

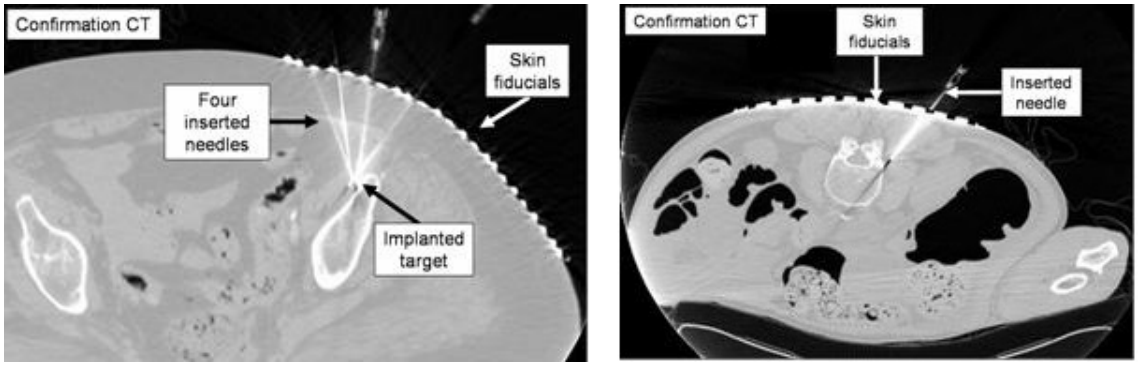

Figure 2.23: Musculoskeletal needle interventions: a) Confirmation CT of pilot needle insertion for MSK biopsy, in cadaver . b) Confirmation CT of needle placement for spine pain management, in cadaver *(perk.cs.queensu.ca)*.

Sampling of the bone marrow and soft tissues for analysis has been recognized for several decades [79]. Image-guided percutaneous needle biopsy is a relatively recent development and is rapidly gaining popularity as the standard of care in the assessment of musculoskeletal tumors. The percutaneous biopsy has several advantages over open biopsy. It is minimally invasive, allowing access to different parts of the lesion rather than the surgically exposed area alone. The imaging modality often can direct the biopsy needle to the most likely areas to yield suitable specimens. Typically the procedure includes the appropriate imaging scan (CT/MR) and identifying the target using the image volume. Then the physician performs the free hand needle insertion using the ultrasound image-guidance followed by the use of multiple CT scans to confirm the needle position (Figure 2.23 a). The minimally invasive approach reduces recovery time and patient morbidity. The procedure has a high reported accuracy, which ranges from 68% to 97% [80] [81] [82] [83] [84] [85] [86]. Generally, percutaneous image-guided needle biopsy for the musculoskeletal regions has been found to be an effective alternative to open biopsy.

Spine injection

Spinal disorders are the leading cause of pain, disability, and compromise of health-related quality of life. Back pain is the second most expensive musculoskeletal condition at an estimated $193.9 billion (between 2002 to 2004) [87], affecting 27.2% of the US population [88] and is the leading physical complaint prompting physician visits. Image guided minimally invasive procedures involving modalities such as CT fluoroscopy and MRI have gained a lot of interest lately. The interventional radiologist with an efficient image-guided technique (for example, CT-guidance), can increase the precision of the procedures allowing an improvement of the outcomes and reducing the complications. Typically the procedure includes ultrasound image-guided needle insertion across the superficial soft tissue, and the use of multiple CT scans to confirm the needle position (Figure 2.23 b) as it is advanced. The outcomes of these procedures are usually measured as spatial accuracy of needle placement. The longer procedure times and repeated radiation exposure are usually associated with the occasional misplacement of the needle, often several times, before its correct position is confirmed.

By overlaying the scanned image volume over the patient using the image overlay concept, the physician can browse the image volume over the patient and identify the target point right inside the patient body. There is no need for the physician to look at the monitor and hence the hand-eye coordination and mental 3D registration can be eliminated. The need for ultrasound or multiple scans to guide the needle can be avoided and the procedure duration could be reduced eventually minimizing the radiation exposure and number of punctures above the patient.

2.5.2 Parathyoidectomy

The conventional parathyroidectomy involved an open procedure with a neck incision up to 2 to 4 inches, followed by the inspection of all four parathyroid glands and removal of the offending gland or glands. There are usually two glands on each side of the thyroid, as shown in Figure 2.24, although 3-7% of the population may have an accessory (or supernumerary) parathyroid, and 3-6% may have fewer than four glands. The glands may occasionally *descend incompletely*, or too far, and lie in aberrant locations [89], and in such cases, the surgery requires longer incision leaving visible scar, as shown in Figure 2.25 a and Figure 2.25 b on the patient neck and longer procedure duration resulting in increased post-operative complications and longer stay in the hospital.

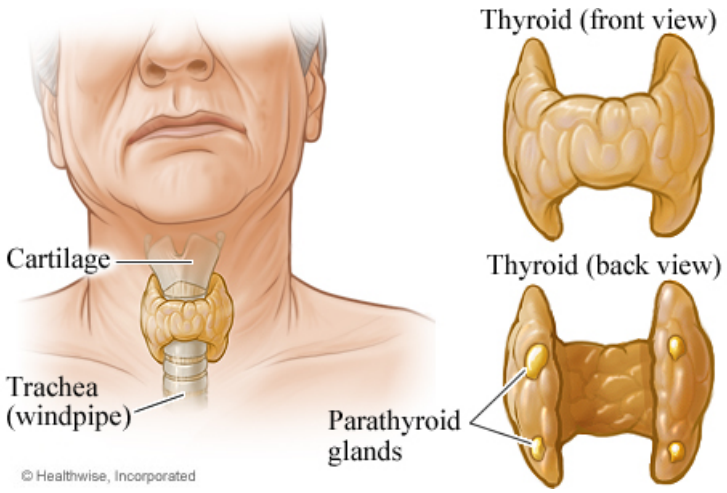

Figure 2.24: Graphical representation of parathyroid gland location (*Healthwise Inc.)*.

Figure 2.25: Conventional parathyroidectomy procedures [24]. A) Longer incision required *(wikipedia.com)*. B) Longer visible scar.

There has been a constant push from the public and the surgical community for minimally invasive procedures with the goal of decreased incision length (reduced visible scar), decreased procedure time, decreased recovery time and post-operative complications. The conventional open (four gland) parathyroid exploration was considered the standard of care for the treatment of primary hyperparathyroidism until the 1990's, the advancements in imaging techniques made limited (less than four gland) exploration, a feasible concept [24]. Now, many expert centers worldwide have adopted limited parathyroid exploration as their preferred surgical approach [90] [91] [92] [93].

The reason for limited exploration method as preferred choice of procedure is due to the fact that about 90% of the patients associated with hyperparathyroidism have only one diseased gland [94] (Figure 2.26). The challenge here is to successfully find the diseased gland prior to the procedure. The essential imaging techniques used to localize the solitary parathyroid adenomas are parathyroid sestamibi (a nuclear

medicine test, SPECT - Single Photon Emission Computed Tomography) and ultrasound [95] [96].

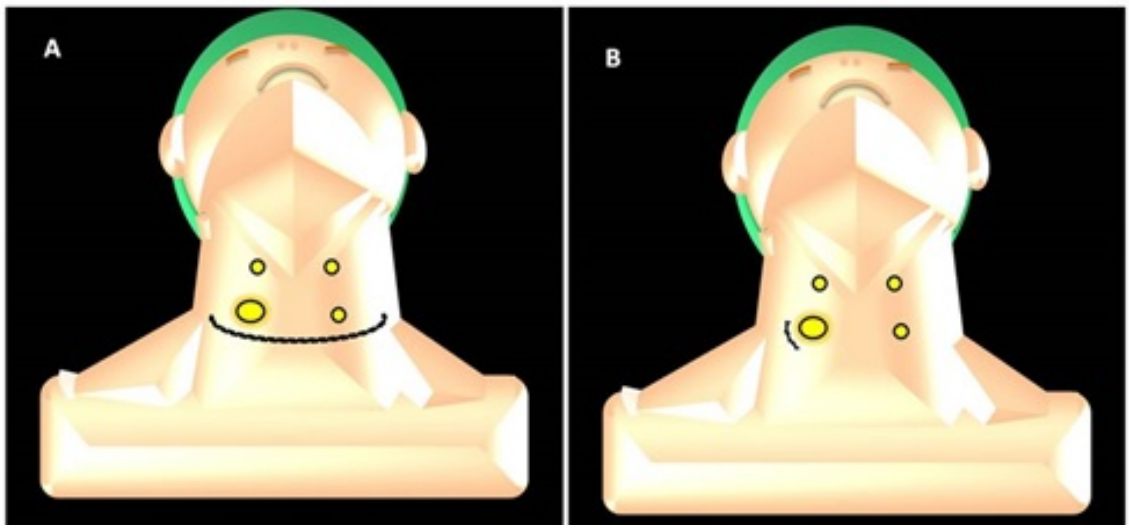

Figure 2.26: Graphical representation demonstrating the advantage of limited exploration method to locate the disease gland [25]. a) Open surgery. b) Minimally invasive surgery.

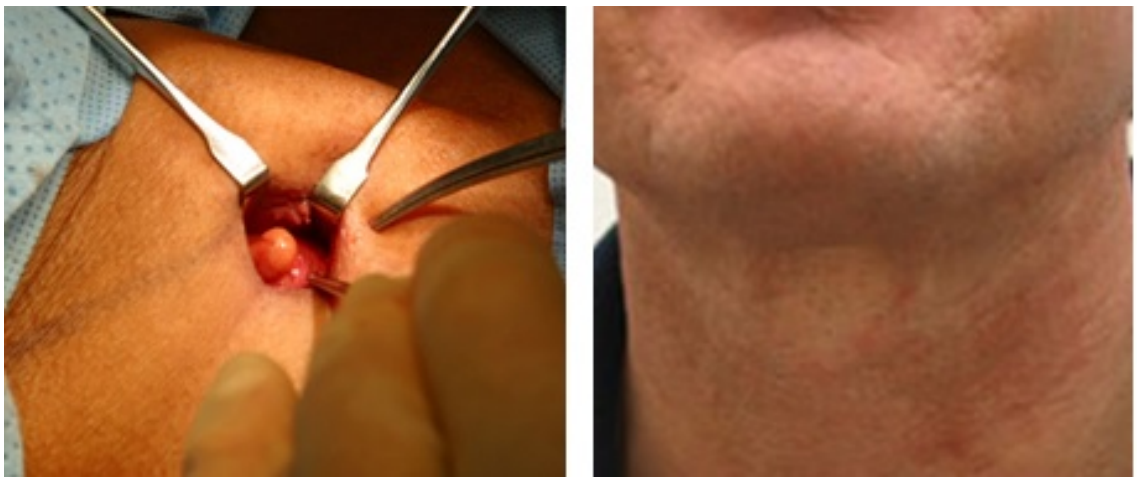

Figure 2.27: Benefits of minimally invasive exploration procedure for parathyroidectomy (*UCLA Endocrine Surgery*) (left) shorter incision and (right) scar almost invisible.

Minimally invasive exploration procedure (Figure 2.27) has resulted in incision length 1.5-2.0 cm (approx. .75") [97] and 90% of operations being completed in less than 30 minutes [98] as compared to the conventional open surgery. Significant amount of time was spent in exploring the location of parathyroid gland using the ultrasound imaging. It is further possible to reduce the procedure duration and incision length by overlaying the SPECT scan data upon the patient using the proposed augmented reality concept. The image volume can be explored over the patient to localize the diseased parathyroid gland. The application of augmented reality image overlay concept for the parathyroidectomy procedure was proposed by our clinical collaborators at Harvard Brigham and Women's Hospital, Boston USA.

2.5.3 Percutaneous nephrolithotomy

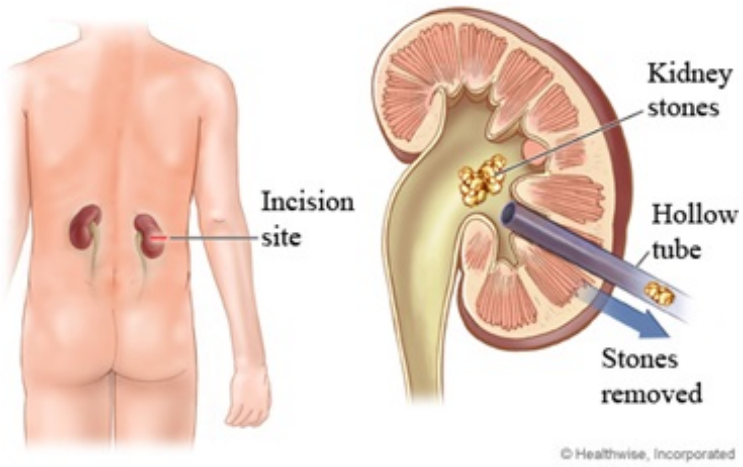

Figure 2.28: Graphical representation of percutaneous nephrolithotomy procedure (*Healthwise Inc.*)

Percutaneous nephrolithotomy (PCNL) involves the removal of kidney stones percutaneously through the skin, as shown in Figure 2.28. Kidney stones are a common

problem affecting people irrespective of their geographical, cultural or racial differences [99]. Approximately 14% of men and 6% of women will develop a kidney stone disease during their lifetime [100] [101]. PCNL is accepted as the procedure of choice for the treatment of large or complex renal calculi [102].

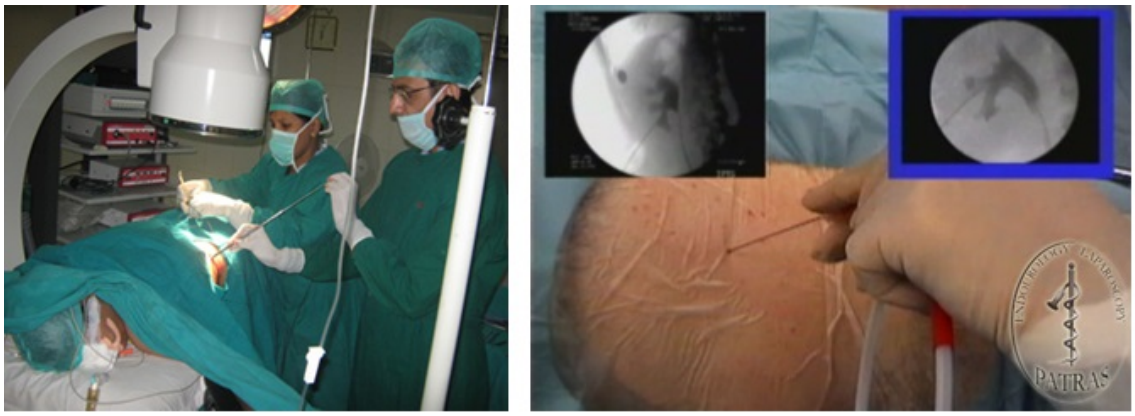

Figure 2.29: Surgeons using fluoroscopic guidance to guide the wire into kidney (*wecareindia.com and University of Patras*)

Kidney stones are diagnosed by X-ray, ultrasound scan and CT scan. Compared to X-ray and ultrasound, CT scans are more sensitive in picking up stones in the kidney or the structures which drain the urine from the kidney into the bladder (ureter). The key challenge associated with the procedure is gaining access into the kidney percutaneously through the skin. This is achieved by inserting a guide wire with the aid of ultrasound or fluoroscopic imaging. Fluoroscopic guidance is the preferred technique for the most stone therapies with PCNL (Figure 2.29).

The primary outcome measures are usually associated with access-related complications such as bleeding, failure to access, pneumothorax, or other organ injury [103]. The other problems associated with this procedure are increased duration and increased radiation exposure due to use of continuous fluoroscopic imaging [47] to

guide the wire.

In order to minimize the radiation exposure, CT-guided PCNL procedure has been proposed to gain access into kidney using the image-guidance. The main challenge associated with CT-guided PCNL is transporting the patient between the procedure room and CT room resulting in increased procedure duration and the possibility of patient infection. We propose to overlay the CT image volume over the patient using the proposed augmented reality image overlay concept, and provide the physician the 'X-ray' vision to guide the wire into kidney resulting in reduced radiation exposure, procedure duration and post-operative complications.

2.6 Research motivation

Compared to many image-guided navigation methods discussed in this chapter, the 2D image overlay concept is relative simple, low cost ($3,300) [23] and reliable. The reflected virtual image is optically stable, multiple users can simultaneously view the same image, and it does not require spatial tracking of all actors and components. The successful pre-clinical trials conducted with the system have clearly demonstrated the clinical importance of the image overlay concept.

The static image overlay system required careful and tedious calibration of the virtual image overlay plane. There was no significant economic interest as the initial setup time was much higher than the actual procedure duration. The system lacked dynamic tracking and was prone to misalignments due to structural deformation or unintended physical contact during the procedure. The system was either fixed to a CT/MR machine or floor-mounted frame and this limited access to the physician around the patient and excluded clinically relevant ranges of motions of the tool and

physician. The system is always in the OR (operation room) or procedure room even when the procedure is not done and thereby consuming the useful OR space. The system can provide only transverse image guidance thereby limiting the number of possible clinical applications. The accurate positioning of the system over the patient was difficult due to limited precision of movement by the patient table.

In spite of numerous efforts by our research group in simplifying the concept and enhancing the features, the system has still not seen its presence in clinical space mainly due to ergonomic and mechanical issues of the system. The main objective of this thesis project is to enable the clinical translation of the image overlay concept by simplifying the mechanical design, improve the system ergonomics, integrate dynamic tracking, reduce calibration duration, simplify laser and virtual plane alignment, enhance image quality and improve virtual plan tracking accuracy.

Chapter 3

Adjustable Image Overlay System

The material in this chapter is the extension of the conference paper published as Anand *et al.* The Hamlyn Symposium on Medical Robotics (2013), pp 47-48 [104], where I was the primary author and responsible for the system concept, design and development.

3.1 System description

The adjustable image overlay system was proposed to overcome the ergonomic and mechanical issues associated with previously proposed static image overlay systems [20] [21] [22]. The system design was aimed at introducing system mobility, increasing degrees of freedom for the mirror-monitor setup, and integrate an optical tracking system for dynamic tracking and improve virtual plane calibration accuracy.

The conceptual view of the adjustable overlay system is shown in Figure 3.1 and consists of mirror-monitor setup called a "viewbox" similar to [21] [22] and attached to a floor-mounted counterbalanced, articulated arm. The system is equipped with optical markers on the viewbox to measure the pose of the image overlay plane during

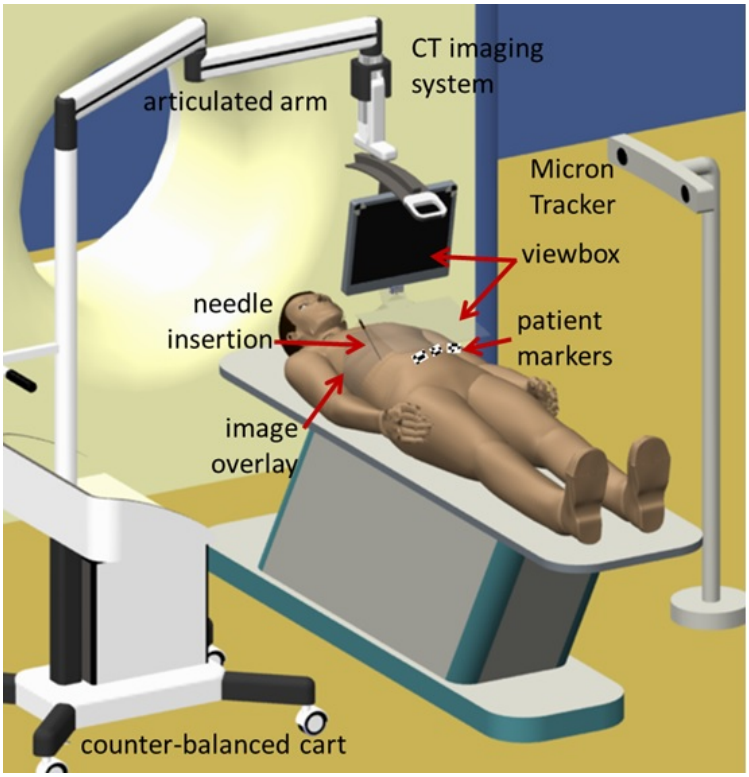

Figure 3.1: Conceptual view of the proposed adjustable image overlay system with viewbox mounted upon the articulated arm with mobile cart and optical dynamic tracking system integrated.

the procedure. Another set of optical markers are fixed upon the patient for co-registration of scanned image volume and the system together. The system can be used for exploration of image volume by moving the viewbox over the patient. The image re-slicing software will display the correct image in real time corresponding to the 3D position of the image overlay plane tracked by the optical tracker with respect to the patient. After locating the target point in the image overlay plane inside the patient, the system is locked in this position and a virtual needle path is drawn on the image slice using the software, which gets updated in the image overlay plane for needle guidance.

The adjustable system overcomes the practical difficulty of accurately positioning the static image overlay system [21] [22] by increased degrees of freedom and motion tracking of the viewbox. The mobility enables the system to be moved out of the procedure room when not in use and thereby not using the precious procedure room space. Mounting the viewbox over an articulated arm increases the degrees of freedom to provide oblique and sagittal image guidance in addition to transverse image guidance thereby increasing the possibility of adding more clinical procedures. The integration of optical tracking system minimizes the initial setup time and eliminates the problem of misalignments as the system is continuously tracked.

The mechanical design was done using the Parametric Modeling CAD tool "Creo 2.0" *(Parametric Technology Corporation Inc. MA USA)*. The MicronTracker *(Claron Technology Inc. ON Canada)* was chosen for optical tracking, 3D Slicer *(slicer.org)* software for image re-slicing and 3D visualization, and PLUS *(plustoolkit.org)* for communicating 3D Slicer with MicronTracker.

3.2 Driving clinical applications

Musculoskeletal procedures such as biopsies, orthographies, and spinal injections will continue to be the driving clinical application for the adjustable image overlay system due to its economic benefits and large number of procedures being performed annually. These procedures have been successfully tested using previously developed image overlay systems [73] [23] [5] [4]. Spine needle injections and parathyroidectomy are the two driving applications that define the constrains for the system design. Spine needle injection requires needles of length up to 7 cm and oblique rotation of $\pm$ 35°. The parathyroidectomy procedure requires enough clearance between the device and

the patient head when place above the neck to explore the image volume. The image overlay concept potentially can reduce the radiation exposure, procedure duration and minimize post-procedure complications.

The key technical specifications for the system design are derived from the driving clinical applications and they are as follows:

- System shall support the needle of length up to 7 cm (requirement for all MSK procedures)
- Image overlay plane oblique rotation of $\pm$ 35° for spine injection procedure
- Sufficient clearance above the patient to avoid possible interference with the patient's head during parathyroidectomy procedure

At each development phase, the design was verified against the requirements by simulation using the CAD tool, as shown in Figure 3.2. The manikin 3D model used represents the 95^{th} percentile adult male population.

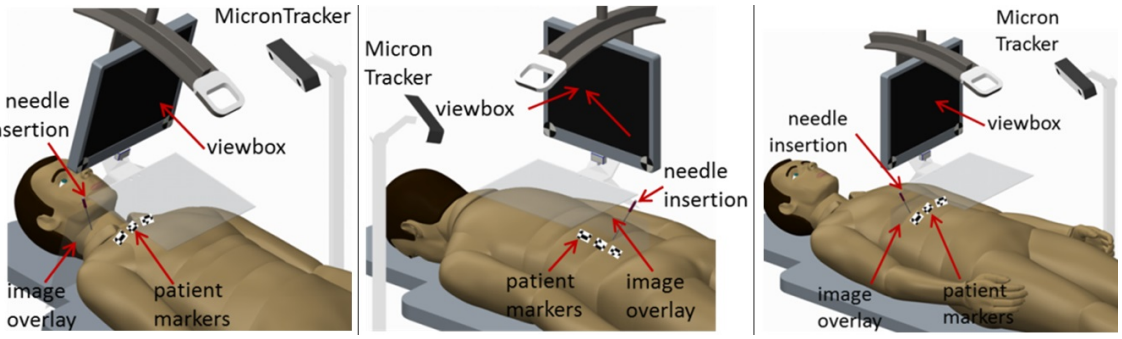

Figure 3.2: CAD simulation of clinical applications for the adjustable image overlay system: Left) Parathyroidectomy. Middle) MSK procedure. Right) Percutaneous nephrolithotomy.

3.3 Workspace analysis

The workspace analysis is the study aimed to determine the optimal assembly dimensions between the display monitor and mirror considering the constraints defined by the targeted clinical applications. The spine needle injection and parathyroidectomy are the two critical procedures which will define the constraints for the workspace analysis. The expected outcome of the study is to define the mirror-monitor configuration satisfying the following requirements:

- Optimum included angle between the mirror and display monitor to achieve maximum user viewing angle, through which the physician can view the complete depth of virtual image overlay plane when "seen through" mirror
- Orientation of viewbox with respect to the articulated arm and degrees of freedom required
- Sufficient gap between the viewbox and patient while the system is positioned over patient for parathroidectomy procedure
- Oblique image display of $\pm$ 35° required to guide the needle between the vertebrate for facet (spine) injection procedure
- Sufficient clearance between the display monitor and mirror for accommodating the needle length of minimum 7 cm and enough space for the user to hold the needle

Initially, a 60-degree design similar to the previous systems [20] [21] [22] was considered for the study and several prototype configurations, as shown in *Appendix A* were developed to define the optimal assembly dimensions between the mirror and

display monitor; however, none of these solutions were satisfactory and hence other design configurations (angle between mirror and display monitor) were explored.

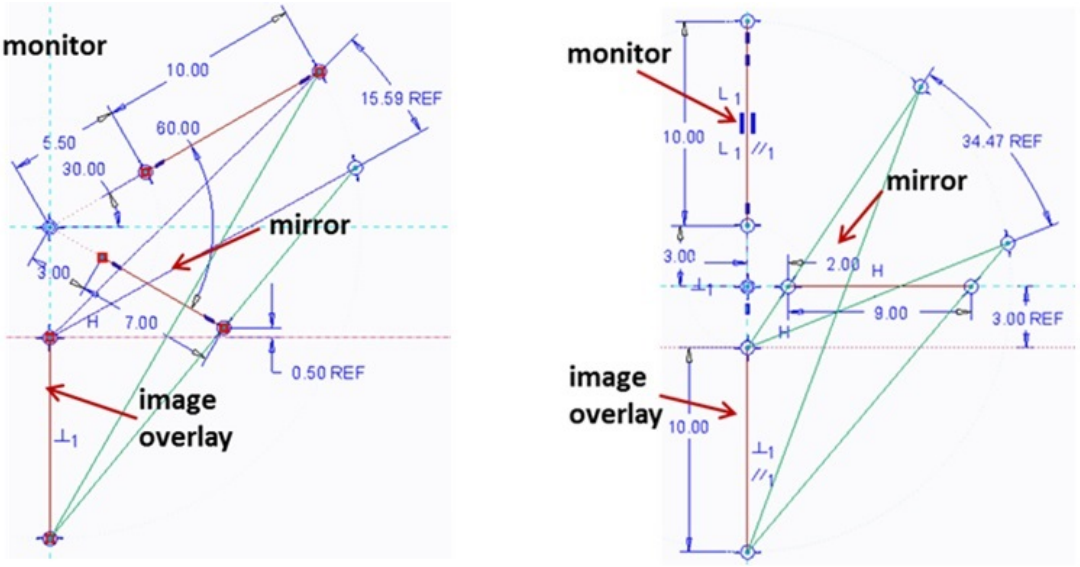

Figure 3.3: 2D sketch simulation study using "Creo 2.0" CAD tool : Left) 60-degree. Right) 90-degree.

Method

A mechanical CAD tool "Creo 2.0" was used for simulation (Figure 3.3) and all configurations between 60-degree and 90-degree, as shown in Figure 3.4 were explored. The 90-degree design represents the newly proposed mirror-monitor configuration. The 2D sketch module of the CAD tool was used to create skeleton structure of the concept. The display device and mirror are represented by the line with the actual component dimensions being considered. The reflected virtual image is created at the same angle between the mirror and display device. The dimensions between the mirror and display device were adjusted by trial and error method and the outcomes were compared with the clinical requirements described

in the previous section. The study was done for all configurations between 60-degree and 90-degree and the results were reported.

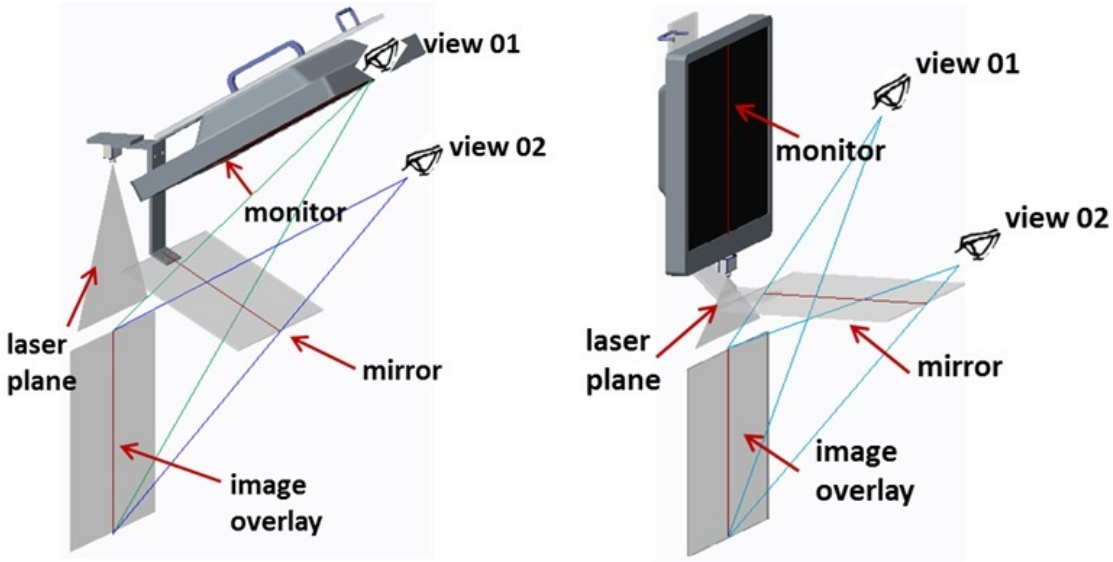

Figure 3.4: Workspace concept using the output of 2D sketch simulation study, as shown in Figure 3.3: Left) 60-degree. Right) 90-degree.

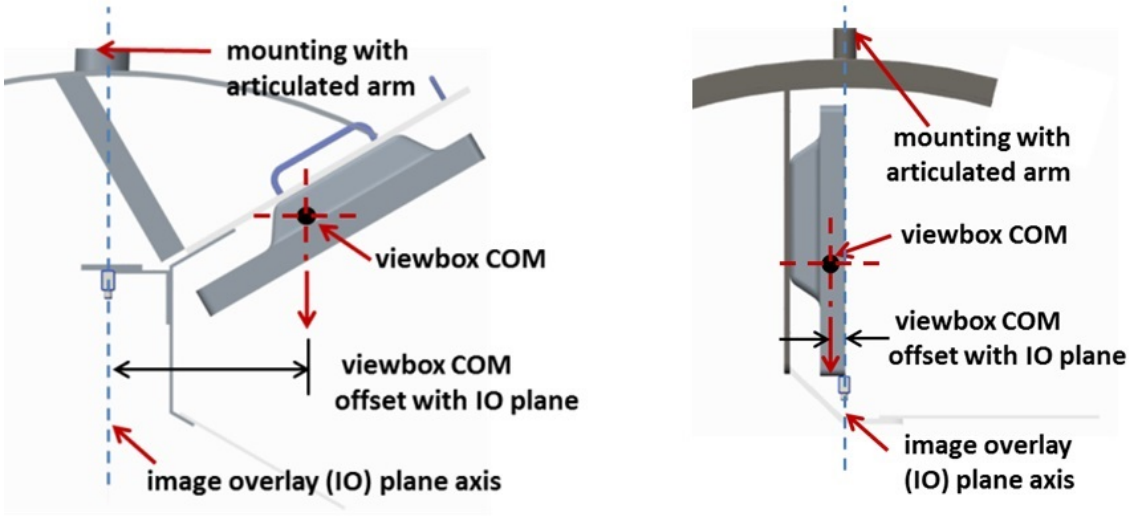

Figure 3.5: Center of mass (COM) offset from the vertical axis of rotation about the image overlay plane: Left) 60-degree. Right) 90-degree.

Table 3.1: Results of workspace analysis between 60-degree and 90-degree mirror-monitor configuration for the adjustable image overlay system

System configuration	***60-degree***	***90-degree***
Design principle	Similar to earlier system	Newly proposed design
User viewing angle	15 degree	35 degree
Center of mass offset	17.5 cm	1.0 cm
Oblique rotation	0 degree	15 degree
Viewbox weight	27.3* kg	8.2 kg
System weight	145* kg	45* kg

∗*approximate weight of the system calculated using 3D design models created*

The results of the workspace analysis are presented in Table 3.1; the study reported the newly proposed 90-degree design to be optimal solution as compared to the previously proposed 60-degree design. The increased viewing angle of the 90-degree design gives more flexibility for the physician to work around the patient and allows more than one user to view the same image through the mirror. Due to zero clearance above the patient for 60-degree design, a compromise in depth of the image overlay plane was required to gain additional clearance. The 90-degree design has minimum of 7.5 cm clearance above the patient while still permitting to view the complete image overlay depth of 25 cm. Both designs were able to accommodate needle of length 7 cm along with enough space for the user to hold the needle (12 cm approx. in total required). The center of mass of the 90-degree design is in-line with the axis of vertical rotation shown in Figure 3.5 as compared to 17.5 cm offset for the 60-degree design. The center of mass offset from the vertical axis of rotation creates

additional torque about the rotational joints, decreases the bearing performance and increases the effort required for user to maneuver the system during procedure. In order to minimize these problems, the 60-degree design should be counterbalanced, as shown in Figure 3.5, but this would increase the viewbox and overall system weight, and prototype development cost.

The viewbox and the overall system weight for 90-degree design was 3.3 times lighter compared to the 60-degree design. The other advantages of 90-degree design compared to 60-degree design are:

- Increased clearance between the mirror and the patient
- Reduced system inertia as the system is mechanically balanced about the vertical axis of rotation along the image overlay plane
- Increased viewing angle which also improves the view-ability for MicronTracker

3.4 Oblique image overlay plane rotation

Many solutions discussed in the previous chapter require pre-planning of the procedure with the scanned image volume. The main drawback with pre-planning is the amount of time spent in aligning the viewbox to view the preplanned image at correct location over the patient. In order to eliminate the need for pre-planning, the virtual image overlay plane needs oblique rotation. The oblique rotation of the viewbox enables the physician to browse through the image volume, and identify the target and appropriate needle entry point. Browsing through the image volume over the patient is more convenient as the physician can define the target and entry point at the fixed location of the viewbox over the patient.

In order to achieve the oblique rotation, the viewbox is rotated about the target point with remote center of rotation (RCM). Three concepts were studied:

1. Five bar link mechanism
2. Monitor rotation mechanism
3. Arc guide rotation

Five bar link mechanism

The viewbox is mounted upon a five bar link mechanism and rotated about the fixed remote center of rotation (RCM). The schematic representation of the concept is shown in Figure 3.6 a. The main limitation of this concept was the mechanical interference of linkages with the patient (and table), increased number of mechanical parts adding additional weight to the suspended mass with increased manufacturing cost.

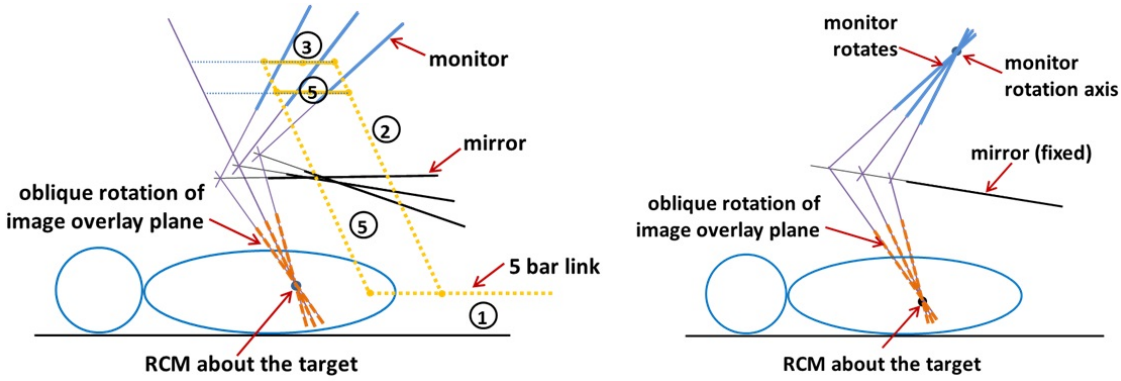

Figure 3.6: Oblique rotation: A) Five bar link mechanism. B) Monitor rotation mechanism.

Monitor rotation mechanism

In this concept (Figure 3.6 b), the monitor is rotated about an axis and the reflected image through the mirror is also rotated causing the oblique rotation

of virtual image overlay plane. Although the monitor rotation was simple but the mirror and laser plane needs translation as the monitor rotates adding more complexity for the mechanical design.

Arc guide rotation

In this concept shown in Figure 3.7, the viewbox is mounted upon a custom made arc-guide. The axis of rotation of the arc guide is about the remote center of rotation of the image overlay plane. The viewbox can be rotated about the fixed RCM to browse the image volume over the patient to determine the optimal needle insertion path.

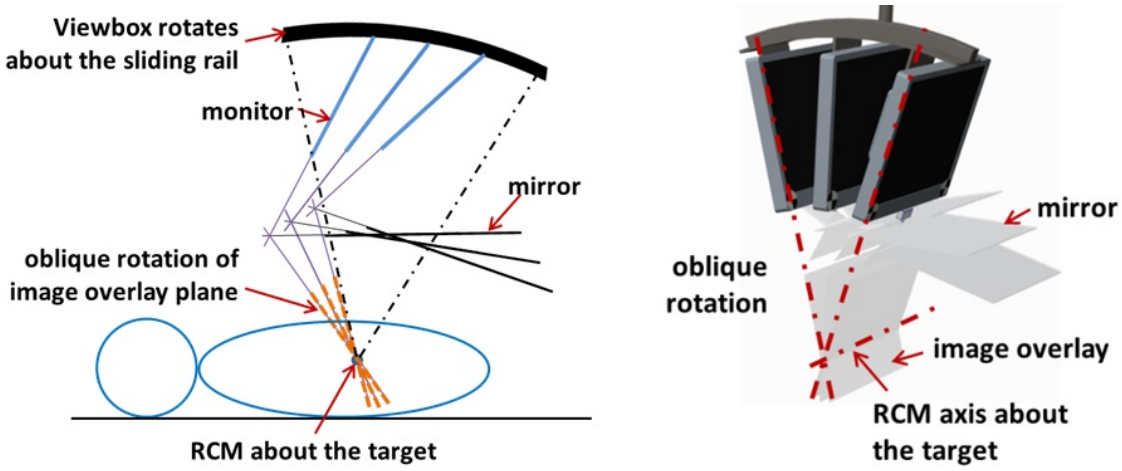

Figure 3.7: Arc guide concept for oblique image overlay plane rotation: Left) Schematic representation. Right) Viewbox design.

The oblique rotation of the viewbox using arc guide rotation was practically feasible as compared to five bar link mechanism or monitor rotation concept. The requirement of ± 35° oblique rotation was not met with either of the viewbox configurations (60-degree and 90-degree) due to reduced user viewing angle and mirror interference with the patient. The optimal oblique rotation of ± 15° was

practically feasible for 90-degree design, as shown in Figure 3.8 and it will be considered as a limitation of the adjustable image overlay system. Alternatively, the system can be rotated about 90° around the vertical axis, as shown in Figure 3.9 to view the needle insertion path in the virtual image overlay plane along sagittal plane.

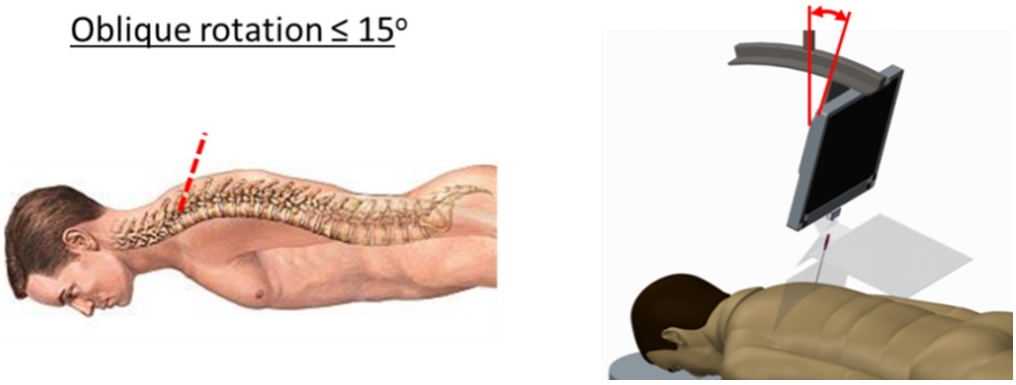

Figure 3.8: Viewbox rotation about the RCM for oblique rotation of $\leq \pm 15°$.

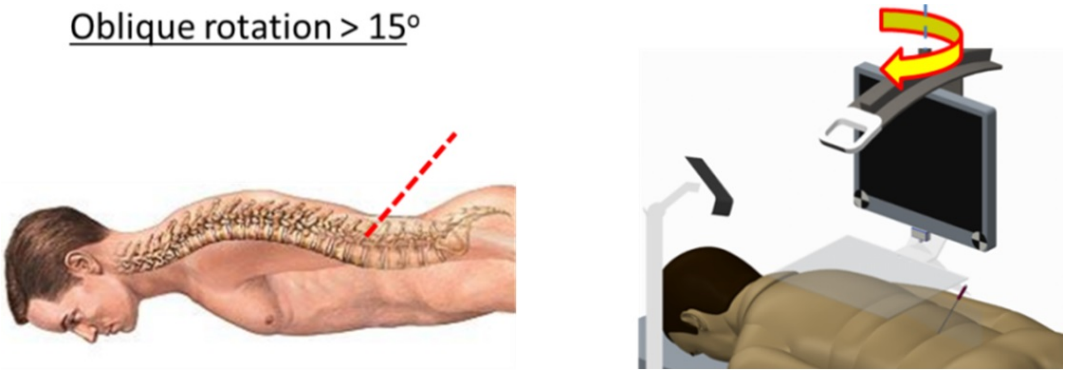

Figure 3.9: Viewbox rotation about the vertical axis for oblique rotation of $> \pm 15°$.

Different directions of motions for viewbox

The viewbox conceptual design based on the outcomes of workspace analysis is shown in Figure 3.10. The angle between the display monitor and mirror is 90° and the viewbox is mounted upon the arc-guide rail. The system shall have four directions

of motion, as shown in Figure 3.10:

1. Movement of ± 5 cm along the longitudinal axis *(X)*
2. Rotation of ± 90° about the vertical axis *(Z)*
3. Oblique rotation of ± 15° about the target point of needle insertion
4. Movement of ± 10 cm along the vertical axis *(Z)* to accommodate patients of different abdominal size.

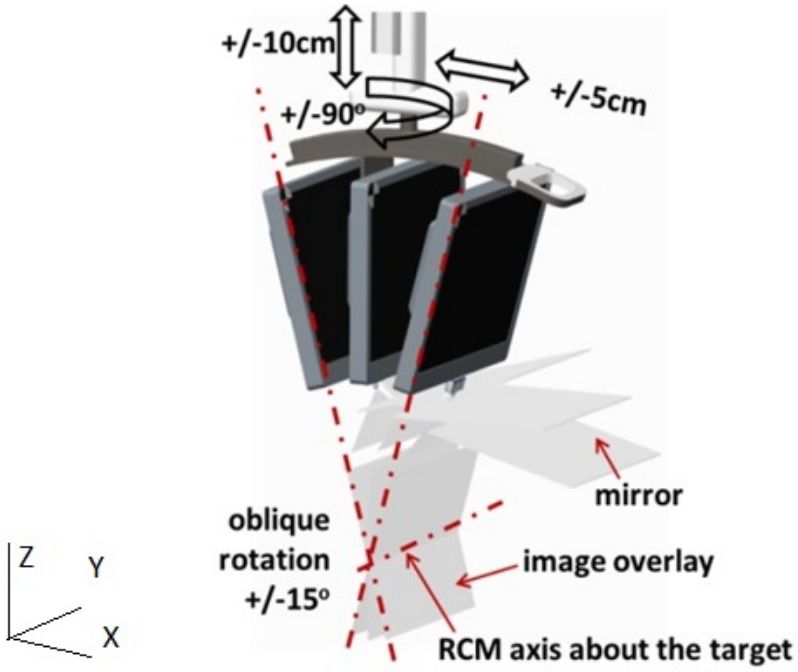

Figure 3.10: Viewbox conceptual design based on the workspace analysis outcomes.

3.5 Viewbox design

The detailed engineering design of the 90-degree viewbox is shown in Figure 3.11 and the first prototype developed is shown in Figure 3.12. The standard T-slotted

aluminium profiles (25mmx25mm) were used for building the prototype. The aluminum profiles are standard, light weight, low cost, easy to machine, easy to build and compatible with other standard profiles, connectors and accessories. The aluminuim profiles are connected together using joining plates and brackets, M6 T-nuts, and anchor fasteners. The structural rigidity between the monitor and mirror was maintained by additional 45° supports, as shown in Figure 3.11. The standard pivot joints were made of zinc with the powder coating and used for rotation joint about the vertical axis. High-cycle double flange linear bearings were used for linear adjustment of the viewbox about the longitudinal and vertical axis. A linear braking kit was used to secure the linear bearings in the desired position.

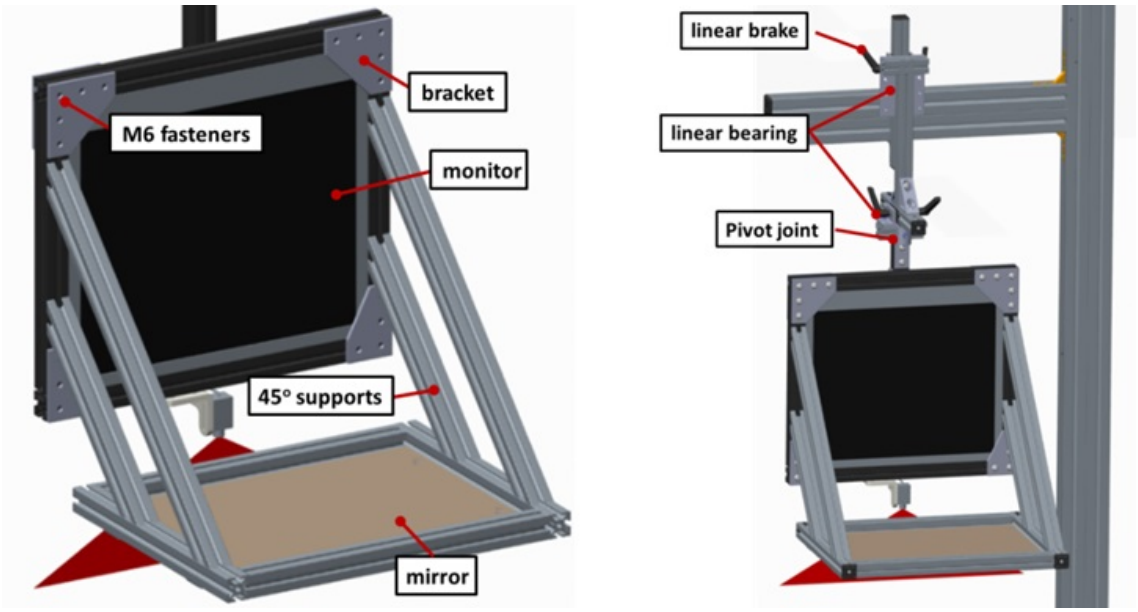

Figure 3.11: 90-degree viewbox design: Left) Viewbox. Right) All joints shown.

A standard 15" LCD monitor and semi-transparent mirror similar to earlier static systems [20] [21] were used as display device and mirror respectively. A red line type laser diode (RoHS compliant) of power output 1mW similar to the earlier systems

[20] [21] was used to indicate the position of the virtual plane upon the patient. A custom designed laser mount shown in Figure 3.13 was used to attach the laser diode upon the viewbox and provides three degrees of freedom to align the laser plane with the virtual image overlay plane.

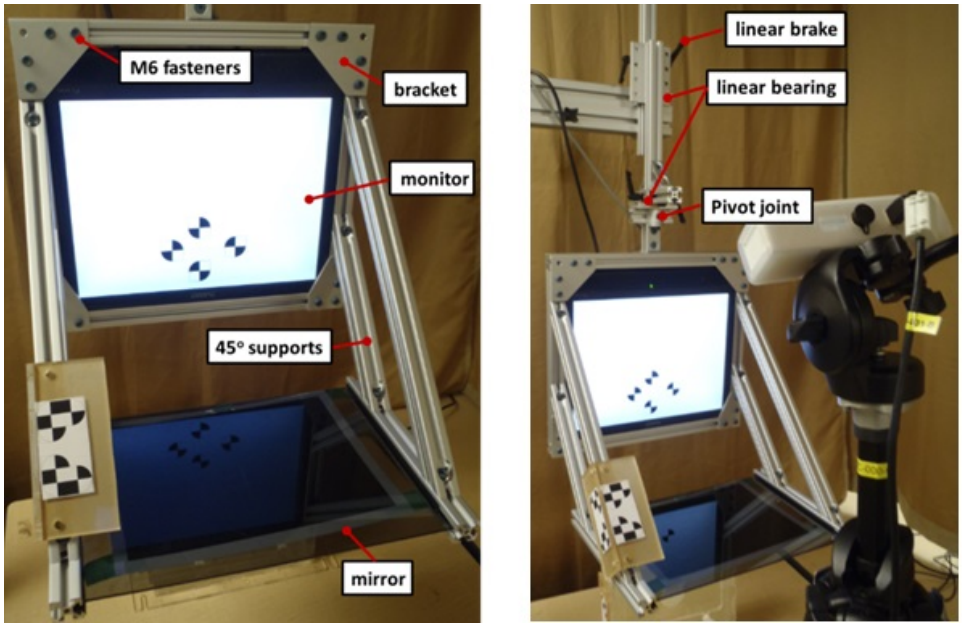

Figure 3.12: 90-degree viewbox prototype: Left) Viewbox. Right) All joints shown.

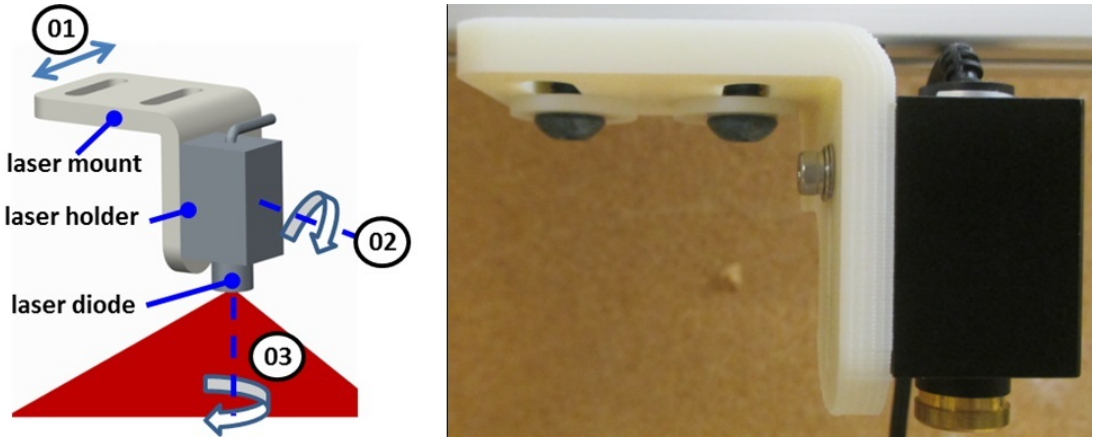

Figure 3.13: Laser mount: Left) Design with 3 DOF's. Right) Prototype developed.

After the prototype assembly, the viewbox inclination, as shown in Figure 3.14 a was observed due to offset in the center of mass from the vertical axis of rotation. The offset in the center of mass was due to significant weight of aluminium structures supporting the mirror (includes weight of 45° supports, mirror and mirror support), variation in manufacturing tolerances and clearances in the pivot joint and linear bearings. The manufacturing tolerances and clearances can be improved by using precision manufacturing and custom parts resulting in increased development and increased manufacturing cost.

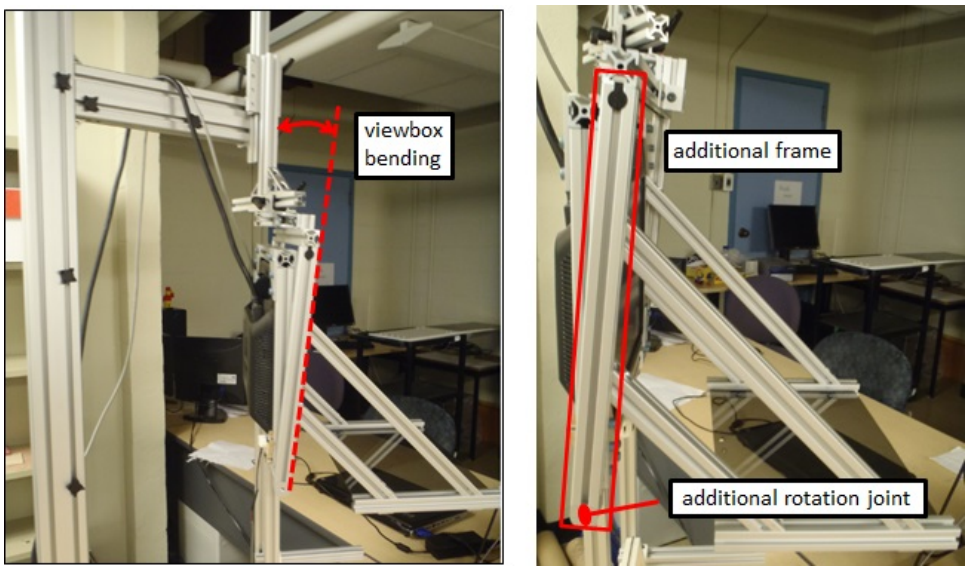

Figure 3.14: Standard pivots and bearings used: A) Viewbox inclination observed. B) Design modified to compensate the inclination by additional joints.

For the prototype development, an alternative design modification was considered by adding additional pivot joint at the bottom of the monitor on each side, as shown in Figure 3.14 b. The vertical orientation of the monitor was manually adjusted and fixed with the aid of spirit level. The proposed design modification ($30) was cost effective as compared to high precision pivot joints and linear bearings ($400 each).

3.6 Counterbalanced cart design

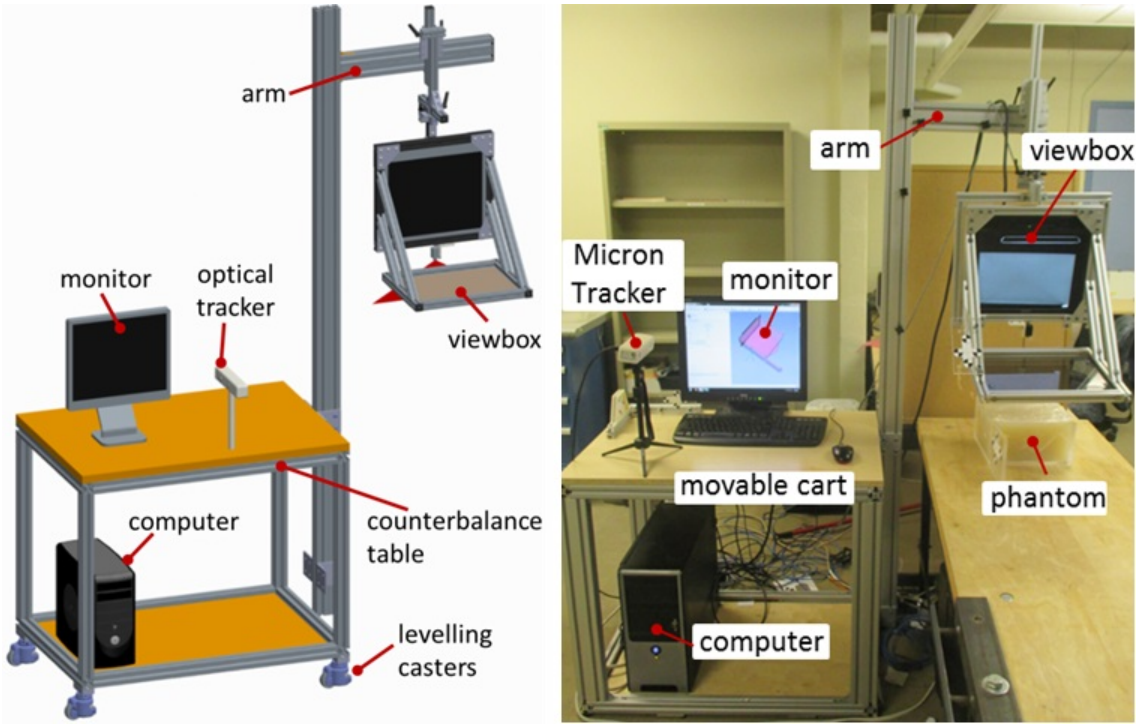

Figure 3.15: Counterbalanced mobile cart and simplified arm: A) Concept design. B) Prototype developed.

A custom designed articulated arm with mobile cart was used to support the suspended viewbox over the patient and transport the system in and out of the procedure room. The detailed design of the cart is shown in Figure 3.15 a and the prototype developed is shown in Figure 3.15 b. The weight of the mobile cart and the desktop computer above the cart counterbalances the suspended weight of the viewbox. A desktop computer machine was required for supporting image re-slicing software. The arm (vertical and horizontal structure) supporting the viewbox was built using T-slotted aluminium profile (40mmx80mm). The arm is attached to customized cart which counter balances the weight of the suspended viewbox.

The leveling casters (4X) attached to the cart allow the system to be movable. The leveling feature of the caster provides braking function to lock the system during the procedure. The optical tracking system is also placed upon the cart so that the patient and the viewbox are in the field of measurement of the tracking device. The arm design was simplified by removing articulation feature for prototype development; however, for the final product an articulated arm similar to shown in Figure 3.1 could be used.

3.7 Laser plane alignment method

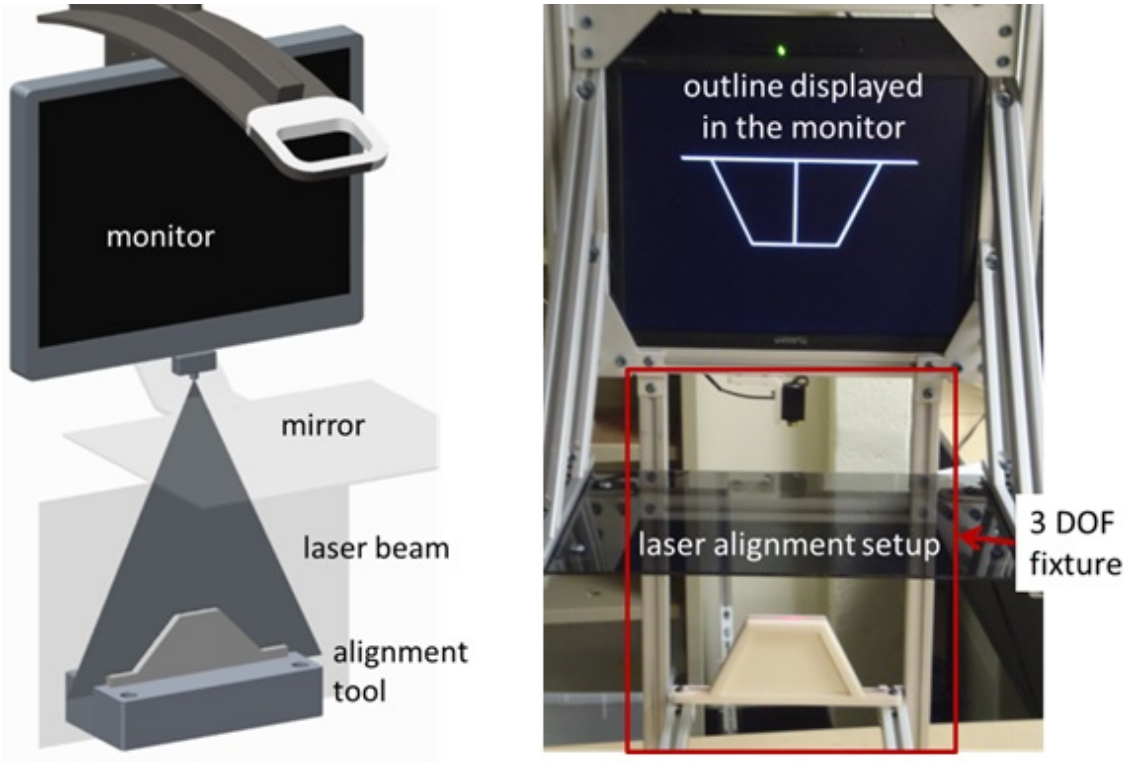

Figure 3.16: Laser alignment setup: A) Concept. B) Prototype implementation.

The physical location of the virtual image overlay plane over the patient is indicated by a laser line upon the patient. The laser plane aids the physician to locate the needle entry point upon the patient and align along the virtual image overlay plane. The laser plane must be aligned with the virtual image overlay plane before the system calibration and initial setup for the procedure. The earlier systems [20] [21] [22] were designed so that the virtual plane was parallel to the scanner inner transverse plane and the laser plane was aligned either inline [20] or parallel [21] [22] to scanner laser plane. Since the laser source was attached to the viewbox which had four degrees of freedom, aligning the laser plane with scanner inner laser plane was challenging and tedious. To simplify the laser alignment, an alignment tool was developed, as shown in Figure 3.16 a and its implementation is shown in Figure 3.16 b.

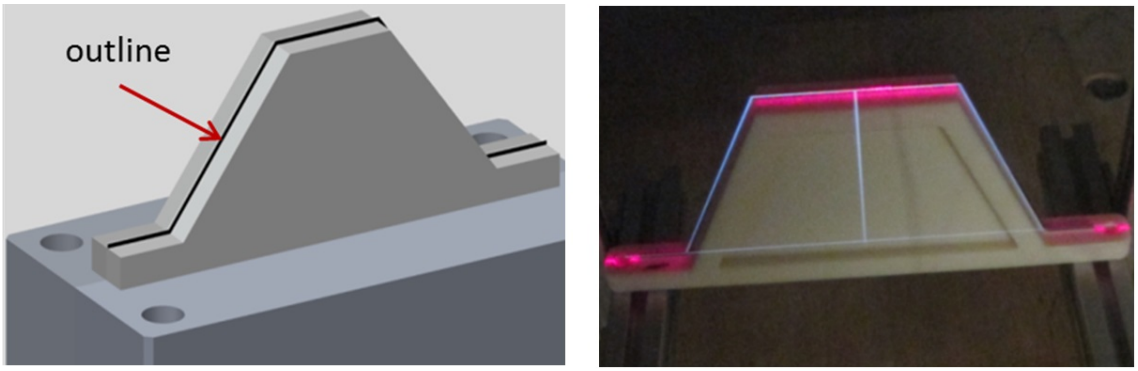

Figure 3.17: Laser plane alignment: A) Trapezoid-shaped tool with outline shown. B) Alignment of reflected 2D sketch, tool outline and laser line confirming correct alignment of laser plane with virtual plane.

The laser plane alignment setup consists of trapezoid shaped 3D-printed tool with a dark outline of 2 mm thick in the center of the part, as shown in Figure 3.19 a. The tool is attached to the viewbox using a customized fixture with three degrees of freedom, as shown in Figure 3.16 b. The 2D outline sketch of the trapezoid-shaped

alignment tool is displayed upon the monitor and the reflected image is shown in the virtual image overlay plane. Using the fixture, the alignment tool is adjusted so that the reflected image of the 2D sketch when "seen through" the mirror is overlaid upon the dark outline of the alignment tool, as shown in Figure 3.19 b. At this position, the alignment tool is firmly fixed to the fixture and the laser diode mounted upon the laser mount (Figure 3.13) is adjusted until the laser plane (line) aligns with outline of the laser alignment tool. The laser plane alignment is considered to be successful when the laser line, alignment tool outline and 2D outline of the virtual image are aligned together when "seen through" the mirror, as shown in Figure 3.19 b. For the commercial version of the device, the laser plane alignment shall be a pre-factory setting and needs to be done once. The structure between the mirror and monitor shall be rigid and hence there is no need to realign the laser plane before each procedure. However a calibration step can be defined to confirm the laser alignment periodically.

3.8 Optical dynamic tracking

Figure 3.18: Optical tracking systems: A) MicronTracker *(Claron Techecnology Inc.)*. B) Polaris Tracker *(NDI Medical Inc.)*.

The problem of misalignment of the previous static systems [20] [21] [22] were due to unintended physical contact with the system and / or mechanical deformation due

to large suspended mass. The previous systems lacked dynamic tracking to account for these misalignments. The adjustable image overlay system shall be equipped with an optical tracking system for continuous tracking of the viewbox and the patient together. Two different tracking devices were considered for the system.

1. MicronTracker *(Claron Technology Inc. Canada)* shown in Figure 3.18 a uses passive planar markers and stereoscopic camera for real time tracking of the marked objects

2. Polaris Tracker *(NDI Medical Inc. Canada)* shown in Figure 3.18 b uses passive spherical, retro-reflective markers and infrared light to track the marker in real time

Each set of markers are mounted upon the viewbox and patient for simultaneous tracking in real-time. MicronTracker was the chosen optical tracker for adjustable system and it was based on the outcome of the image overlay calibration method study.

3.9 Image overlay plane calibration

The image overlay plane calibration was required to determine the pose of the virtual image overlay plane with respect to physical reference or the scanner coordinates. Depending upon the position of virtual image overlay plane with respect to the patient (or phantom), the software displays the right image slice on the monitor and by reflection into the virtual image overlay plane.

The main limitation of the previous static image overlay system was longer duration required for initial setup which was higher than the actual procedure duration.

The image overlay plane calibration was done using Z-frame registration [20] method using a specific calibration phantom. The image volume displayed in the virtual plane was aligned with the phantom manually by the user and the virtual image overlay plane was registered with scanner coordinates. The procedure being completely manual was tedious, requires additional phantoms and CT scans. A stereotactic calibration method [20] was developed by the same group to improve the accuracy of calibration and reduce the human error; however, the longer calibration duration remained the same.

The calibration method for the adjustable image overlay system was aimed at simplifying the calibration steps with reduced duration with simplified phantom if required. Two calibration methods were studied for the adjustable image overlay system. The motivation for the new calibration methods wwas due to optical tracking system used for dynamic tracking.

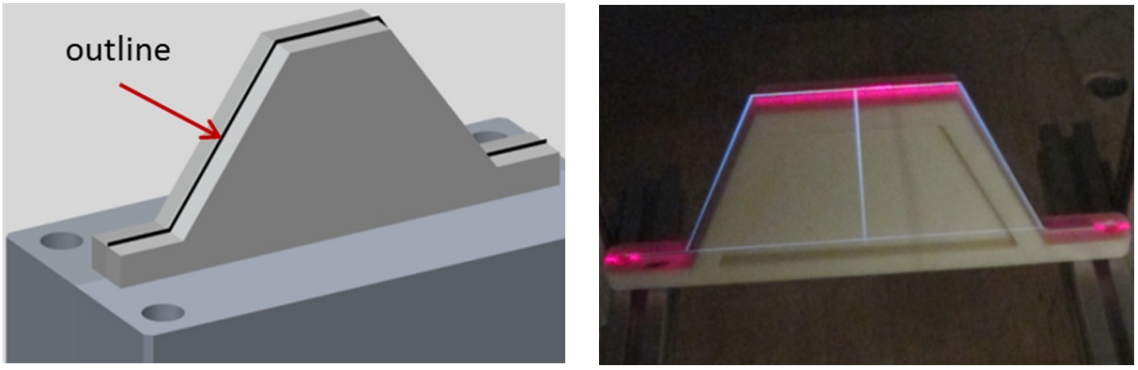

Figure 3.19: Laser plane alignment: A) Trapezoid-shaped tool with outline shown. B) Alignment of reflected 2D sketch, tool outline and laser line confirming correct alignment of laser plane with virtual plane.

1. Indirect calibration (Figure 3.20)

2. Direct calibration (Figure 3.21)

3.9.1 Indirect calibration

The indirect calibration method is similar to the conventional calibration procedure used in the earlier systems [20] [21] [22] and uses the reflective spherical marker based Polaris optical tracker system. The conceptual representation of the indirect calibration method using the Polaris system is shown in Figure 3.20. The calibration phantom proposed is similar to the laser alignment tool and is attached with 3D reflective spherical markers. Another set of spherical markers are attached upon the viewbox (monitor) for dynamic tracking of the viewbox during the procedure. The 2D outline sketch of the calibration phantom is displayed upon the monitor and the reflected image through the mirror is aligned manually with the outline of the calibration phantom. After successful alignment, the 3D reflective markers pose upon the calibration phantom (${}^{PM}T_{OT}$) and the viewbox (${}^{FM}T_{OT}$) shall be recorded with respect to the tracker coordinates using Polaris optical tracker. The transform between the virtual image overlay plane (IO) and physical marker upon the viewbox (FM) are determined by applying the following transforms:

$$ {}^{FM}T_{IO} = {}^{FM}\,T_{OT}\ {}^{OT}T_{PM}\ {}^{PM}T_{IO} $$

${}^{PM}T_{IO}$ = Identity transform obtained by manually aligning the 2D outline sketch of the virtual image overlay plane with outline upon the calibration phantom when "seen through" mirror.

3.9.2 Direct calibration

The proposed direct calibration method is a novel approach to automatically register the virtual image overlay plane to the physical reference upon the viewbox and uses MicronTracker optical tracking system with passive planar makers'. The calibration

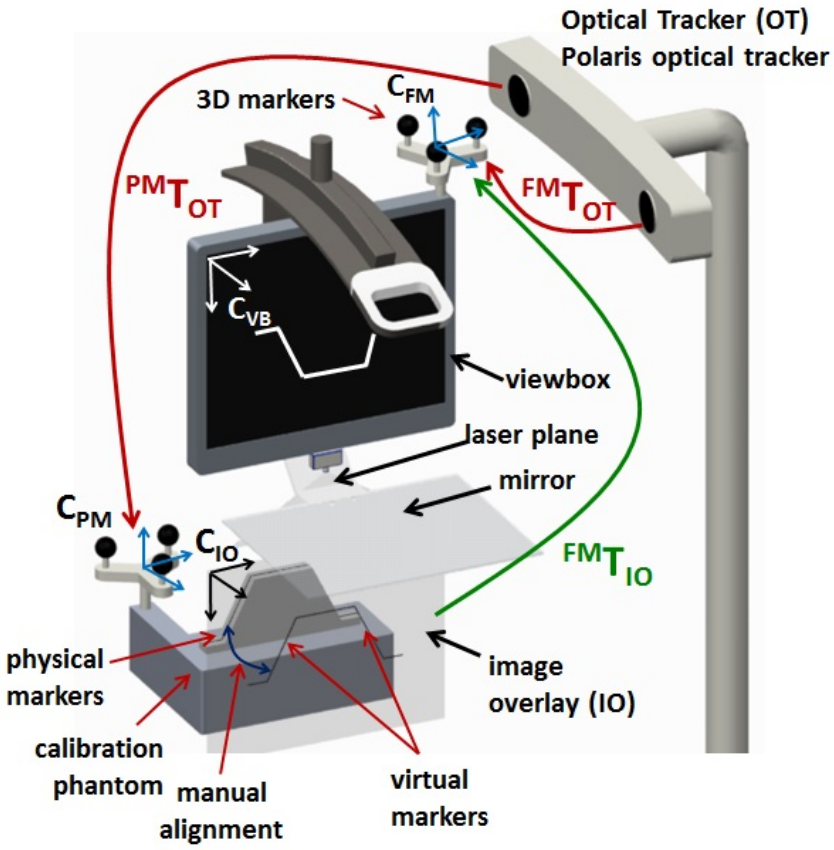

Figure 3.20: Indirect image overlay plane calibration using Polaris optical tracker system and manual alignment of virtual plane with phantom.

principle shown in Figure 3.21 is based on the ability of the tracker camera to see through the mirror and detect the marker pose displayed in the virtual plane. A set of planar markers' are displayed upon the monitor and by reflection through the mirror, the virtual markers are displayed in the image overlay plane. Another set of markers are attached upon the viewbox for dynamic tracking during the procedure. The tracker is positioned in front of the viewbox so that the virtual markers in the image overlay plane and physical markers upon the viewbox are within the field of measurement of the tracker. The virtual marker pose ($^{IO}T_{OT}$) and viewbox markers

pose ($^{FM}T_{OT}$) are recorded simultaneously. The transform between the virtual image overlay plane (IO) and the physical marker upon the viewbox (FM) are determined by applying the following transforms:

$$^{FM}T_{IO} = ^{FM}T_{OT}\ ^{OT}T_{IO}$$

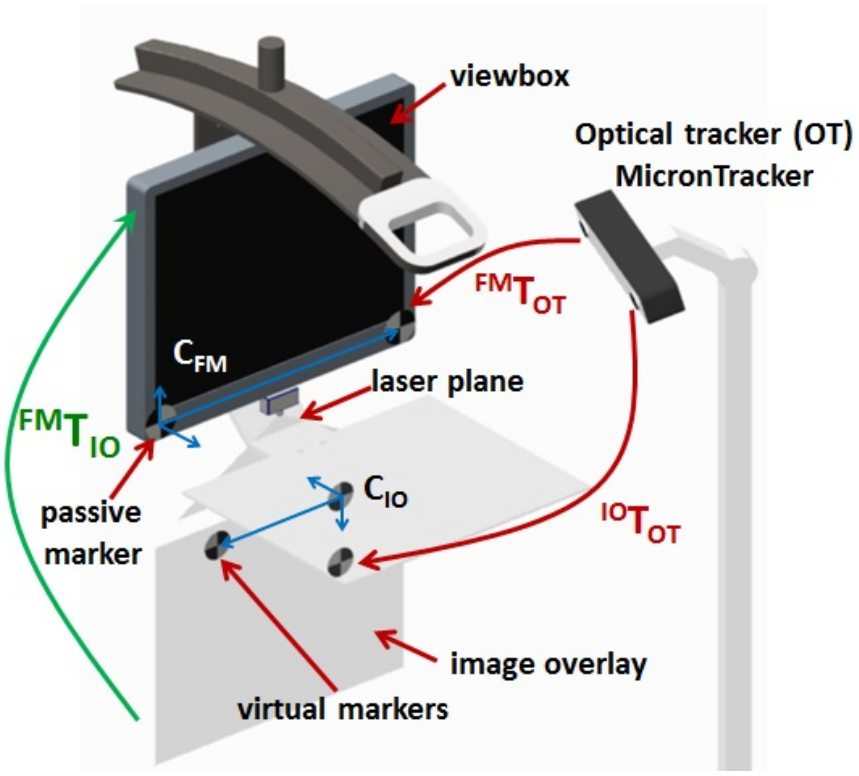

Figure 3.21: Direct automatic image overlay plane calibration using MicronTracker, the MicronTracker sees through the mirror and determines the virtual markers pose.

3.9.3 Selection of calibration method

Both MicronTracker and Polaris tracker are having similar performance; however, the decision of tracker system for the adjustable system was based upon the calibration method chosen. The comparisons between the two calibration methods are summarized in Table 3.2.

Table 3.2: Summary of comparison between direct and indirect calibration methods

Calibration Method	***Indirect calibration***	***Direct calibration***
Calibration phantom	Required	Not required
Method of calibration	Manual	Auto
Tracker system	Any tracking system	Stereo tracking system
Marker type	Tracker dependent	Passive planar markers
Effort and time	High and Tedious	Low and Simple
Effect of ambient light	No	Yes

The direct calibration method is automatic with simplified calibration steps and does not require additional calibration phantom. The indirect calibration method requires additional phantom and manual alignment of the viewbox which is a very tedious job, requires more time and effort. Direct calibration can be done away from the patient table and independent of scanner coordinates. The calibration time with direct method is expected to be lower as compared to indirect method and conventional Z-calibration methods [20]. The only limitation of direct calibration is the effect of ambient light for visibility of virtual markers by the tracker camera. Based on the comparative outcomes summarized in Table 3.2, direct calibration is

the chosen method for the adjustable image overlay system. The effect of ambient light is addressed in further sections of this chapter and later in chapter 4.

3.9.4 Implementation of auto-direct calibration

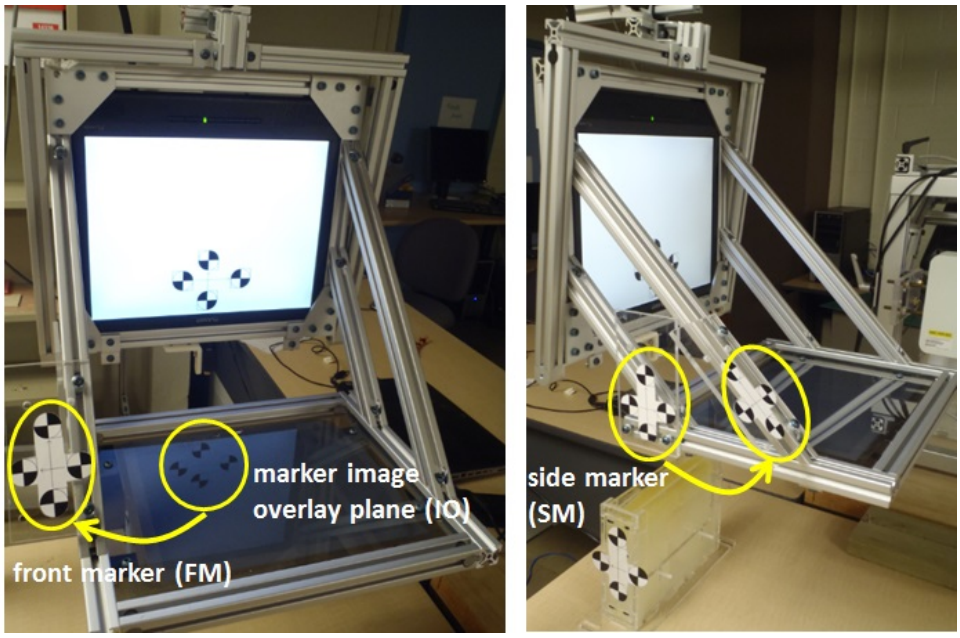

Figure 3.22: Viewbox with planar marker for image overlay calibration.

The viewbox equipped with three different markers i.e. virtual marker, front marker, and side marker for implementation of the direct calibration method is shown in Figure 3.22. The virtual marker is formed by reflection through the mirror. The side marker was required for dynamic tracking of the viewbox during the procedure as the tracker is placed towards the side of the patient and system. It was not possible to ensure both the side marker and the virtual marker within the tracker field of measurement and hence a front maker was required. The positions of all markers upon the viewbox were optimized to ensure visibility within the tracker field of measurement.

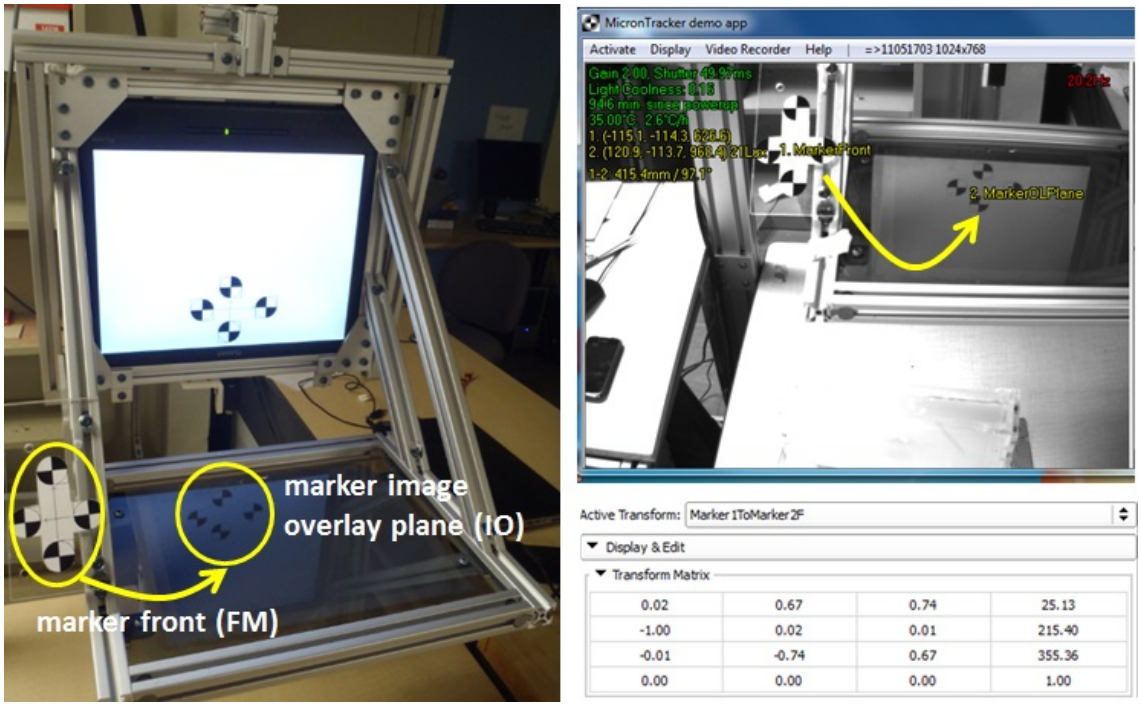

Figure 3.23: Auto-direct calibration Step 1: Left) Transform (${}^{FM}T_{IO}$) ⇒ front marker (FM) to marker image overlay plane (IO). Right-top) MicronTracker camera image indicating markers pose. Right-bottom) Transform obtained using the *"Transform recorder"* Perk Tutor module of 3D Slicer.

The image overlay plane calibration with viewbox side marker can be done in two steps, as shown in Figure 3.23 and Figure 3.24. The tracker is placed in front of viewbox so that the virtual marker and front marker are within the tracker field of measurement. Using the *"Transform Recorder"* module from the PerkTutor extension "(perktutor.org)" for 3D Slicer, the transform (${}^{FM}T_{IO}$) between the front marker (FM) to the virtual marker in image overlay plane (IO) is determined. Next, the MicronTracker is placed at the side so that both the front marker and the side marker are in the tracker field of measurement. The transform ${}^{SM}T_{FM}$ between the side marker (SM) and the front marker (FM) is determined. The transform (${}^{SM}T_{IO}$) between the side marker (SM) to the image overlay plane marker (IO) are determined

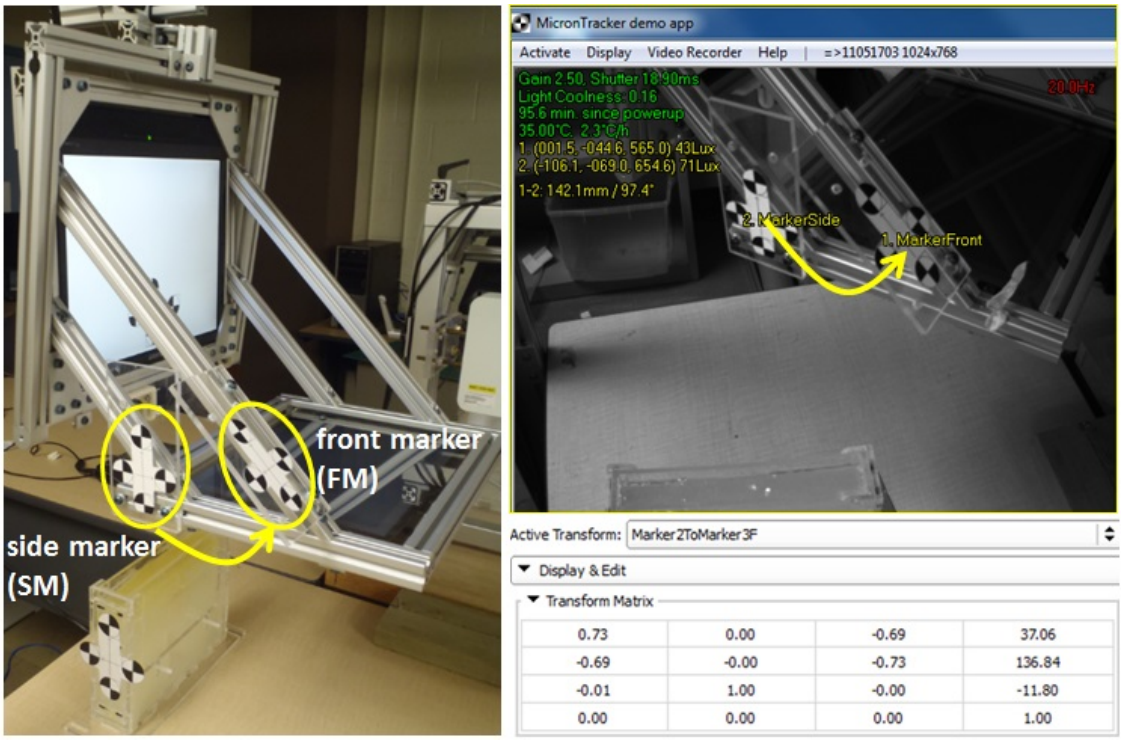

Figure 3.24: Auto-direct calibration Step 2: Left) Transform (${}^{SM}T_{FM}$) ⇒ side marker (SM) to front marker (MF). Right-top) MicronTracker camera image indicating markers' pose. Right-bottom) Transform obtained using the *"Transform recorder"* Perk Tutor module of 3D Slicer.

by applying the following transform:

$$ {}^{SM}T_{IO} = {}^{SM}\ T_{FM}\ {}^{FM}T_{IO} $$

During the procedure, the tracker is placed towards the side of viewbox so that the markers on the phantom (or patient) and side marker of the viewbox are simultaneously seen by tracker (Figure 3.25). By applying the transform (${}^{SM}T_{IO}$) to the side markers, the position of the virtual image overlay plane with respect to the phantom (or patient) is computed in real-time and image re-slicing software displays the correct image slice in the virtual plane.

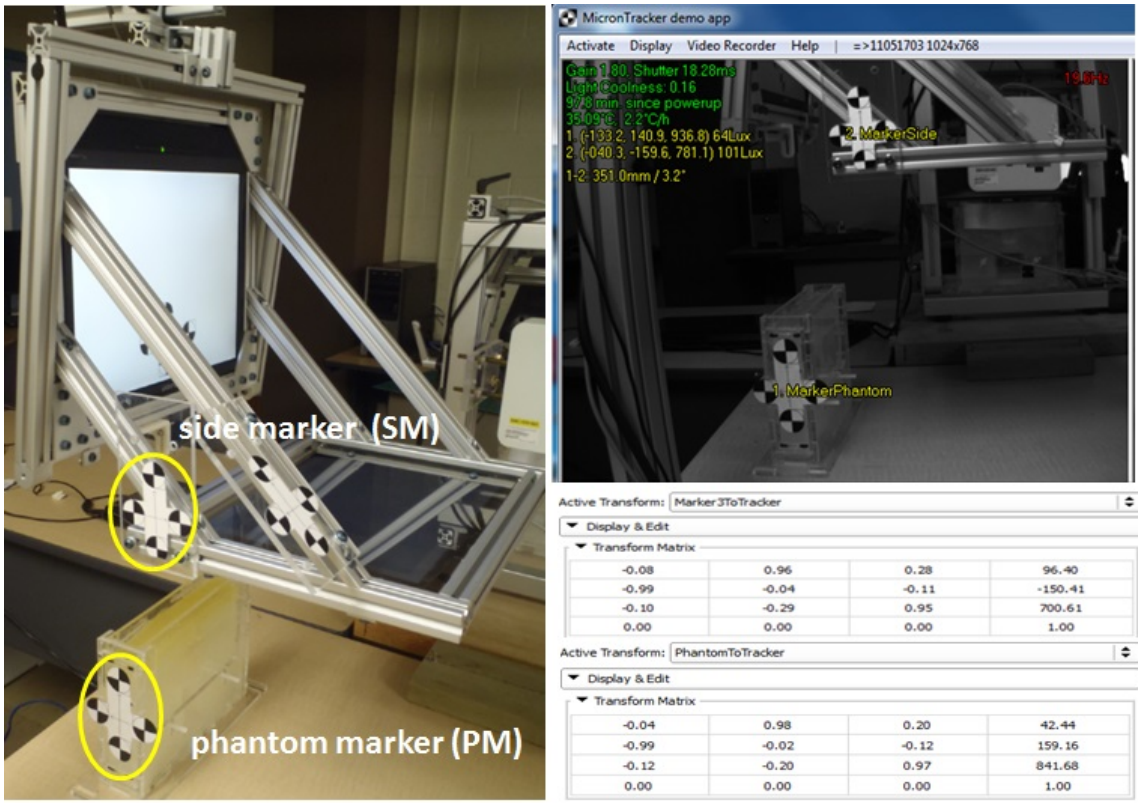

Figure 3.25: Real-time dynamic tracking of patient (phantom) and System: Left) Phantom marker and side marker upon the viewbox. Right-top) MicronTracker camera image indicating markers pose. Right-bottom) Tansform obtained using the *"Transform recorder"* Perk Tutor module of 3D Slicer.

3.10 Limitations of the adjustable system

The optical tracking system, MicronTracker, was integrated into the adjustable image overlay system to dynamically track the device and the patient during the procedure. The initial setup time was minimized by simplifying the image overlay plane calibration procedure, which is completely automatic. The viewbox was adjustable with four degrees of freedom allowing the physician to explore the image volume over the patient and thus avoiding the need for pre-planning. The counterbalanced mobile cart enabled the system to be transported in and out of the procedure room and not

consuming the useful procedure room space when not in use. The adjustable image overlay concept was not considered for further development into clinical translation due to following limitations:

- **Large mechanical structure**: As per the IEC 60601 3rd Edition standard [105] *(same applies for equivaluent FDA standard)*, the factor of safety required for suspended parts (with friction) above the patient is *12X*; the current weight of the viewbox is 8.2 kg. The articulated arm for supporting the viewbox should be designed to withstand 12 x 8.2 kg = **98.4** kg resulting in a large mechanical structure with increased product cost and complexity of mechanical design.

- **Mechanical instability**: Unwanted mechanical vibrations of the viewbox were observed when the user makes unintended contact with the system. The articulated arm length, linear bearings and pivot joints reduced system stiffness causing mechanical instability of the system.

- **Limited precise viewbox movement**: The linear bearings and pivot joints used for the current prototype limited the precise movement of viewbox; however, precise movement of viewbox can be achieved by using high precision linear bearings and pivot joints, which further increases the cost of arm development.

- **Commercial arm**: The further development of adjustable system was inhibited due to non-availability of commercially built articulated arms that could meet the system requirements. The articulated arm design was more complex and expensive as compared to viewbox; hence the economic feasibility was not justified.

- **Ambient light**: The effect of ambient light for the virtual image overlay plane calibration was anticipated during the selection of optical tracking system. The advantage of simplified auto-direct calibration with reduced calibration duration led to the choice of MicronTracker as the optical tracking system for the adjustable image overlay system. The objects below the mirror and the ambient light decreased the visibility of virtual markers in the image overlay plane for the MicronTracker camera when "seen through" the mirror, as shown in Figure 3.26 a. The ambient light effect was minimized by reducing the ambient light (dark room), and the background noise was eliminated by using plain background below the mirror (plain paper). These modifications improved the visibility of virtual markers for MicronTracker through the mirror, as shown in Figure 3.26 b; however, these solutions are not preferred for clinical trials.

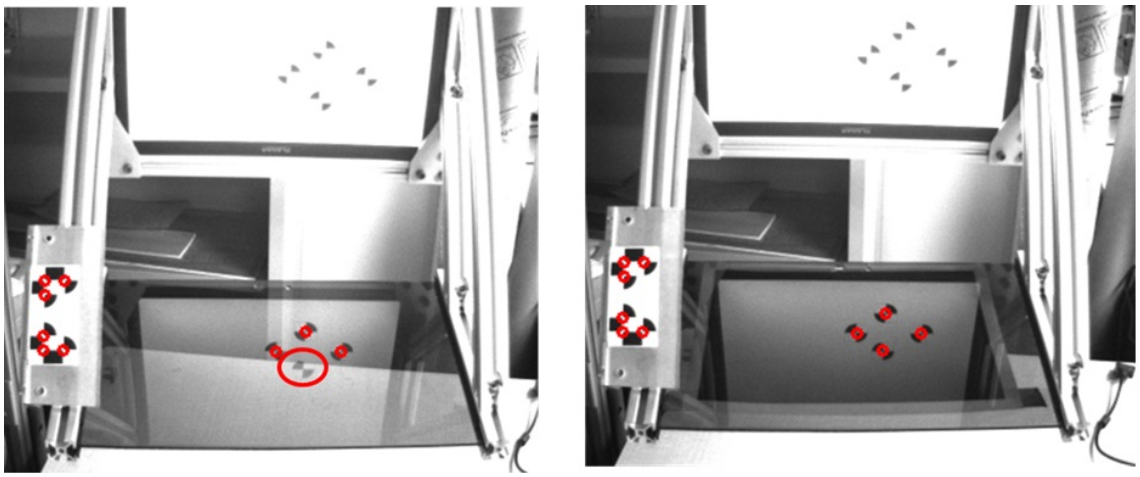

Figure 3.26: Effect of ambient light with virtual markers visibility: A) One X-point not detected under ambient light. B) All X points detected with plain background (paper) below mirror.

The mechanical instability due to vibrations and increased cost of prototype development was mainly due to suspended viewbox weight. Approximately 90% of viewbox

weight was due to display monitor and aluminium structures required to support monitor. Eliminating the need for counterbalanced articulated arm by choosing smaller and lighter displays and improving the virtual markers' visibility by choosing a beamsplitter with high Reflection/Transmission were the motivation and direction for the newly proposed mobile image overlay system presented in the next chapter.

Chapter 4

Mobile Image Overlay System

The material in this chapter is the extension of the conference paper accepted as Anand *et al. "36th Annual International Conference of the IEEE EMBS 2014"* [106], where I was the primary author and responsible for the system concept, design and development.

4.1 Motivation

The development of an adjustable image overlay system led to definition of a new 90-degree workspace configuration between display monitor and mirror, successful integration of MicronTracker for dynamic tracking of the device and patient, and definition of auto-direct calibration of the virtual image overlay plane. The limitations of the adjustable image overlay system were mechanical instability, difficulty in view-box precise movement, increased prototype development cost, and poor visibility of virtual markers in the image overlay plane.

In order to minimize the ergonomic problems of the adjustable image overlay system presented in the previous chapter, we propose a mobile image overlay system that is mobile, light weight and has smaller dimensions. In addition, we aim to improve

the image quality and dynamic tracking accuracy enabling the translation of 2D image overlay concept into clinical space. The 90-degree mirror-monitor configuration, auto-direct calibration and optical dynamic tracking using MicronTracker developed for the adjustable system are implemented for the mobile image overlay system.

4.2 System description

The design of the mobile image overlay system is aimed at reducing the viewbox weight so that the system can be hand-held by the physician and eliminate the need for a large counterbalanced, articulated arm. This is achieved primarily by replacing the 15" LCD monitor with 10.1" tablet display device. The virtual plane image quality and the tracking accuracy can be improved by choosing high brightness tablet display device and a beamsplitter mirror. The conceptual view of the proposed mobile image overlay system is shown in Figure 4.1 and the system consists of:

1. Viewbox
2. Optical tracking system
3. Host computer

The viewbox consists of a display device, mirror and laser source similar to the adjustable system. A host computer was required due to insufficient computational capacity to run image re-slicing software and non-availability of IEEE-1394a interface for an optical tracker with the tablet device. The tablet device is connected as a secondary display with the host computer through wireless network. A line type laser source similar to [21] is used to indicate the physical location of the virtual image overlay plane over the patient. The display device and the mirror are attached

together using 90-degree configuration similar to the adjustable system [104] and the virtual image formed due to reflection through the mirror is floating inside the patient at the correct 3D location. A set of planar markers are displayed in the virtual image overlay plane which is directly seen by the optical tracker for automatic self-calibration. The viewbox is equipped with a planar markers on the side to determine the pose of the image overlay plane during the entire procedure. Another set of markers are fixed upon the patient for co-registration of scanned image volume and the viewbox with respect to patient position.

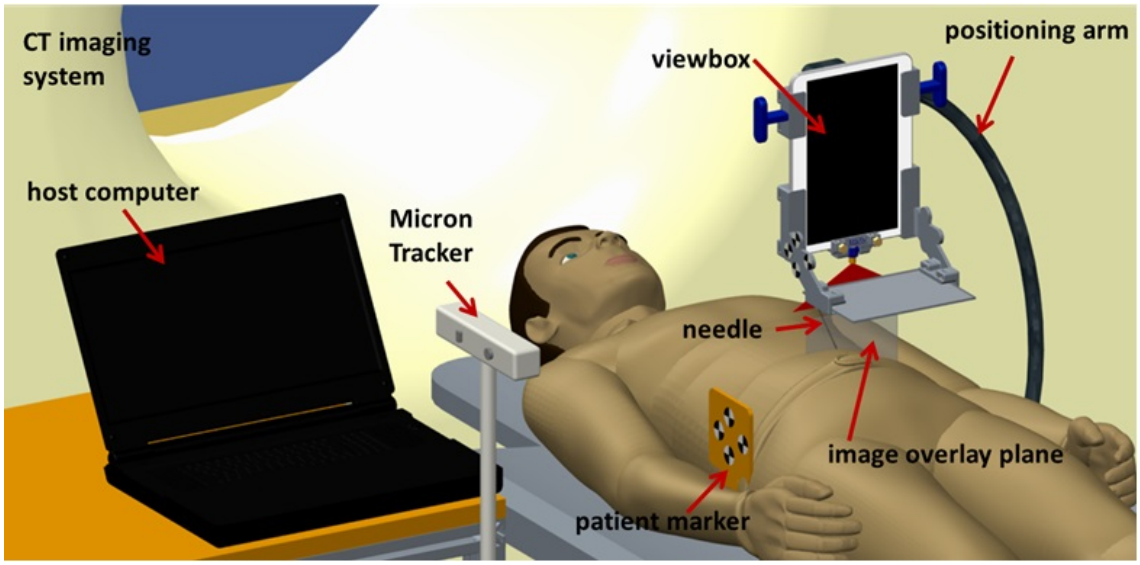

Figure 4.1: Mobile image overlay system concept with viewbox, MicronTracker and host computer in the procedure room.

The system can be possibly hand-held by the physician and used for exploration of image volume over the patient. The image re-slicing software displays the correct image in real-time corresponding to the 3D position of the virtual image overlay plane i.e. the system with respect to the patient. The system mechanical design is done using mechanical CAD tool "Creo 2.0" *(Parametric technology Corporation,*

MA USA). MicronTracker from *Claron Technology Inc. ON Canada*, is chosen for optical tracking. The tracking data is acquired by the PLUS toolkit *(plustoolkit.org)* and visualized by 3D Slicer *(slicer.org)*. The first prototype developed is shown in Figure 4.13 and the appearance of this embodiment of the viewbox resembles the Sonic Flashlight [73] developed for direct visualization of ultrasound images using real-time tomographic reflection.

The newly proposed mobile image overlay system is designed to perform as indicated without causing injury or harm to the patient or the user. Hence the mobile system shall be classified as Class II medical device as per FDA standards [107], Class IIa as per Annex IX of the Council Directive 93/42/EEC (MDD) and corresponds to Class II device as per the guidance for the Risk-based Classification System published by Health Canada. Classification of mobile image overlay system as Class II medical device does not require extensive verification and validation activities, require only the manufacturer's declaration of device safety and effectiveness. This would reduce the product development cost to a greater extent and increase the commercialization possibilities.

4.3 Driving clinical applications

The clinical applications presented in the previous chapter for the adjustable system shall continue to be the potential clinical applications for the mobile image overlay system. The specifications for the system design are derived from the targeted clinical applications. The proposed design shall support needle insertion depth up to 7 cm, oblique image overlay plane rotation of $\pm$ 35° and sufficient clearance above the patient.

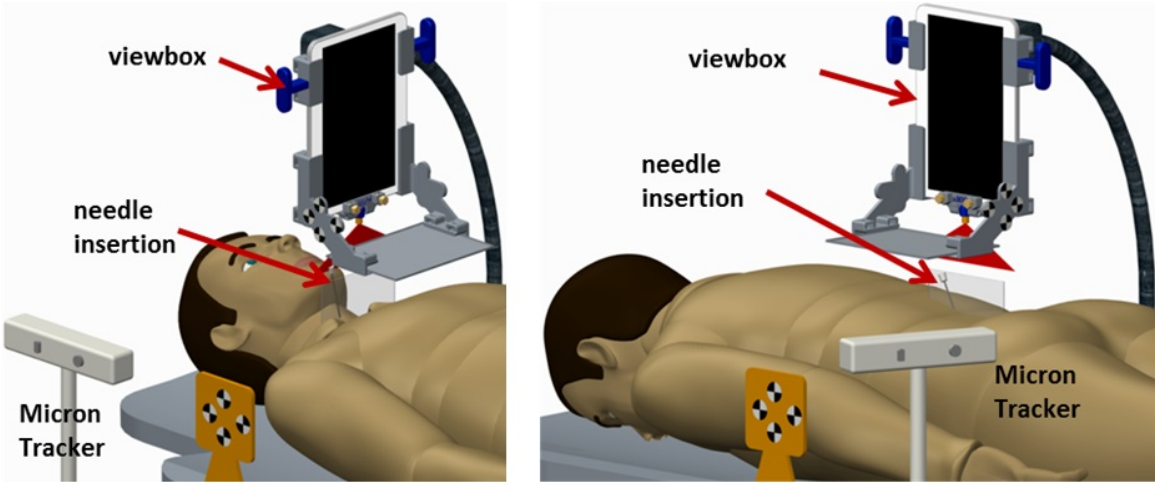

Figure 4.2: Potential clinical applications for mobile image overlay system: Left) Parathyroidectomy. Right) Percutaneous nephrolithotomy.

At each development phase, the design is verified against the requirements by simulation using CAD tool as shown in Figure 4.1 (MSK procedures) and Figure 4.2 (parathyroidectomy and percutaneous nephrolithotomy). The manikin 3D model used represents the 95^{th} percentile adult male population.

4.4 Viewbox design

The viewbox consists of a display device, mirror and laser diode similar to the adjustable system. The viewbox for the mobile image overlay system was designed with two objectives:

1. Reducing the system weight so that it can be possibly hand-held by the physician and eliminate the need for an articulated arm

2. Improve the image quality and image overlay plane calibration accuracy by choosing an appropriate display device and mirror

The image quality and accuracy of dynamic tracking of the virtual plane can be improved by increasing the brightness of the reflected image by choosing high brightness display device and high reflection mirror. In the following sections, we will discuss workspace analysis defining the optimal mirror-monitor configuration and selection of display device, mirror and laser diode.

4.4.1 Workspace analysis

As discussed in the previous chapter, the objective of workspace analysis was to define the optimal angle and the assembly dimensions between the display monitor and mirror. The spine needle injection and parathyroidectomy shall continue to be the critical procedures which define the constraints for workspace analysis. The expected outcome of this study is to define the mirror-monitor configuration satisfying the requirements mentioned in Section 3.3.

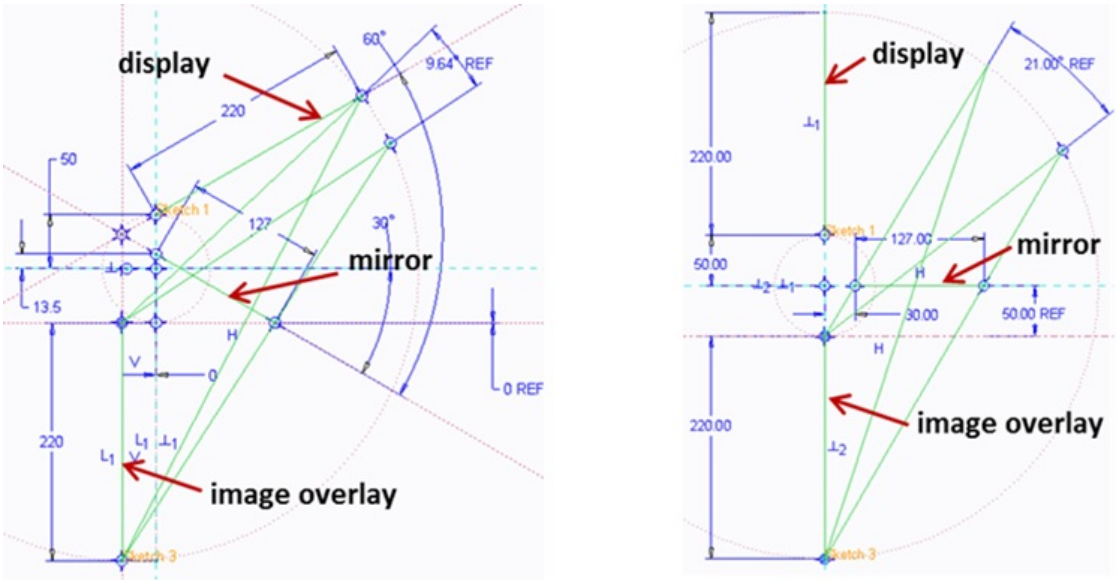

Figure 4.3: 2D sketch simulation study using "Creo 2.0" CAD tool: Left) 60-degree. Right) 90-degree.

All mirror-monitor configurations between 60-degree and 90-degree, as shown in Figure 4.4 were considered for the study. The mechanical CAD simulation for workspace analysis shown in Figure 4.3 was done with all component dimensions and constraints from relevant clinical application. The 60-degree design represents the design similar to previously proposed static image overlay system [20] [21] [22] and the 90-degree design represents the newly proposed mirror-monitor design similar to the adjustable image overlay system.

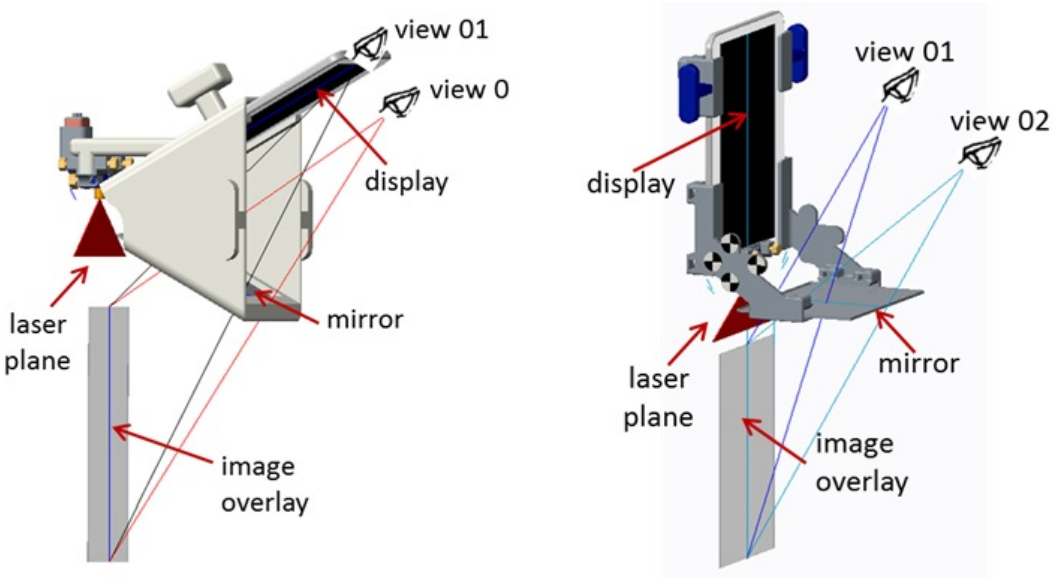

Figure 4.4: Workspace concept using the output of 2D sketch simulation study, as shown in Figure 4.3: Left) 60-degree. Right) 90-degree.

The results of the workspace analysis for the mobile image overlay system are summarized in Table 4.1; similar to the results of the adjustable image overlay system presented in Table 3.1. The study for the mobile system also reported the newly proposed 90-degree design to be optimal as compared to the previously proposed 60-degree design. The increased viewing angle of the 90-degree design gives more flexibility for the physician to work around the patient and allows more than one user

Table 4.1: Results of workspace analysis between 60-degree and 90-degree mirror-monitor configuration for mobile image overlay system

System configuration	***60-degree***	***90-degree***
Design principle	Similar to earlier system	Newly proposed design
User viewing angle	9.5 degree	21 degree
Oblique rotation	$>$ 35 degree	$>$ 35 degree
System (viewbox) weight	1.3* kg	1.0 kg

∗approximate weight of the system calculated with 3D design models created

to view the same image through the mirror simultaneously. Due to zero clearance above the patient for the 60-degree design, a compromise in depth of the image overlay plane was required to gain additional clearance. The 90-degree design has minimum clearance of 5.0 cm above the patient while still permitting the user to view the complete image overlay of depth 22 cm. Both designs were able to accommodate the needle of length 7 cm and provide oblique image overlay plane rotation of $\pm$ 35°. The viewbox (and overall system weight) for the 90-degree design (1.0 kg) was 1.3 times lighter compared to the 60-degree design (1.3 kg). Finally, the housing design of the 90-degree system was simpler and manufacturable. This opens up new possibilities for commercialization and large scale deployment of the 2D image overlay concept into clinical space.

4.4.2 Selection of display device

The display monitor was the main contributor for mechanical instability and increased cost of the adjustable image overlay system due to monitor self-weight (approx. 3.0

kg) and supporting structures (4.4 kg) for the monitor. The tablet computers were the chosen display device for the mobile image overlay system due to lighter weight and smaller dimensions. The second important parameter for choosing the display device was brightness. The reflected virtual image quality in the overlay plane depends upon the brightness of the display device. The tablet device display brightness (luminance) for several commercially devices are summarized, as shown in Figure 4.5.

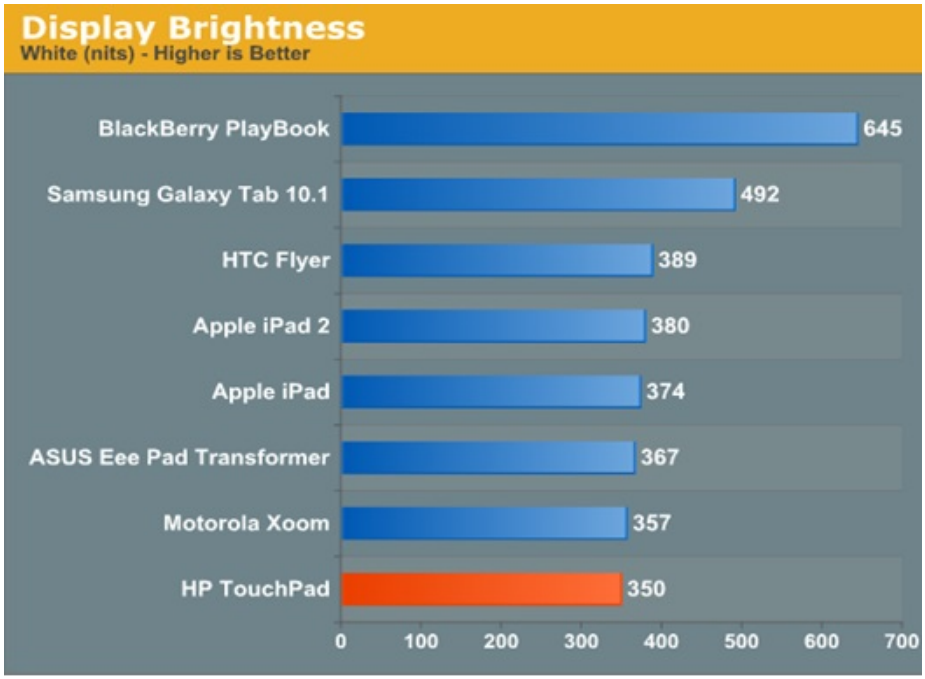

Figure 4.5: Comparison of display brightness for commercially available tablet devices *(www.anandtech.com/show/4508/hp-touchpad-review/15).*

The luminance is a photometric measure of the luminous intensity per unit area of light traveling in a given direction. It defines the amount of light that is emitted from a particular display device. The SI unit for luminance is candela per square meter ($^{cd}/_{m^2}$). The previous systems [20] [21] [22] [104] were equipped with a display monitor of luminance 250 ($^{cd}/_{m^2}$). The Playbook *(BlackBerry Inc. Canada)* has the

highest luminance value of 645 ($^{cd}/_{m^2}$), followed by Galaxy Tab 10.1 *(Samsung Inc. South Korea)* with luminance value of 492 ($^{cd}/_{m^2}$).

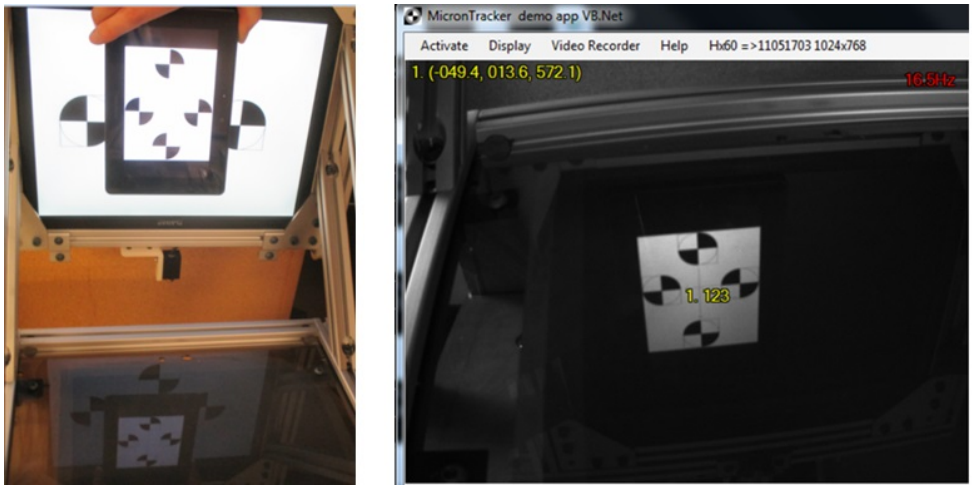

Figure 4.6: Tablet display device (Playbook) feasibility study: Left) Marker displayed upon Playbook device. Right) Pose of the virtual reflected marker determined by MicronTracker.

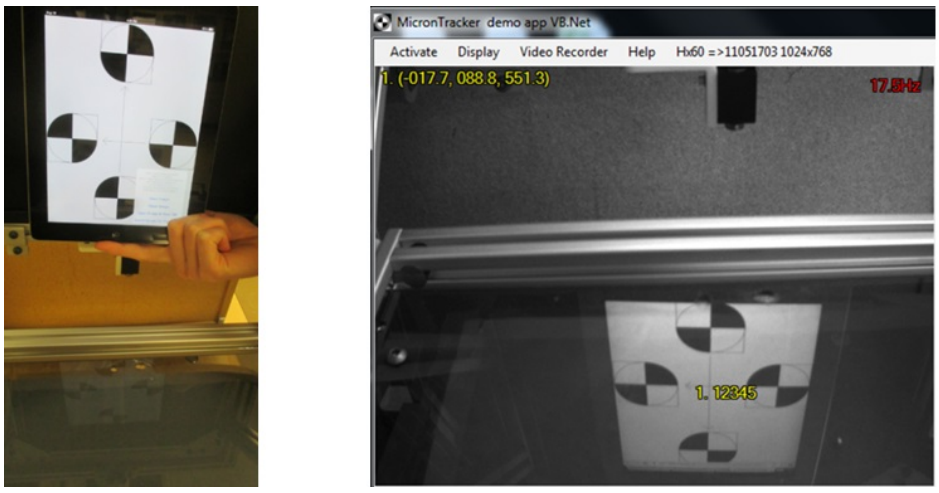

Figure 4.7: Tablet display device (iPad2) feasibility study: Left) Marker displayed upon iPad2 device. Right) Pose of the virtual reflected marker determined by MicronTracker.

The feasibility of using tablet devices for the mobile image overlay system was

demonstrated by pose measurement of virtual markers using MicronTracker. The Playbook and iPad2 *(Apple Inc. USA)* were the two tablet devices immediately available in our lab and the MicronTracker pose determination using these two devices are shown in Figure 4.6 and Figure 4.7 respectively. The brightness of the display device has a direct impact upon the virtual markers pose measurement rate by the MicronTracker. The MicronTracker pose acquisition was higher with increase in the display device brightness as summarized in Table 4.2.

Table 4.2: Summary of comparison for different display devices with respect to image overlay parameters.

Device	***Acquisition rate (poses recorded per second)***	***Display brightness*** $(^{cd}/_{m^2})$	***Device weight (kg)***	***Display Dimension (cm)***
15" LCD monitor	1	250	3	30.5 X 22.8
Playbook	10	645	0.425	9.0 X 15.3
iPad 2	8	380	0.6	14.8 X 19.7
Galaxy Tab 10.1	10	492	0.565	13.6 X 21.8

The virtual markers pose were measured for 15" LCD monitor setup under dark room (reduced visible light) conditions and tablet device (Playbook and iPad2) under normal (laboratory setup) lighting conditions. The acquisition rate using the tablet device was at least 10 times faster compared to normal 15" LCD monitor.The mirror used for the LCD monitor, Playbook, and iPad2 was a polycarbonate semi-tranparent mirror and for the Galaxy Tab 10.1 was a beamsplitter.

The tablet devices in general were lighter by 5 to 6 times and pose measurement rate was at least 10 times higher as compared to the LCD monitor thus indicating the improved image quality in the reflected virtual image overlay plane. The Samsung Galaxy Tab 10.1 (Figure 4.13) was the chosen display device for the mobile image overlay system due to its 10.1" display size, Android platform and discontinued service for Playbook. The Android platform would be the preferred choice due to few commercially available Apps to use the tablet device as the secondary display device for the host computer. The display height of Galaxy Tab 10.1 is similar (21.8 cm) compared to the 15" LCD monitor (22.8 cm) and hence there was no compromise in the depth of virtual image overlay plane. The tablet display width is 2.3 times smaller than the LCD monitor. The reduced display width has no impact as the mobile system can be moved along the transverse plane to view the complete image slice over the patient. Further validation should be done by actual clinical trials. The ambient light has minimal effect upon the virtual image quality as pose measurements were done under normal lighting conditions for tablet devices, unlike dark room conditions required for the LCD monitor.

4.4.3 The host computer and *iDisplay* software.

A host computer was required due to insufficient computational capacity to run image re-slicing software (3D Slicer) and non-availability of IEEE-1394a interface for MicronTracker with the tablet device. The tablet device shall be used as a secondary display device for the host computer using a software solution through wireless connection. Several commercially available Android apps (iDisplay, AirDisplay and TeamViewer) were evaluated to support the tablet device as secondary display device and iDisplay *(Shape Inc. Germany)*, with a better image update rate, was the chosen solution. The scanned image volume shall be loaded into image re-slicing software on the host computer and the re-sliced image is displayed upon the tablet device through the iDisplay App wirelessly.

4.4.4 Selection of mirror

The 2D image overlay concept works mainly due to partial reflection/transmission property of semi-transparent mirrors. The users can simultaneously see the reflected image of the computer screen and see through the object below the mirror. The previous systems [20] [21] [22] [104] used a semi-transparent mirror made of polycarbonate sheet with transparent thin film coating of aluminium on one side, which allows a percentage of reflected light to pass through while reflecting the reminder. There is no evident literature available to support the reflection capability of the polycarbonate semi-polished mirror; however, the aluminium film coating results in a dark grey colored mirror, as shown in Figure 4.7 a and reduces the transparency. The brightness of the virtual image displayed in the image overlay plane depends upon the display device luminance and percentage reflection of the mirror. The reduced transparency

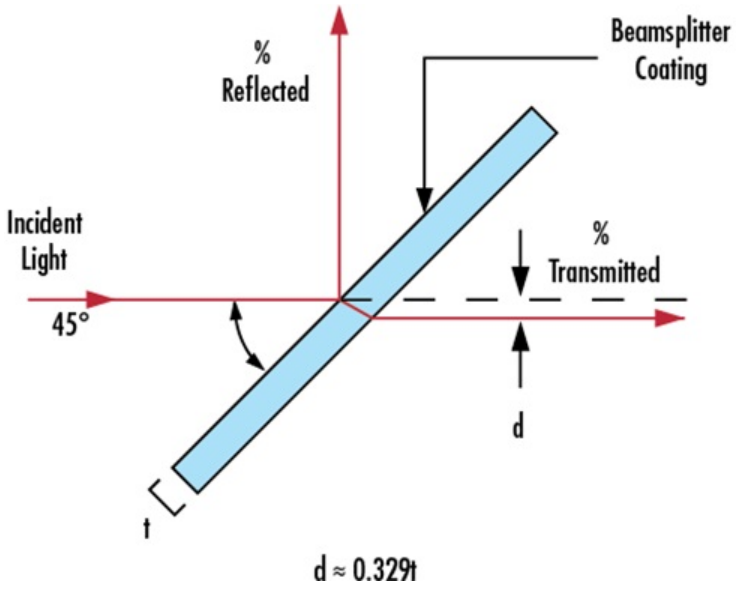

Figure 4.8: Beamsplitter working principle *(Edmund Optics Inc. USA)*. The incident light upon the mirror is partially reflected and partially transmitted through the mirror.

decreases the reflected image quality, affecting the virtual marker pose measurement precision.

Table 4.3: Image acquisition rate comparison between semi-transparent mirror and beamsplitter using Galaxy Tab.

Mirror type used	***Acquisition rate (poses recorded per second)***
Acrylic semi-transparent mirror	10
Beamsplitter (75/25 R/T)	20

In order to improve the reflected image quality and see through transparency, a beamsplitter was used for the mobile image overlay system. Beamsplitters are

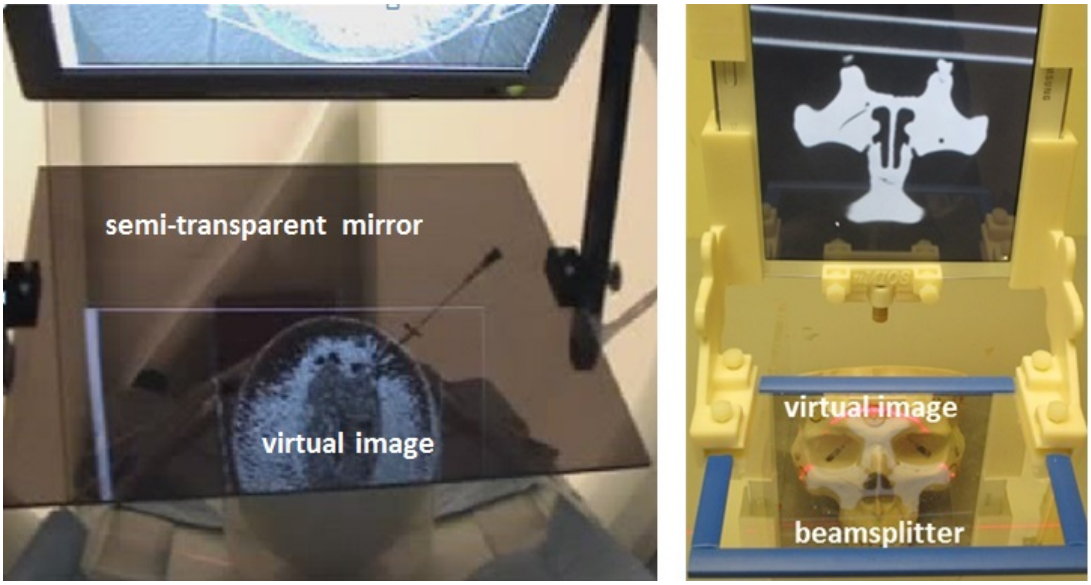

Figure 4.9: Reflected virtual image and the see through object below the mirror: Left) Polycarbonate semi-transparent mirror with poor visibility of the reflected image and the object [20]. Right) Beamsplitter of R/T = 75/25 with clear view of the object and improved virtual image quality

optical components used to split incident light at a designated ratio into two separate beams (reflected and transmitted), as shown in Figure 4.8. Beamsplitter consists of a thin, flat glass plate with substrate coating on one side and anti-reflection coating on the other side. The beamsplitter mirror is almost transparent as seen in Figure 4.9 b, unlike the dark grey color of the polycarbonate semi-transparent mirror. A beamsplitter with highest Reflection/Transmission ratio (75/25) was used for the mobile image overlay system. The benefits of using a beamsplitter are high reflection capability and a clear see through image which is clearly demonstrated by a pose measurement rate twice as high as the polycarbonate semi-transparent mirror as summarized in Table 4.3.

4.4.5 Selection of laser diode

The physical location of the virtual image overlay plane over the patient is indicated by a laser line upon the patient. The laser line (plane) aids the physician in locating the needle entry point upon the patient and aligning the needle along the virtual image overlay plane. The laser line should be visible under procedure room light conditions (boom lights). The previous systems [20] [21] [22] [104] were equipped with a 650nm red line type laser diode of power output 1mW which satisfies FDA class II category [108] and is considered to be safe for human eye; however, poor visibility under the normal (procedure room) lighting conditions were reported by our research group with the previous systems [20] [21] [22].

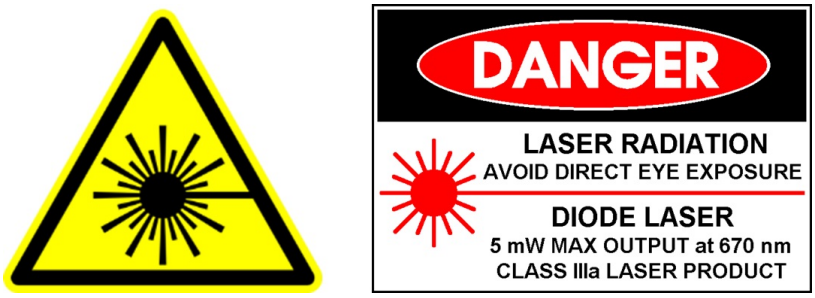

Figure 4.10: "Caution" labels for products using class IIIa laser diodes: A) Label placed closer to laser diode and visible to the user. B) Label placed on the product and visible to user

Further understanding of FDA standards related to laser devices used in medical devices (laser diodes of power output up to 5mW) falls under class IIIa [108] and can be used without additional verification requirements. The class IIIa represent the safe operating limits without causing injury to the human eye if handled carefully. The medical devices using class IIIa laser diodes shall have *"Caution"* labels, as shown in Figure 4.10 to comply with FDA standard requirements. Hence, a 5mW output

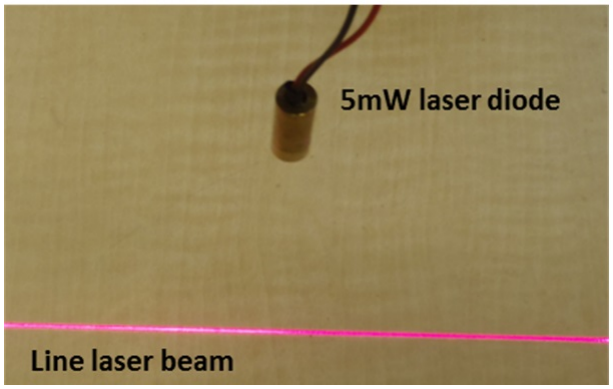

Figure 4.11: Laser diode *(ER56L 650nm 5mW Red Laser Line Diode 9x22 mm, Laser Guy Inc. USA)* used for the mobile image overlay system.

source laser diode *(Laser Guy Inc. USA)* shown in Figure 4.11 which satisfies the requirements of FDA class IIIa was chosen.

4.4.6 Design and development of a viewbox

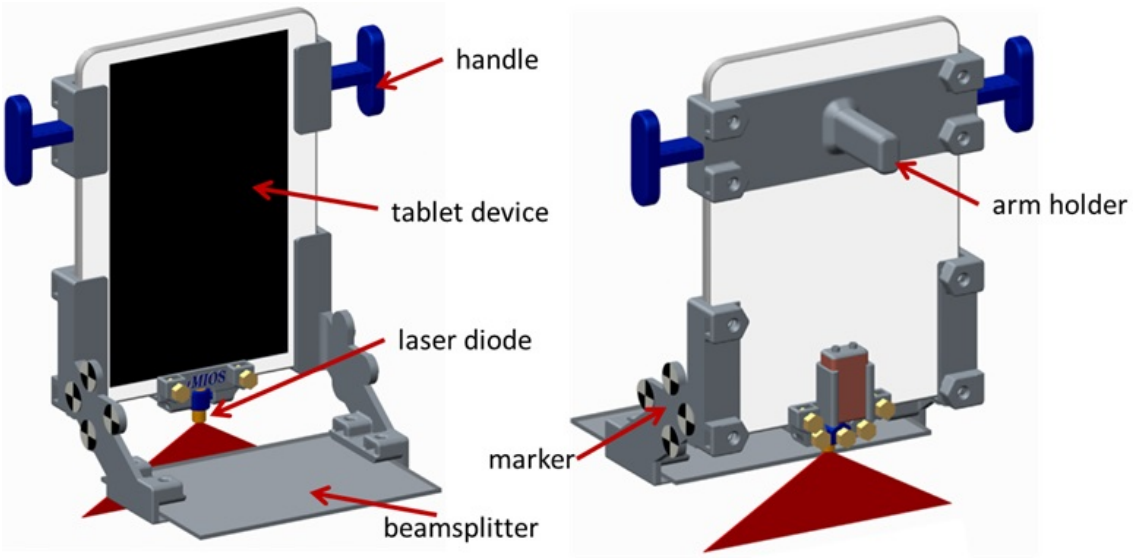

Figure 4.12: Viewbox design with 90-degree workspace configuration, tablet display device, and beamsplitter mirror. Markers attached on each side for dynamic tracking during the procedure. Right). Front view and Left). Back view

The detailed engineering design for the mobile image overlay system based on the results of workspace analysis and components selection is shown in Figure 4.12. The 90-degree viewbox design was the optimal solution, Samsung Galaxy Tab 10.1, 75/25 (R/T) beamsplitter and 5mW power output laser diode were the chosen display device, mirror and laser source for the newly proposed system respectively. The first prototype developed is shown in Figure 4.13. The display device and the mirror are attached together with the 3D-printed brackets. All mechanical dimensions between the display device and mirror were derived from the workspace analysis. A 3D-printed handle attached to the display device is used for holding the system by hand for exploration over the patient. The arm holder allows the device to be fixed over the patient during needle insertion using a positioning arm. All parts are held together using M6 (metric) plastic fasteners. A set of planar markers are attached on each side for dynamic optical tracking of the viewbox during the procedure.

The laser diode is attached to the display device using a custom designed laser mount, as shown in Figure 4.14. The laser mount provides three degrees of freedom to aid laser plane alignment with the virtual image overlay plane. The laser diode is attached to the display device using laser mount and M6 plastic fasteners. The laser mount (updated new design) also supports a battery power source (9V alkaline battery) along with a switch to operate the laser diode. Powering the laser source using a battery was required to ensure the viewbox was free from wires and enabling the physician to freely move the device over the patient.

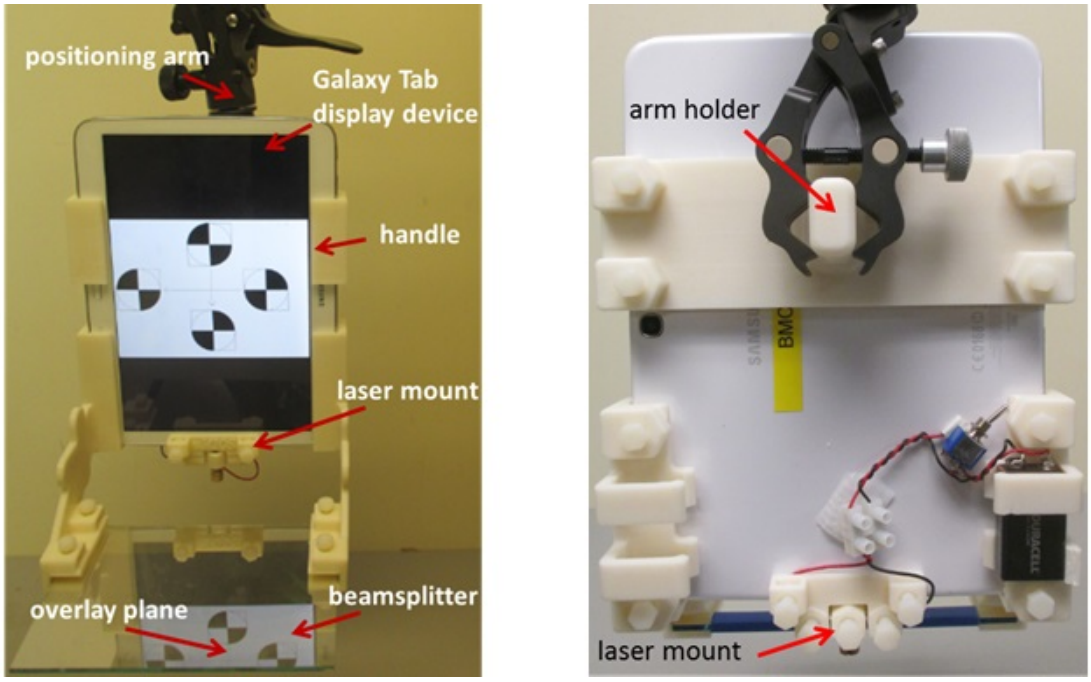

Figure 4.13: Viewbox of the mobile image overlay system first prototype developed for the Samsung Galaxy Tab 10.1 and beamsplitter. The first version of laser mount design can be seen in the prototype with the battery and switch attached to the housing.

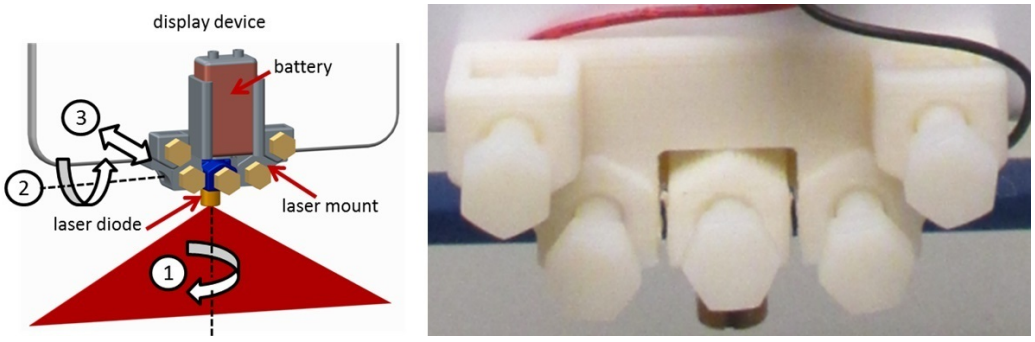

Figure 4.14: Laser mount to support laser diode with three degrees of freedom attached upon the viewbox: Left) Design. Right) Prototype developed.

4.5 MicronTracker

The direct calibration method developed for the previous adjustable system [104] was adopted for the newly proposed mobile image overlay system. MicronTracker was the

chosen optical tracking device for dynamic tracking of the patient and the viewbox. MicronTracker is an optical pose tracking device used for real-time (10Hz or faster) tracking of specially marked objects in the camera field of measurement and reports the pose (location and orientation) of each detected object. It is fully passive and uses visible light illumination to detect the targets stereoscopically. It is simpler, more reliable, low-cost, light weight, use printable markers and can practically track an unlimited number of makers (objects) concurrently. *The material in this section is referenced from the MicronTracker developer's manual MTC 3.6* [26].

Working Principle

MicronTracker consists of two (or three) stereo cameras (left and right) to detect and correlate visual patterns of markers matching the predefined marker templates in the database. Once the marker template is identified in the images, the exact 3D position of its target points are calculated by triangulating the two projection lines associated with the two image positions in which the target center is observed (see Figure 4.15).

Marker design

A marker consists of one or more rigid facets and each facet consist of two vectors (one vector is longer than the other) on a rigid configuration. A vector is formed between two Xpoints arranged so that one's BW Xline is aligned (co-linear) with the other's WB Xline. An Xpoint is formed at the intersection of the painted flat surface as show in Figure 4.15. From the possible list of markers, the chosen marker design for the mobile image overlay system is shown in Figure 4.16. These markers consist of two facets perpendicular to each other and are more suitable for reporting accurate orientation of the planar objects. At-least five different markers

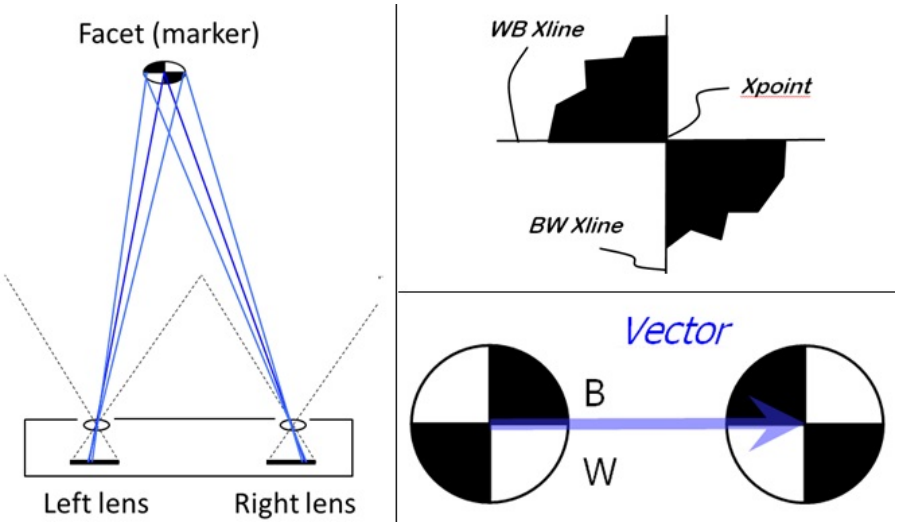

Figure 4.15: MicronTracker working principle [26]: *Starting from left* A) 3D position of the marker determined using triangulation principle. B) Xpoint formation. C) Vector formation between two facets.

were required for the mobile image overlay system, and the variants of the chosen design are achieved by varying the distance between Xpoints (i.e. vector length).

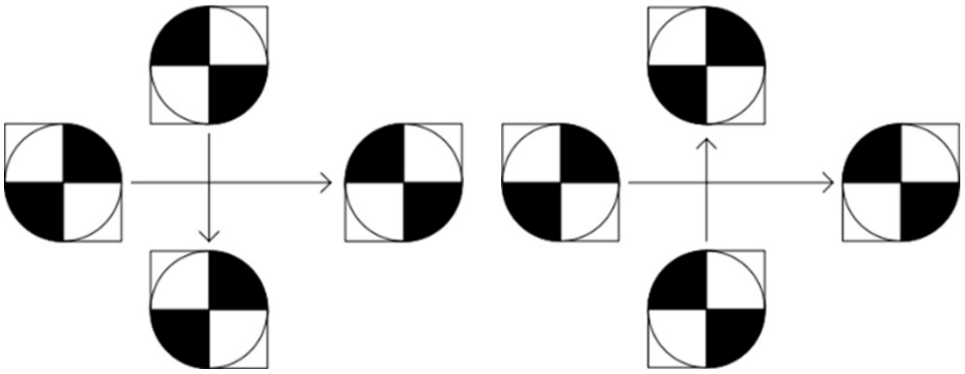

Figure 4.16: Marker templates (design) with four facets (and different orientations) used for mobile image overlay system.

Registering new multi-facet marker templates

The newly designed multi-facet marker is placed in the tracker field of measurement (Figure 4.17 a). Using the template creation module of the MicronTracker

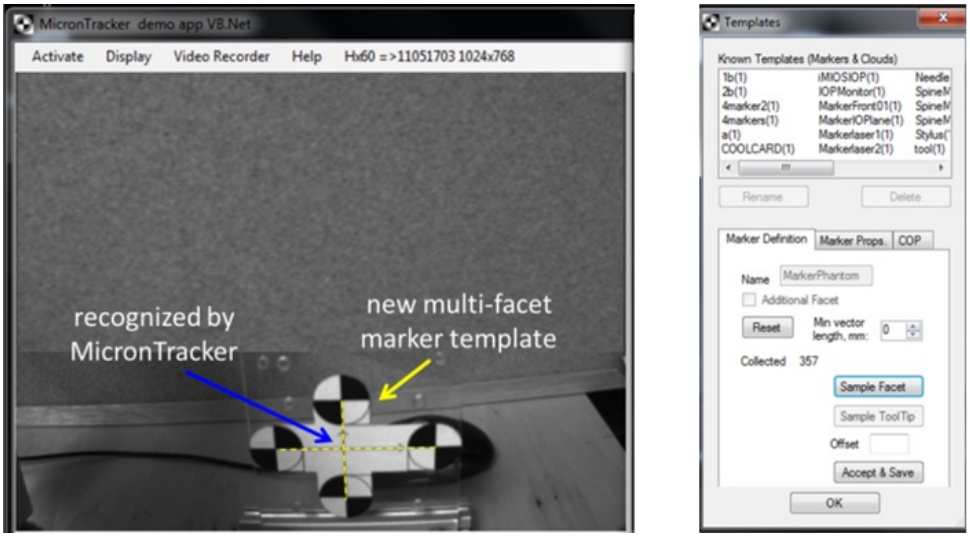

Figure 4.17: Multi-facet marker template registration: A) New marker recognized by MicronTracker. B) Template creation module of the software to collect pose and register new marker.

software (Figure 4.17 b), a minimum of 300 facet samplings are recorded and the software automatically creates a new marker template in the database.

4.6 3D Slicer image overlay module

Image re-slicing software is required to display the correct image slice into the virtual image overlay plane depending on the position of the device tracked with respect to the patient. This image overlay software is developed as a module of 3D Slicer which is an open source image processing tool that provides image registration, image processing, an interface with external devices (ex. MicronTracker) for image guidance support, and volume rendering. The image overlay module projects the re-sliced image upon the secondary tablet display and creates needle insertion path based on the needle entry and target point defined by the physician. The software architecture developed for the mobile image overlay system is shown in Figure 4.18. The scanned

image volume (raw scan data) is processed by threshold based image segmentation using 3D Slicer visualization software and and an appropriately rendered 3D model is created for visualization purpose. Through the *OpenIGTLink* and *PLUS* toolkit, 3D Slicer communicates with MicronTracker and pose details of the tracked objects are obtained. The *Volume Reslice Driver* module re-slices the image volume depending upon the pose information obtained from the MicronTracker and re-sliced image is projected onto the tablet display device through the image overlay module and iDisplay software wirelessly.

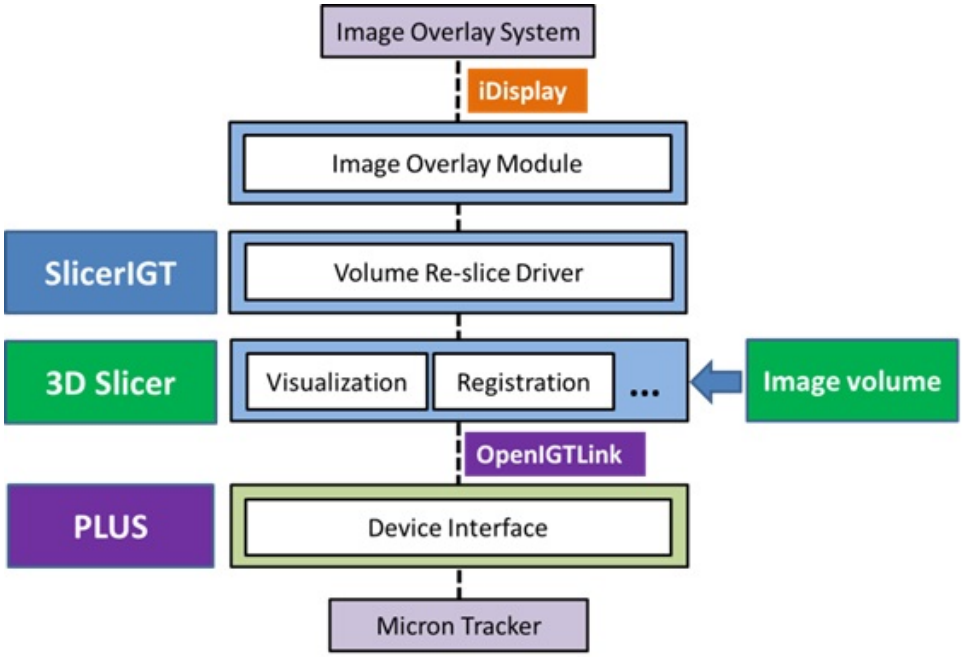

Figure 4.18: Software architecture for the image overlay using 3D Slicer, PLUS and Slicer IGT. MicronTracker and image overlay system are the hardwares.

During the procedure, the image overlay device is used to browse the image volume over the patient. Depending upon the device position with respect to patient the software projects the right image slice onto tablet display device and by reflection the virtual image appears inside the patient at the correct 3D location. After locating the

target inside the patient body, the target and entry point are marked by the physician using the image overlay module. Then, the virtual needle insertion path along with the needle length is displayed over the re-sliced image and can be seen in the virtual image overlay plane (Figure 4.19).

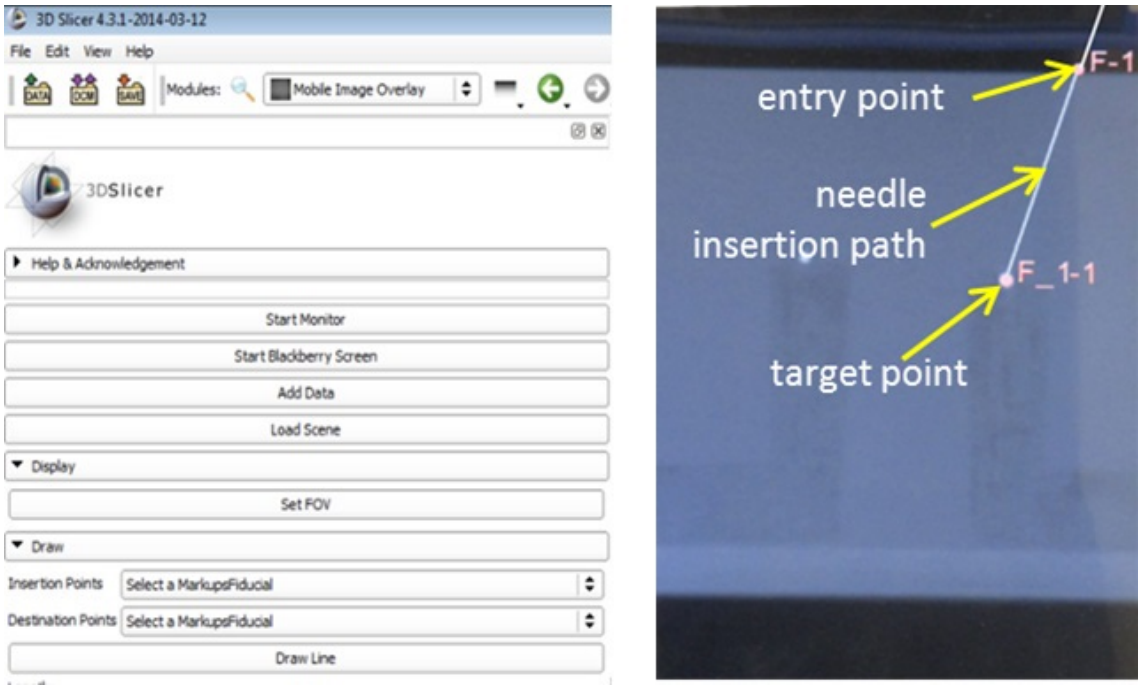

Figure 4.19: 3D Slicer image overlay module: Left) User interface. Right) Needle insertion path created by the software with entry and target point defined by physician.

4.7 Image overlay calibration method

The auto-direct calibration method using MicronTracker implemented for the previous adjustable image overlay system was adopted for the proposed image overlay system. The viewbox consists of three different markers (i.e the virtual marker, front marker, and side marker) for implementation of the direct calibration method as

shown in Figure 4.20. The virtual marker in the overlay plane was formed by reflection of the marker displayed in the tablet device. The side marker is required for dynamic tracking of the viewbox during the procedure as the tracker is placed towards the side of the patient and system. It was not possible to ensure both side marker and virtual marker were within the tracker field of measurement and hence a temporary front maker was required. The positions of all markers upon the viewbox were optimized to ensure visibility within the tracker field of measurement. The marker displayed in the virtual image overlay plane is directly seen by the MicronTracker through the beamsplitter mirror. The transform between the two markers are calculated by the average of 300 transforms recorded using *"Transform Recorder"* module from PerkTutor extension of 3D Slicer.

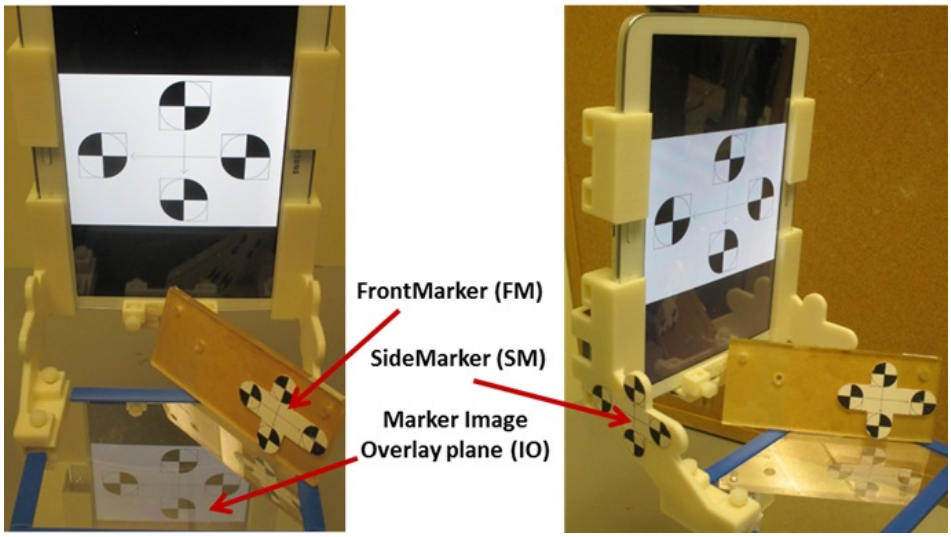

Figure 4.20: Planar markers attached upon the viewbox for auto-direct image overlay calibration.

The image overlay plane calibration with the viewbox side marker can be done in two steps, as shown in Figure **??** and Figure **??**. The tracker is placed in front of the viewbox so that the virtual marker and the front marker are within the tracker

field of measurement. Using the *"Transform Recorder"* module from the PerkTutor extension for 3D Slicer, the transform ${}^{FM}T_{IO}$ between the front marker (FM) and the virtual marker in the image overlay plane (IO) is determined. Next the MicronTracker is placed at the side so that both the front marker and the side marker are in the tracker field of measurement and the transform (${}^{SM}T_{FM}$) between the side marker (SM) and the front marker (FM) can be determined. The transform (${}^{SM}T_{IO}$) between the side marker (SM) to image overlay plane marker (IO) is determined by applying the following transform:

correct image slice in the virtual image overlay plane. 4.8 Laser plane alignment method

The laser plane alignment method using the trapezoid shaped tool as discussed in the previous chapter requires the user to manually align the 2D outline in virtual plane when "seen through" the mirror with the outline of the trapezoid tool. Our experience with the previous alignment was tedious as it requires the user to simultaneously view the virtual 2D outline through mirror and the alignment requires tool movement in all directions. Particularly, it was not easy to make the decision if the trapezoid tool should be adjusted vertically or horizontally to align with the virtual 2D outline.

We propose an optical tracker aided laser alignment method to eliminate the need for a virtual 2D outline and seeing though the mirror during alignment. The proposed method uses a 3D-printed trapezoid tool, MicronTracker, and 3D Slicer visualization module. The virtual plane and the center plane of the trapezoid tool are tracked in real-time by MicronTracker and visualized by rendering in 3D Slicer (Figure 4.24).

The alignment tool consists of two markers, A and B, attached perpendicular to each other as shown in Figure 4.24, and the transform ${}^{LA}T_{LB}$ between the markers

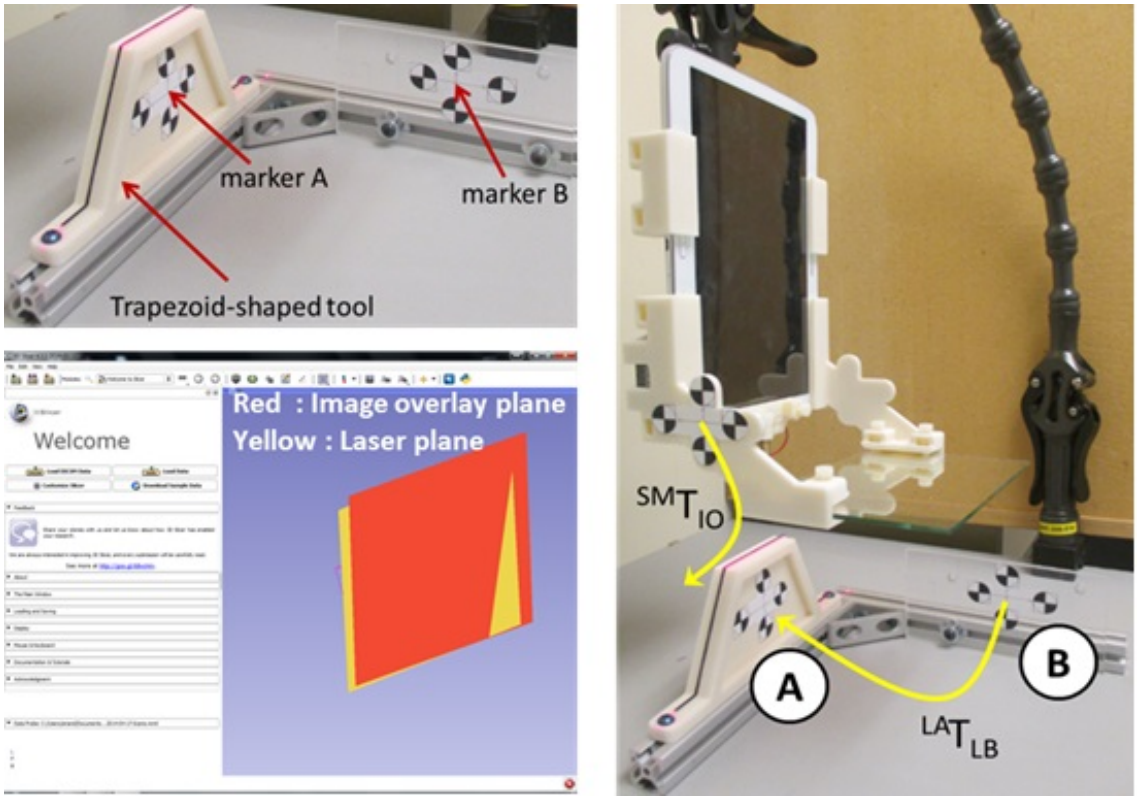

Figure 4.24: Tracker aided laser plane alignment: *Starting from right* A) Tool with two markers (A and B). B) Rendering of overlay plane and laser plane in 3D Slicer for visualization. C) Laser plane aligned with virtual plane using the alignment tool, 3D Slicer software and MicronTracker.

is predetermined. Marker A consists of a trapezoid shaped 3D printed part with a dark outline at the center representing the laser plane rendered in the image re-slicing software and it is continuously tracked by the MicronTracker through Marker B and applying the transform ${}^{LA}T_{LB}$. The dynamic pose of the virtual image overlay plane with respect to the viewbox side markers is determined by continuous tracking of the side marker (SM) by MicronTracker and applying the transform (${}^{SM}T_{IO}$) determined previously during the image overlay calibration. The laser plane is aligned with the virtual image overlay plane in two steps:

1. Manually align the viewbox until the image overlay plane aligns with the laser plane in the 3D Slicer screen (Figure 4.24)

2. Adjust only the laser mount until the laser line cuts through the center dark line upon the alignment tool indicating the position of marker A.

The real-time tracking and rendering in 3D Slicer provided visual guidance for the user to adjust the alignment tool center plane with the virtual image overlay plane. The newly proposed method was simpler and entire alignment procedure was completed in less than 10 minutes.

4.9 Phantom design

The accuracy of the proposed mobile image overlay system shall be validated by performing image-guided needle insertion with a custom designed validation phantom. The conceptual design of the validation phantom is shown in Figure 4.25 and is made of an acrylic box consisting of four sets of 3D-printed blocks. Each block is set at different height and consists of four pillars.

Two different types of fiducial markers shown in Figure 4.26 are used for validation phantom design. Fiducials markers are objects that appear bright and consistent in the scanned image volume used for localization and navigation in computer-assisted interventions. CT-Spot fiducials *(Beekley Corporation, USA)* are placed upon each pillar and seven PinPoint multi-modality fiducials *(Beekley Corporation, USA)* are placed upon the top surface of phantom side walls. The PinPoint fiducials are conical in shape with center hole of 1.27 mm diameter and generally used for image volume registration with the physical object (phantom or patient). The CT-Spot fiducials are spherical in shape with diameter 2 mm and used as target points for needle insertion.

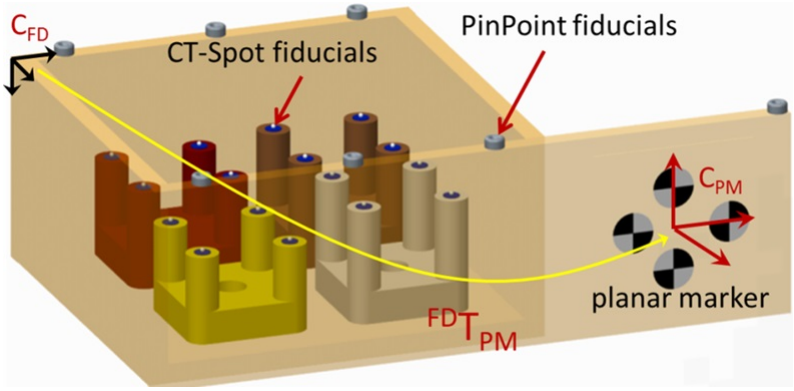

Figure 4.25: Validation phantom conceptual design with passive planar markers; PinPoint fiducials upon the acrylic sheets and CT-Spot fiducials upon 3D printed pillars.

A planar marker is used for continuous tracking of the phantom with respect to the image overlay plane by the MicronTracker. The acrylic box is filled with tissue mimicking gel made of agar and gelatin. The phantom prototype developed is shown in Figure 4.27 and CT scanned for ground truth.

Figure 4.26: Fiducials markers: Left) CT-Spot fiducials used as target points for needle insertion. Right) PinPoint fiducials for phantom image volume registration, *(Beekley Corporation, USA)*.

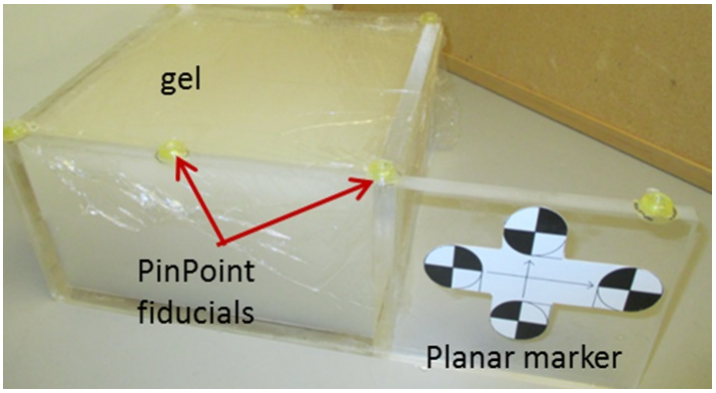

Figure 4.27: System accuracy validation phantom: Prototype developed with tissue mimicking gel. PinPoint fidcuials and planar marker can be seen.

4.10 Stylus tip design

The phantom (or patient) and the scanned image volume are registered together using fiducial registration. The locations of the fiducial points upon the phantom are determined by probing the PinPoint fiducials using custom designed stylus continuously tracked by MicronTracker. The 3D-printed stylus prototype with the stainless steel tip is shown in Figure 4.28 a, and the design is similar to the commercially available tool probe, as shown in Figure 4.28 b. Two sets of marker facets are attached upon the stylus for real-time tracking of the stylus tip. The stylus tip is calibrated to the marker coordinates using the TTBlock (for Tool-Tip calibration block) available as part of the MicronTracker SDK toolkit.

Stylus Tip calibration

The stylus tip is placed at the center of TTBlock and oriented perpendicular to the TTBlock surface, as shown in Figure 4.29. The center of the TTBlock marker is predetermined by the manufacturer. The MicronTracker is positioned so that the markers upon the stylus and TTBlock are in tracker's field of measurement.

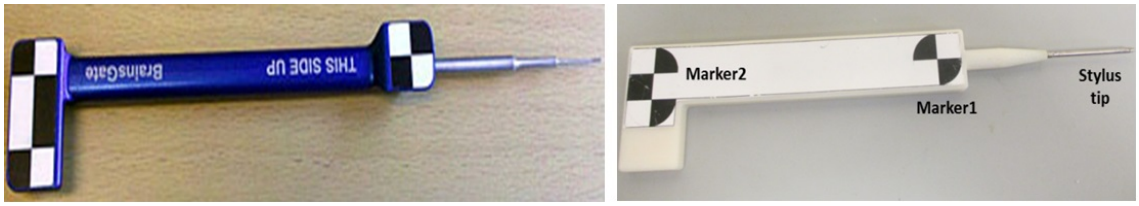

Figure 4.28: Tracked stylus: A) Commercially available tool probe *(Claron Technology Inc.)*. B) custom-designed 3D-printed stylus with design and markers similar to commerial probe.

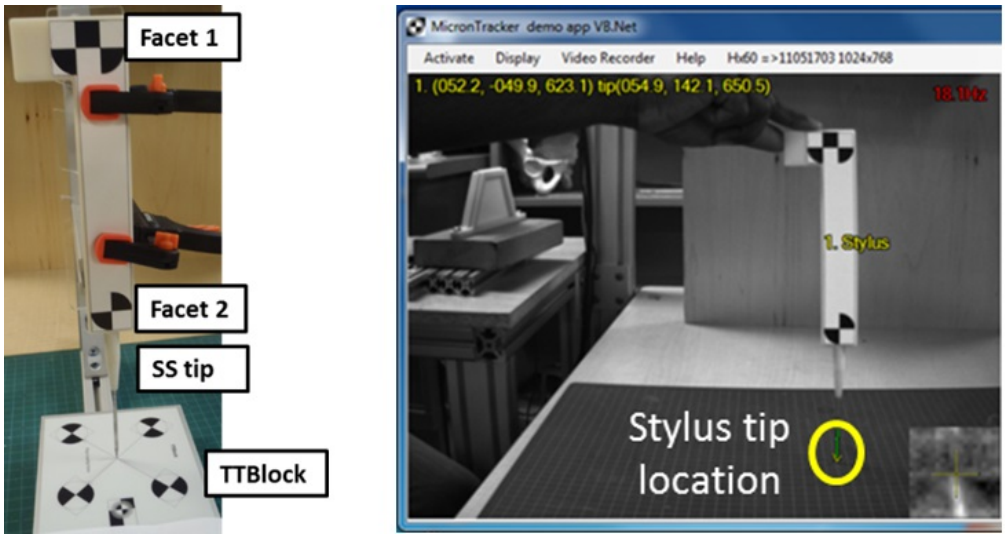

Figure 4.29: Stylus tip calibration: A) Setup with TTBlock tool kit. Right) Stylus tip location determined by MicronTracker in real-time.

Using the marker template registration module as described in section 4.4, minimum of 300 pose measurements were recorded. The transform between the stylus marker coordinates to the center of the TTBlock coordinates are computed by the MicronTracker software and the calculated transform is applied to the stylus markers to locate the stylus tip position in real-time, as shown in Figure 4.29. The length of the stylus is chosen so that the distance between the two Xpoints is at least 150 mm (vector length), similar to commercially available tool probe (Figure 4.28 b) for higher accuracy of stylus tip registration.

4.11 Phantom registration

The CT-scanned raw image volume of the validation phantom is loaded into 3D Slicer for visualization. Using the threshold based image segmentation, the fiducial points are extracted from the CT volume and rendered 3D models are created for visualization purpose, as shown in Figure 4.30 a.

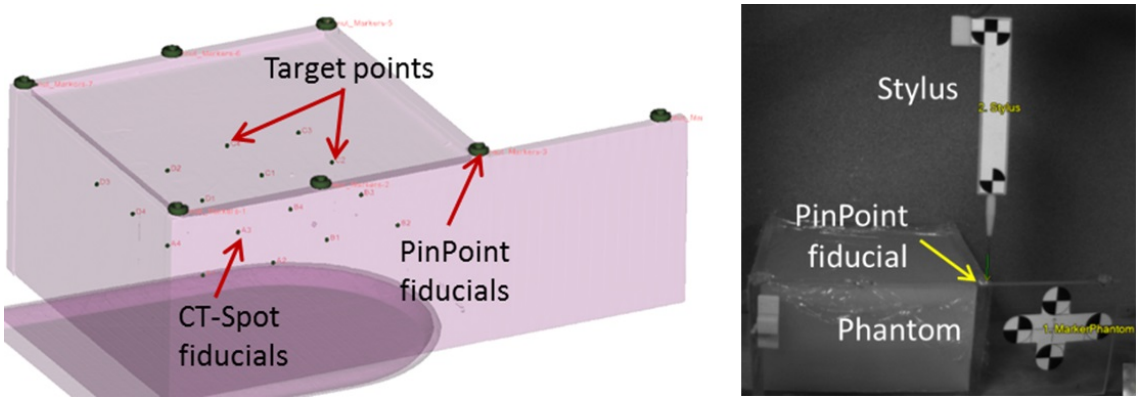

Figure 4.30: Phantom registration: A) 3D Slicer rendered image volume of validation phantom. B) phantom registration using MicronTracker tracked stylus.

The scanned image volume is registered to the physical phantom using fiducial registration. The physical locations of PinPoint fiducials upon the phantom are probed using the tracked stylus, as shown in Figure 4.30 b. Using the *"Fiducial Registration"* wizard of 3D Slicer, the location of the fiducial points are recorded with respect to the planar marker coordinates. The PinPoint fiducial center points are extracted from the image volume using the threshold based image segmentation method from scanned CT volume, as shown in Figure 4.30 b. The image volume is registered to the physical phantom by overlapping the probed physical points with same points in the scanned image volume. The phantom registration using MicronTracker was repeated 10 times and the root mean square error for fiducial registration was 1.35

mm (STD=0.14).

The real-time physical location of the image volume with respect to mobile image overlay device is determined by tracking the planar markers upon the phantom. The position of the virtual image overlay plane with respect to the phantom image volume is calculated by applying the transform (${}^{IO}T_{PM}$) as defined in the section 4.7.

The transform (${}^{SM}T_{PM}$) is computed by continuous tracking of the marker upon the viewbox (SM) and phantom (PM), as shown in Figure **??**. The transform (${}^{SM}T_{IO}$) is determined by image overlay plane calibration as explained in section 4.7.

4.12 System accuracy validation

The accuracy of the mobile image overlay system shall be validated by needle insertion test on the validation phantom. The image overlay plane calibration and phantom registration shall be performed as defined in section 4.7 and 4.11 respectively. The system is hand-held over the validation phantom so that the markers upon the viewbox and phantom are within the tracker's field of measurement. The image volume is browsed over the phantom until the target point (CT-Spot fiducials) is seen in the virtual image overlay plane and the system is fixed at this position firmly using positioning arm.

The needle insertion is planned by choosing the target and needle entry point upon the re-sliced image shown in virtual image overlay plane as (Figure 4.31). The software creates a virtual needle insertion path and shows it in the virtual plane along with depth of insertion. A 0.9 mm diameter needle is used for validation purposes and needle insertion depth is marked. The needle insertion is performed by the following steps mentioned below:

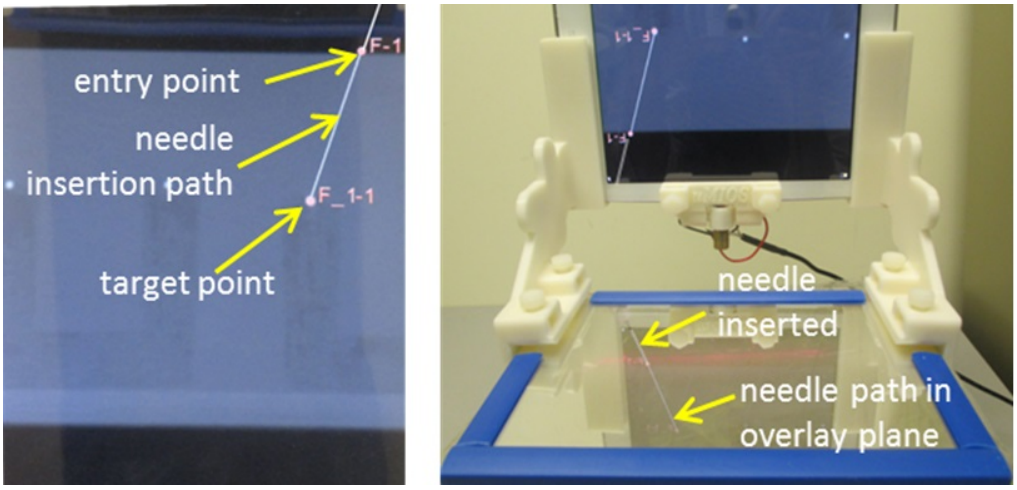

Figure 4.31: System accuracy validation tests: A) Needle insertion planning using image overlay software. Right) Image overlay-guided needle insertion performed.

1. Place the needle tip at the intersection of the laser line upon the phantom and the needle insertion path displayed in the virtual image overlay plane

2. Orient the needle so that the laser line cuts through the center of needle head

3. Align the needle along the needle insertion path displayed in the virtual plane

4. Push the needle into the phantom until mark indicating the insertion depth is reached

The procedure must be repeated for all the targets in the phantom (Figure 4.32). The phantom along with the inserted needles shall be CT-scanned. The new image volume shall be used for measuring the offset between needle tip and target CT-Spot fiducials for validating the accuracy of mobile image overlay system.

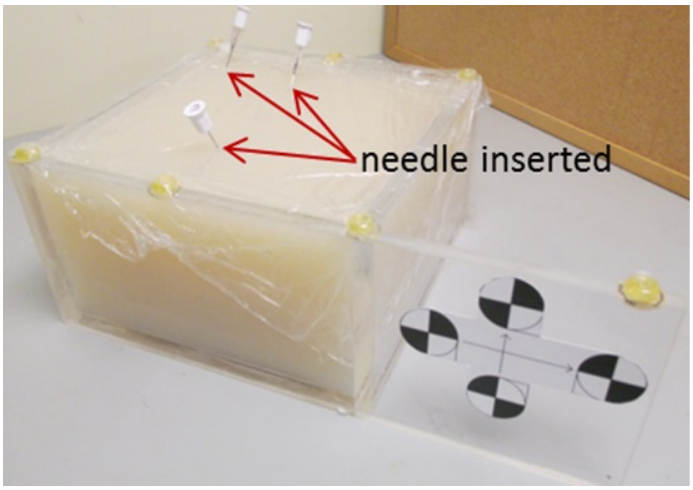

Figure 4.32: Needle insertion performed using virtual image overlay guidance

Chapter 5

Summary and Future Work

The material in this chapter is the extension of the conference paper published as Anand *et al. "The Hamlyn Symposium on Medical Robotics (2013)"*, pp 47-48 [104], and accepted as Anand *et al. 36th Annual International Conference of the IEEE EMBS 2014* [106], where I was the primary author and responsible for the system concept, design and development.

5.1 Experiments and results

5.1.1 Workspace analysis

Referring to the workspace analysis summary presented in Table 3.1 and Table 4.1 for the adjustable and mobile image overlay system, the 90-degree design was considered to be the optimal solution for the viewbox design. The CAD simulation results and viewbox detailed design for 90-degree configuration of the adjustable image overlay system is shown in Figure 5.1.

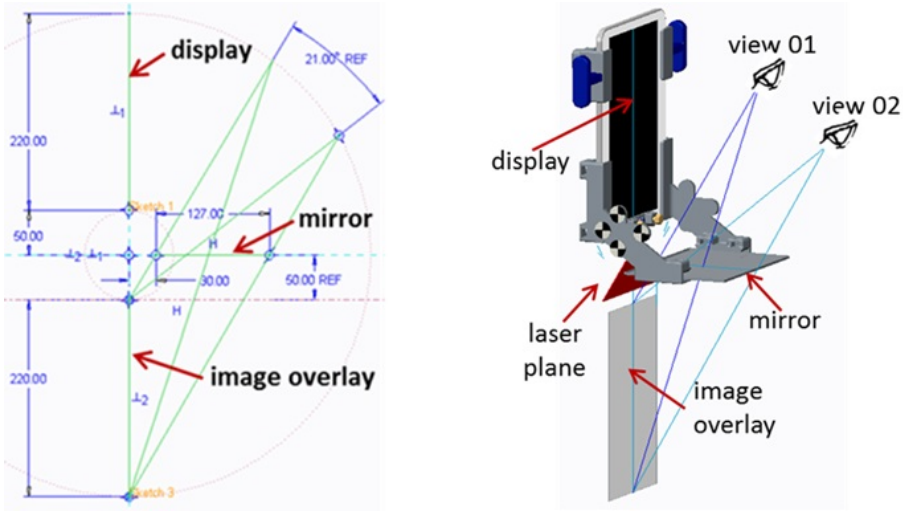

Figure 5.1: 90-degree viewbox design for mobile image overlay system: Left) 2D sketch optimization. Right) Detailed design based upon the outcome of 2D sketch simulation.

The 90-degree design in general was associated with increased viewing angle, higher clearance above the patient, reduced viewbox (and system) weight and simpler viewbox design as compared to 60-degree design. The increased viewing angle provides the physician increased flexibility to work around the patient, simplifies the image overlay plane auto-calibration using MicronTracker and allows more than one user to simultaneously view the same image. The clearance of 5.0 cm above the patient allows the user to view the complete image overlay depth, increases the oblique image overlay plane rotation and accommodates obese patients. The reduced weight of the 90-degree design (<1.0 kg) allows the system to be possibly hand-held by the physician to browse the image volume over the patient. The 90-degree viewbox housing design for the mobile image overlay system was simpler, can be manufactured using injection molding technique, and improves the possibilities for commercialization and large scale deployment of 2D image overlay concept into clinical space. The

appearance of the viewbox resembles the Sonic Flashlight [73] developed for direct visualization of ultrasound images using real-time tomographic reflection.

Table 5.1: 90-degree design workspace analysis: Adjustable and Mobile system

System configuration	***Mobile System***	***Adjustable System***
User viewing angle	21 degree	35 degree
Image overlay depth	21.8 cm	22.8 cm
Image overlay width	13.6 cm	30.5 cm
Oblique rotation	$>$ 35 degree	$<$ 15 degree

The workspace analysis comparison for 90-degree design between the previously proposed adjustable system and newly proposed mobile image overlay system is summarized in Table 5.1. The user viewing angle for the mobile system was less than the adjustable system, but no significant issues were observed for image overlay calibration using MicronTracker. The user angle for the adjustable system can be further increased by choosing a longer beamsplitter mirror (currently standard off-the-shelf component 13.5 cm X 12.7 cm). Increasing the beamsplitter length impacts the oblique angle rotation and hence an optimal solution should be determined if the current viewing angle of 21° is insufficient. The oblique image overlay plane rotation for the mobile system is higher than the adjustable system and meets the requirement for spine injections procedures. This eliminates the need for rotating the system to view sagittal image for spine injection, something which is suboptimal for physicians. The image overlay depth is similar for both systems and width is lower for mobile system. To view the complete image slice, the mobile system can be moved along the transverse image plane (along the patient width).

5.1.2 System weight

The primary objective of the mobile image overlay system was to reduce the viewbox weight and eliminate the need for a counterbalanced, articulated arm. The use of the Galaxy Tablet 10.1 as the display device for the mobile image overlay system effectively reduced the overall system weight. The results of system weight comparison are summarized in Table 5.2.

Table 5.2: System weight comparison: Adjustable and Mobile system

System configuration	***Mobile System***	***Adjustable System***
Viewbox weight	1.0 kg	8.2 kg
System weight	1.0 kg	>45 *kg
Total parts	10	273

∗*approximate weight of the system calculated with 3D design models created*

The viewbox weight of the newly proposed mobile system is 1.0 kg as compared to the previously proposed adjustable system [104] which was about 8.2 kg. The overall system weight of mobile system remains the same as the viewbox weight since no articulated arm was required to support the system. The reduced system weight allows the device to be possibly hand-held by the physician to browse the image volume over the patient and use a positioning arm to fix the device during needle insertion.

5.1.3 Cost analysis

The detailed breakdown of prototype development cost for different generations of image overlay systems are summarized in Table 5.3.

Table 5.3: Protoype build cost: Static, Adjustable and Mobile system.

	Static System [109]	***Adjustable System***	***Mobile System***
Laptop computer	$1,200	$1,200	$1,200
Display device	$300	$175	$400
Mirror	$300	$30	$125
Frame materials and / or 3D printed parts	$1,000	$1,165	$100
Electronic parts and accessories	$500	$200	$11
Total	$3,100	$2,735	$1,841

The arm development for the adjustable image overlay system was minimal (no articular feature was investigated) and hence the prototype cost does not represent the cost as per final design specifications. We estimate the cost of a commercially available articulated arm to be around $5,000 and the total cost of adjustable system as per actual design specifications to be approximately $7,000. The main cost associated with the mobile image overlay system is the tablet display device and the overall cost is at least 3.75 times less expensive than the cost of adjustable system and two times less inexpensive than the static system previously developed. The cost of labor to build the prototype was not considered for the analysis; however, prototype build cost for the adjustable system with approximately 273 parts is higher compared to mobile system with approximately 10 parts. The detailed bills of material for the

adjustable and the mobile image overlay system are presented in the *Appendix B and C* respectively. Including the MicronTracker (educational cost approx. $6,500), the mobile image overlay system cost for clinical research shall be around $8,300 and the 3D Slicer image overlay system module is available free of cost.

5.1.4 Tracker distance from virtual plane: Pose precision

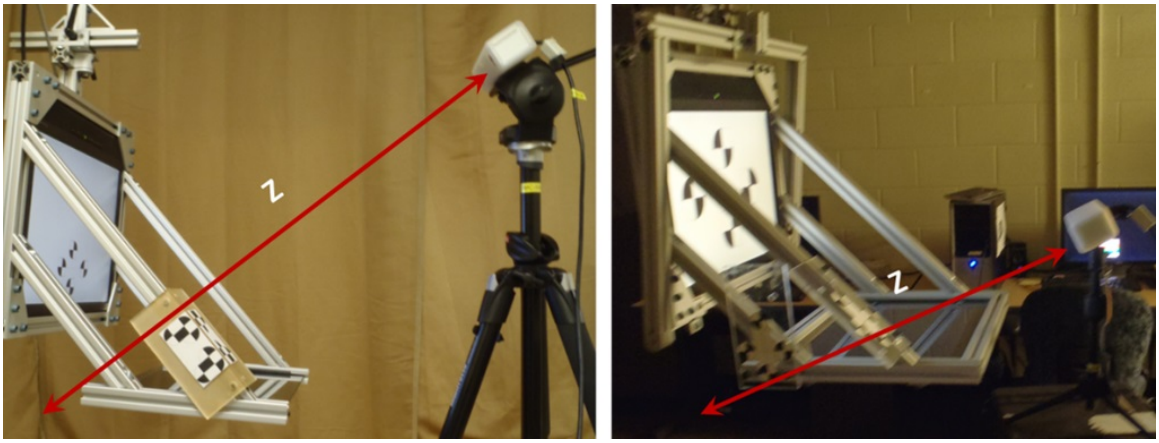

Figure 5.2: Tracker distance from virtual image overlay plane and MicronTracker pose measurement precision: A) Tracker at distance approx. 90 cm. B) Tracker at distance approx. 40 cm.

The pose of the virtual markers are determined by displaying the planar markers in the display screen. By reflection, the virtual markers are seen through the mirror. The MicronTracker is placed above the mirror such that the entire virtual marker is seen the tracker device. Minimum of 300 poses are recorded for each studies and the precision is measured. The precision of MicronTracker as per manufacturer's specification is 0.25 mm RMS (root mean square error) for a single target (Xpoint) measured at depth of 40 - 100 cm with respect to the tracker coordinates; however, a precision of ± 10 mm was observed (average of over 300 poses measured) for adjustable system with LCD monitor and semi-transparent mirror with MicronTracker

approximately 90 cm from the virtual image overlay plane. In order to ensure the virtual marker and front markers were within the field of measurement of the tracker camera, the MicronTracker was required to be placed at a distance of approximately 90 cm (Figure 5.2 a) from the virtual image overlay plane.

Table 5.4: Tracker distance from virtual plane and pose measurement precision

Distance between the virtual plane and MicronTracker coordinates	***Precision measured***
approx. 90 cm	±10 mm
approx 40 cm	±1 mm

The closest possible distance between the tracker and image overlay plane to measure the virtual marker pose was approx. 40 cm (Figure 5.2 b) and precision of ± 1 mm was observed (average of over 300 poses measured). Due to limited field of measurement of tracker camera, it was not possible to have both the front marker and the virtual marker in the field of measurement for transform calculation. A temporary front marker (Figure 5.3 was introduced to overcome the field of measurement limitations and place the tracker as close as possible to improve the pose measurement precision. The temporary marker shall be fixed firmly upon the mirror for the image overlay calibration using adhesive tape and removed after completion of the calibration step. The precision of the virtual markers' pose measurement could be further improved by improving the image quality in the overlay plane.

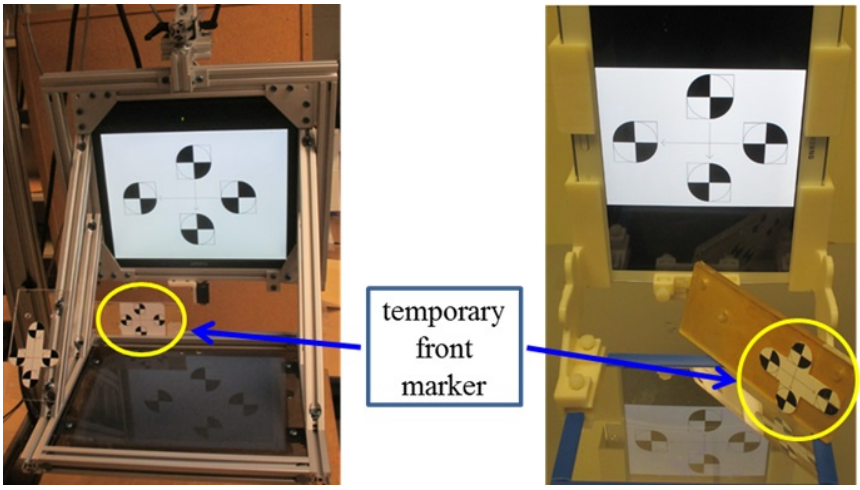

Figure 5.3: Limited tracker field of measurement, temporary front marker used to ensure physical and virtual marker within tracker field of measurement for image overlay calibration: A) Adjustable system. B) Mobile system.

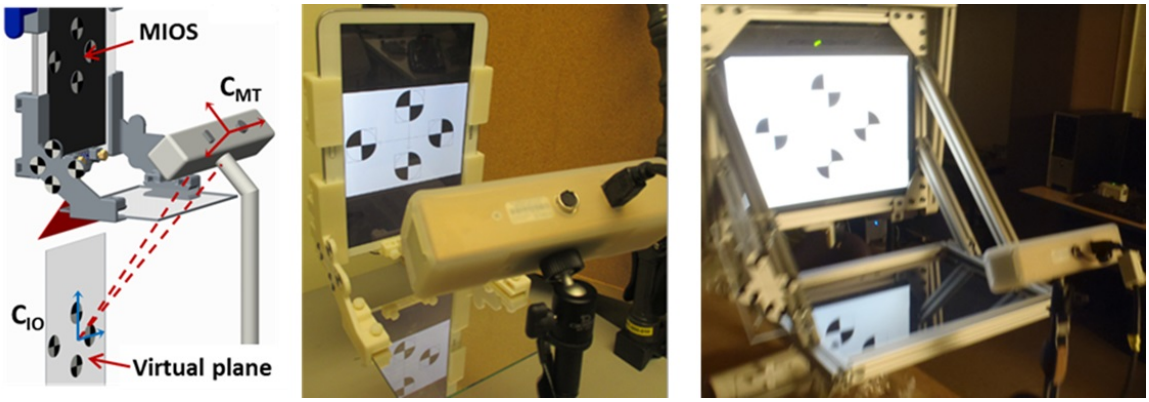

Figure 5.4: Virtual marker pose detection accuracy: A). Pictorial representation. B) Mobile system. C). Adjustable system.

5.1.5 Image overlay plane detection precision

Another objective of the mobile image overlay system was to improve the image quality to increase the dynamic tracking accuracy of the virtual markers. The high luminance tablet display device (Galaxy Tab 10.1) and high reflective mirror (beamsplitter with 75% Reflection) were used for the mobile image overlay system. An experimental

study (Figure 5.4) with 10 repeated trials was conducted to determine the precision of virtual marker pose detection by MicronTracker. For each trial, a minimum of 300 poses were recorded with respect to tracker coordinates using *"Transform Recorder"* module from the PerkTutor extension for 3D Slicer.

Table 5.5: Virtual image overlay plane markers pose measurement precision: Adjustable and Mobile system

	Recorded precision (mm)
Adjustable System	0.55 (STD = 0.05)
Mobile System	0.11 (STD = 0.05)

The recorded precision for mobile and adjustable system were 0.11 mm (STD=0.05) and 0.55 mm (STD=0.05), respectively. The precision of virtual markers detection was comparable to the physical marker precision as specified by the manufacturer. Thus, this validates our initial hypothesis of achieving higher precision with high luminescence display and R/T ratio mirror.

5.2 Outreach and conference demo

The mobile image overlay system being light weight and smaller in dimension has benefited our research group to demonstrate the research theme of Perk Lab *(Laboratory of Percutaneous Surgery)* at various conferences and outreach events. The image overlay device along with the tracker and laptop could be packed into a suitcase of size less than 20" and carried by a single person. The image overlay system very well connected the concept of percutaneous interventions across all age groups i.e. very young children to adults including the university students and the research groups.

Figure 5.5: Demonstration of percutaneous surgery principles at community outreach and conference demos using mobile image overlay systems.

5.3 Summary

Workspace analysis

The main objective of the workspace analysis was to define the optimal mirror-monitor configuration with assembly dimensions to minimize the ergonomic issues of the previous systems [20] [21] [22] and ensure system compatibility for the targeted clinical applications. Based on the study done for adjustable [104] and mobile system

[106], the 90-degree configuration was considered to be optimal with maximum view angle and improved clearance above the patient. The technical benefits of the 90-degree configuration opens the possibilities of exploring new clinical procedures and further strengthening the clinical translation of the image overlay concept. The appearance of the 90-degree configuration (Figure 5.6) for mobile system resembles the soon to be commercialized Sonic Flashlight [73] developed for the direct visualization of ultrasound images using real-time tomographic reflection.

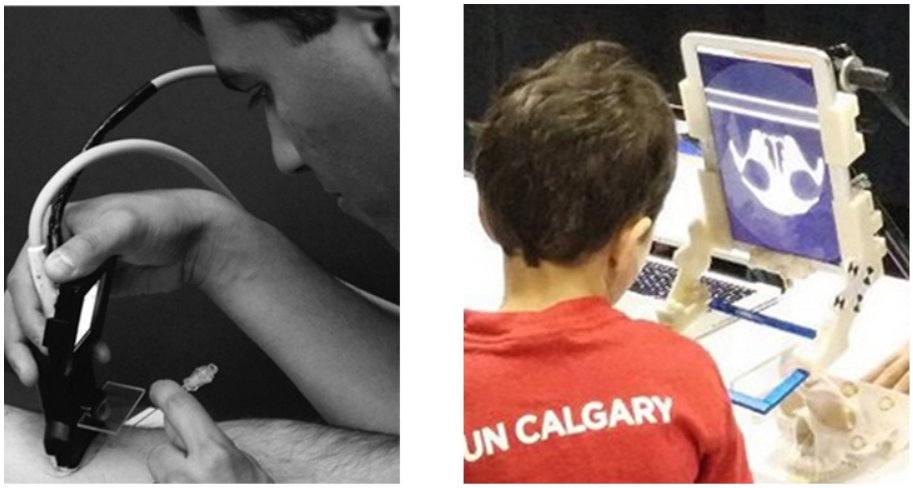

Figure 5.6: Mirror-monitor configuration: A) Sonic Flashlight [27]. B) Newly proposed mobile image overlay system with 90-degree mirror-monitor design.

Integration of optical dynamic tracking

One of the main limitations of the static image overlay system [20] [21] [22] was the absence of dynamic tracking resulting in misalignments due to unintended physical contact with the system during the procedure. We successfully integrated the optical tracking system for continuous dynamic tracking of the image overlay system and patient together. Based on the image overlay plane calibration study[104], MicronTracker was the chosen tracking system for mobile system.

Auto image overlay calibration

The initial setup time for static system was higher than the actual procedure duration, thus inhibiting the clinical translation of the 2D image overlay concept. Auto-direct calibration of the virtual image overlay plane was demonstrated using MicronTracker [104]. The tracker can see through the mirror and determine the pose of virtual markers displayed in the image overlay plane. The image overlay calibration using MicronTracker is simpler with fewer steps, automatic and can be done away from the patient space as compared to the Z-frame registration method described in [78] for the previous static system.

Laser plane alignment

The 5mW output power laser diode satisfying the FDA class IIIa requirements has improved laser line visibility over patient surface under normal procedure room light conditions as compared to previous systems [20] [21] [22] [104]. The optical tracker aided laser plane alignment has simplified the alignment steps with reduced duration as compared to previous systems. The laser line visibility should be tested under procedure room lighting conditions to validate the selection of 5mW output power source laser diode.

Mobile image overlay system

The objective of the proposed new design was to completely mobilize the system and improve the accuracy compared to earlier systems. The viewbox design was simple with only 10% of parts and reduced build time as compared to adjustable system. The use of high luminance tablet display device and high reflection beam-splitter has reduced the viewbox weight (1 kg) by 8.2 times and image overlay plane detection accuracy was improved by 3.2 times compared to the previous

system [20] [21] [22] [104], thus enabling the system to be hand held by the physician and explore the image volume over the patient. The precision of the virtual markers' pose was comparable to that of physical printed markers'. Based on successful pre-clinical testing of the previous system, the mobile image overlay system with reduced weight, increased tracking accuracy and easier maneuverability can be used for wide range of procedures. The clinical procedures such as MSK procedures, parathyroidectomy and nephrolithotomy were validated by simulation using CAD tool.

5.4 Future work

The mobile image overlay system was the first step to overcome the ergonomic limitations of the previous systems and successfully demonstrated the image overlay concept. There has been a radical design change with implementation of 90-degree mirror-monitor configuration; use of tablet display device and beamsplitter; and successful integration of MicronTracker for optical tracking and image overlay plane auto-calibration; however, for effective translation of 2D image overlay concept into clinical space using mobile system, the concept needs further work which is discussed in the following section below.

5.4.1 Phantom and cadaver studies

The thesis project was aimed at design and development of a mobile system to enable the translation of 2D image overlay concept into clinical trials by overcoming the ergonomic issues associated with the previously proposed systems. The needle insertion was performed upon the validation phantom using the mobile image overlay system.

The validation of the concept, however, was not completed due to unavailability of resources (CT scanner) to scan the validation phantom along with the inserted needles. The phantom and cadaver studies should be completed to validate the accuracy of the proposed image overlay system.

5.4.2 3D Slicer image overlay module

A minimal version of 3D Slicer image overlay module prototype software was developed to project the re-sliced image upon the extended secondary tablet display device. The image overlay calibration was done by manually recording the transform, calculating the average of 300 poses recorded and applying the transforms to the volume re-slice driver. The target and entry points are selected by using the *"Markup module"* of 3D Slicer which is outside the image overlay module. To ensure the two markers are visible within the MicronTracker field of measurement for image overlay plane calibration, the MicronTracker software was necessary to visualize the markers and adjust the position of the tracker. Significant amount of time was lost by switching between the two softwares (MicronTracker software and 3D Slicer), switching the modules within 3D Slicer (transform recorder, OpenIGT, volume re-slice driver, markups and image overlay) and calculating the transforms manually. The software workflow and user interface needs further work to add an auto-calibration and a needle insertion planning module. The auto-calibration module shall allow camera images to be "seen through" the 3D Slicer, enable automatic recording for transform calculations and applying to volume re-slice driver. The needle insertion planning module shall enable the physician to select the target and entry point upon the re-sliced image displayed in the virtual image overlay plane without switching to the markups module.

5.4.3 Effect of ambient light

The use of a highly reflective (75%) beamsplitter has improved the image quality and increased the image overlay plane tracking accuracy. The 90-degree configuration does not protect the beamsplitter from the OR boom lights, as shown in Figure 5.7 a, which affect the reflected image quality due to reflected boom light. The housing design can be modified to add reflection protection without reducing the viewing angle, as shown in Figure 5.7 b to minimize the effect of procedure room (OR) boom lights. Further experimental studies should be done to validate the problem and solution.

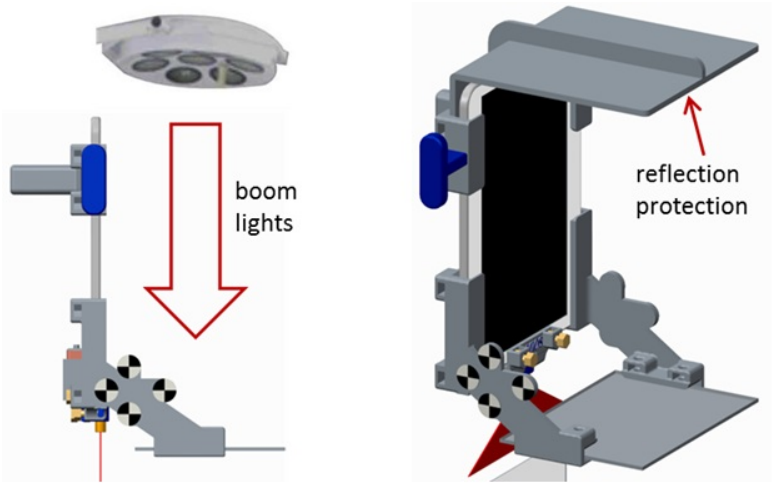

Figure 5.7: Impact of ambient light: A) Reflection of boom lights and interference with virtual image resulting in poor image quality. B) Design modification to add reflection protection and minimize the influence of OR boom light.

5.4.4 Improve the image transfer rate

A slower image update rate between the host computer and tablet device was observed when the image overlay system was used to browse the image volume over phantom.

iDisplay was the preferred commercially available solution to wirelessly connect the tablet device as a secondary display to the host computer. Similar function can be achieved by a desktop sharing software *Team-Viewer (GFI Software Inc. Germany)*. Further development is required to find an alternative solution to improve the image transfer rate between the host computer and the tablet device.

5.4.5 Sterilization

The mobile image overlay system shall be hand-held by the physician using the handle; however, during the procedure there is a high risk of body fluids coming in contact with the device and hence there is risk of contamination and infection to the patient. Therefore the device must be sterilized before each procedure to avoid body fluid contamination and risk of infection to the patient. The housing (bracket and handle) and beamsplitter are the high risk parts compared to display device and laser assembly. One possible solution (Figure 5.8) is to redesign the housing so that the display device and beamsplitter can be disassembled for sterilization purpose and reassembled after sterilization for the procedure. The laser plane alignment shall be a factory adjustment procedure and delivered to the hospitals pre-aligned. The risk associated with this proposal is misalignment of laser plane with image overlay plane due to separation and reassembly of parts during the procedure. The housing construction shall be rigid to reproduce the same position of beamsplitter during each assembly and hence no change in alignment of laser and virtual plane. Repeatability and reproducibility tests should be done to evaluate the misalignment error between the laser plane and virtual plane.

The display device along with the laser assembly can be sterilized either by chemical cleaning of the device or bagging/shrink wrapping. The chemical cleaning may not be effective due to small gaps between the plastic covers of the tablet device and the laser mount needs a more sophisticated design. The bagging or shrink wrapping requires additional custom designed bag or shrink wrapping equipment which increases the effective procedure cost. The mechanical housing and the beam splitter can be sterilized by conventional methods such as heat, gas and chemical.

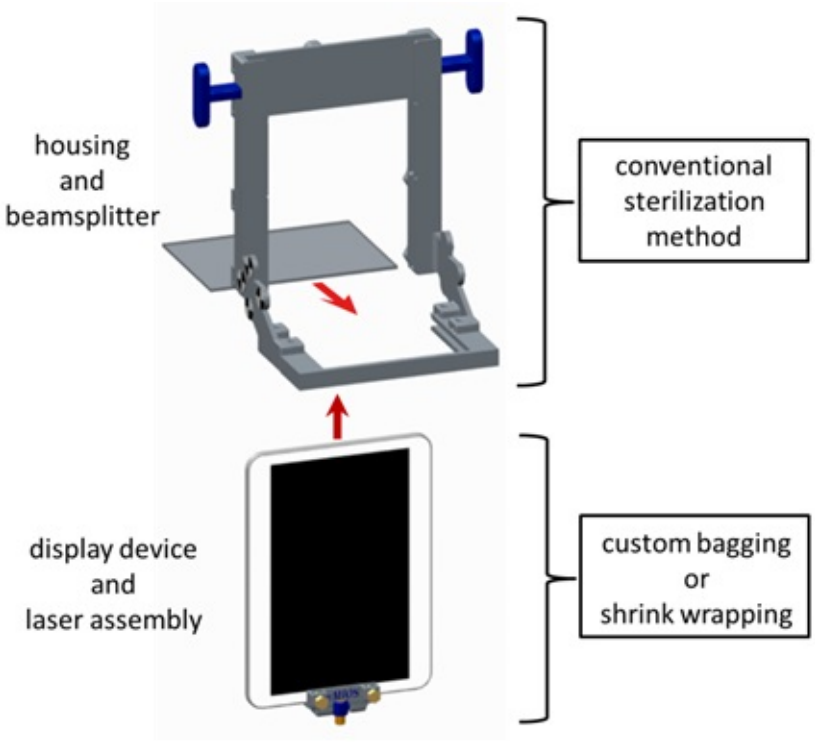

Figure 5.8: Concept proposed for managing sterialization before each procedure for the mobile image overlay system.

5.4.6 MR compatible mobile image overlay system

Increased radiation exposure and poor soft tissue contrast with CT or fluoroscopic imaging systems have pushed the physicians to explore MR imaging system as the modality of choice for many diagnostics in musculoskeletal radiology [110]. Magnetic Resonance (MR) imaging is an excellent imaging modality for soft tissues and provides accurate information about pathological tissues around the normal tissues. For musculoskeletal procedures, MR imaging provides good visualization of pathology and its superior soft tissue contrast helps to avoid critical structures in the puncture route [111] [112]. The advances in the MR systems coupled with fast pulse sequences have contributed to increasing interest in interventional MRI.

The biggest concern with MR technology is the presence of metallic parts in the magnetic field. An MR compatible image overlay system was proposed by our research group [113] and an MR compatible LCD monitor was used. The monitor used in the MR compatible system was bulky, heavier (20 kg), specially-made equipment that is heavy on shielding and light on functionality. Large misalignments were observed due the to large suspended mass of the monitor. The use of the current mobile system for MR-guided procedures shall be inhibited due to the MR incompatible tablet display device used. The aluminium structure, hard disk and glue used to join the parts together pose huge risk of using the tablet device in MR environment. Concurrently, the research group at *The Kim Butts Pauly Research Lab* at Stanford University is working on developing an MR compatible HP Touchpad based tablet device by removing parts such as speakers and its haptic component (which makes the device vibrate). The future availability of MR compatible tablet devices shall further strengthen the clinical deployment of the mobile image overlay system.

5.4.7 AMOLED display devices

The Applied Science Group of Microsoft Research is currently developing SpaceTop [114] concept that fuses 2D and spatial 3D interactions in a single see through desktop workspace, as shown in Figure 5.9. The device uses AMOLED see through displays to fuse 2D image with 3D interactions of the user which is tracked using Kinect system. AMOLED *(active-matrix organic light-emitting diode)* is a display technology for use in mobile devices and televisions. OLED describes a specific type of thin-film-display technology in which organic compounds form the electroluminescent material, and active matrix refers to the technology behind the addressing of pixels. AMOLED's along with a compatible operating system could be a potential image overlay system replacing monitor-mirror configuration by single see through AMOLED display device.

Figure 5.9: SpaceTop: Integrating 2D and spatial 3D Interactions in a see through desktop environment. *(Microsoft Research, Applied Sciences Group)*

5.5 Thesis achievements

The major achievements of the current thesis are as follows:

- Workspace analysis resulted in introduction of a newly proposed 90-degree view-box design with highest viewing angle
- Integration of a tablet computer and beamsplitter as a display device and mirror for 2D image overlay concept
- Novel technique to calibrate the virtual plane using the MicronTracker to "see-through" the mirror and determine virtual markers pose
- Integration of MicronTracker for dynamic tracking of the device and patient during the procedure. Patient respiration can be tracked in real-time using the MicronTracker, this further improves the needle placement accuracy
- Red line type 5mW power output laser source used to improve visibility and development of optical tracker aided laser plane alignment
- Design and development of a smaller and light weight (<1 kg) image overlay system which can possibly be held in a physician's hand to browse the image
- Simplified virtual plane calibration and laser plane alignment resulted in initial setup time much lower compared to actual procedure duration
- Virtual image quality improved with clear visibility of the object below the mirror and tracking precision (0.11mm STD 0.05) similar to physical markers

Bibliography

[1] Bettyann Kevles. *Naked to the bone: Medical imaging in the twentieth century*. Rutgers University Press, 1997.

[2] Andreas H Mahnken and Jens Ricke. *CT-and MR-guided Interventions in Radiology*, volume 22. Springer, 2009.

[3] Edward W. Lee, Christine Chen, Steven Sauk, and Nagesh Ragavendra. How diagnostic is ultrasound-guided neck mass biopsy (fine-needle capillary sampling biopsy technique)?: Evaluation of 132 nonthyroid neck mass biopsies with pathologic analysis over 7 years at a single institution. *Journal of Ultrasound in Medicine*, 28(12):1679, 2009.

[4] Jan Fritz, Paweena U-Thainual, Tamas Ungi, Aaron J. Flammang, Edward F. McCarthy, Gabor Fichtinger, Iulian I. Iordachita, and John A. Carrino. Augmented reality visualization using image overlay technology for mr-guided interventions: Cadaveric bone biopsy at 1.5 t. *Investigative Radiology*, 48(6):464–470, 2013.

[5] Jan Fritz, Paweena U-Thainual, Tamas Ungi, Aaron J. Flammang, Gabor Fichtinger, Iulian I. Iordachita, and John A. Carrino. Augmented reality visualisation using an image overlay system for mr-guided interventions: technical

performance of spine injection procedures in human cadavers at 1.5 tesla. *European radiology*, 23(1):235–245, 2013.

[6] Geir Arne Tangen, Ford Manstad-Hulaas, Brekken Reidar, and Hernes Toril A. N. *Navigation in Endovascular Aortic Repair, Aortic Aneurysm - Recent Advances*. 2013.

[7] Antoine Hakime, Frederic Deschamps, Enio Garcia Marques De Carvalho, Ali Barah, Anne Auperin, and Thierry De Baere. Electromagnetic-tracked biopsy under ultrasound guidance: preliminary results. *Cardiovascular and interventional radiology*, 35(4):898–905, 2012.

[8] Paul R. Detmer, Gerard Bashein, Timothy Hodges, Kirk W. Beach, Eric P. Filer, David H. Burns, and D. E. Strandness. 3d ultrasonic image feature localization based on magnetic scanhead tracking: In vitro calibration and validation. *Ultrasound in Medicine & Biology*, 20(9):923–936, 1994.

[9] P. Reittner, M. Tillich, W. Luxenberger, R. Weinke, K. Preidler, W. Kle, H. Stammberger, and D. Szolar. Multislice ct-image-guided endoscopic sinus surgery using an electromagnetic tracking system. *European Radiology*, 12(3):592–596, 2002.

[10] Kyle Wu Aaron Martin Timothy Kane Craig A Peters Kevin Cleary Raj Shekhar Xin Kang, Wilson Emmanuel. Stereoscopic augmented reality for laparoscopic surgery. *Society of American Gastrointestinal and Endoscopic Surgeons*, Feb 2014.

[11] Andrei State, Mark Livingston, William Garrett, Gentaro Hirota, Mary Whitton, Etta Pisano, and Henry Fuchs. Technologies for augmented reality systems: realizing ultrasound-guided needle biopsies. pages 439–446. ACM, 1996.

[12] Jeremy D. Ackerman. *Application of Augmented Reality to Laparoscopic Surgery*. Phd thesis dissertation, Department of Biomedical Engineering; The University of North Carolina, 2002.

[13] Hong Hua, Chunyu Gao, Jannick P. Rolland, and Frank Biocca. An ultra-light and compact design and implementation of head-mounted projective displays. In *Proceedings of the Virtual Reality 2001 Conference (VR'01)*, VR '01, pages 175–, Washington, DC, USA, 2001. IEEE Computer Society.

[14] Christopher Schmandt. Spatial input/display correspondence in a stereoscopic computer graphic work station. pages 253–261. ACM, 1983.

[15] Mike Blackwell, Constantinos Nikou, Anthony M. DiGioia, and Takeo Kanade. An image overlay system for medical data visualization. In *Proceedings of the First International Conference on Medical Image Computing and Computer-Assisted Intervention*, MICCAI '98, pages 232–240, London, UK, UK, 1998. Springer-Verlag.

[16] Jing-Ren Wu, Min-Liang Wang, Kai-Che Liu, Ming-Hsien Hu, and Pei-Yuan Lee. Real-time advanced spinal surgery via visible patient model and augmented reality system. *Computer methods and programs in biomedicine*, 113(3):869–881, 2014.

[17] G Stetten, V Chib, and R Tamburo. System for location-merging ultrasound images with human vision. In *Applied Imagery Pattern Recognition (AIPR) Workshop*, pages 200–205, 2000.

[18] Caitlin T Yeo, Tamas Ungi, Andras Lasso, RC McGraw, and Gabor Fichtinger. The effect of augmented reality training on percutaneous needle placement in spinal facet joint injections. *Biomedical Engineering, IEEE Transactions on*, 58(7):2031–2037, 2011.

[19] Gregory S Fischer. *Enabling technologies for MRI-guided interventional procedures*. PhD thesis, Johns Hopkins University, 2008.

[20] Gabor Fichtinger, S. J. Zinreich, Anton Deguet, Gregory Fischer, Iulian Iordachita, Emese Balogh, Ken Masamune, Russell H. Taylor, Laura M. Fayad, and Michelle de Oliveira. Image overlay for ct-guided needle insertions. *Computer aided surgery : official journal of the International Society for Computer Aided Surgery*, 10(4):241–255, 2005.

[21] Gabor Fichtinger, Anton Deguet, Ken Masamune, Emese Balogh, Gregory S Fischer, Herve Mathieu, Russell H Taylor, S James Zinreich, and Laura M Fayad. Image overlay guidance for needle insertion in ct scanner. *Biomedical Engineering, IEEE Transactions on*, 52(8):1415–1424, 2005.

[22] Jan Fritz, Paweena U-Thainual, Tamas Ungi, Aaron J. Flammang, Gabor Fichtinger, Iulian I. Iordachita, and John A. Carrino. Augmented reality visualization with use of image overlay technology for mr imaging-guided interventions: assessment of performance in cadaveric shoulder and hip arthrography at 1.5 t. *Radiology*, 265(1):254–259, 2012.

[23] Jan Fritz, Paweena U-Thainual, Tamas Ungi, Aaron J. Flammang, Gabor Fichtinger, Iulian I. Iordachita, and John A. Carrino. Augmented reality visualization using image-overlay for mr-guided interventions: Accuracy for lumbar spinal procedures with a 1.5-tesla mri scanner. *American Journal of Roentgenology*, 198(1):266–273, 2012.

[24] Sanoop K. Zachariah. Gas-less video-assisted thyroidectomy for a solitary thyroid nodule: Technical report of the first case performed at a rural teaching hospital in india and review of literature. *Journal of surgical technique and case report*, 4(1):27, 2012.

[25] Yeh M., Barraclough B.M., Sidhu S.B., Sywak M.S., and Delbridge L.W. 200 consecutive parathyroid ultrasound studies by a single ultrasonologist. endocrine practice. In press.

[26] Caron Technology Inc. *MicronTracker Developers Manual, MTC3.6*, 02 2011.

[27] Gaurav Shukla Angela Bayless David Weiser Adam Scharl Derek Mockel Christopher Banks Bernadette Mandella Roberta Klatzky David Wang, Nikhil Amesur and George Stetten. Peripherally inserted central catheter placement with the sonic flashlight initial clinical trial by nurses. *Journal of Ultrasound in Medicine*, 28(5):651–656.

[28] Terry Peters and Kevin Cleary. *Image-guided interventions: technology and applications*. Springer, 2008.

[29] Laura Liberman. Percutaneous image-guided core breast biopsy. *Radiologic clinics of North America*, 40(3):483–500, 2002.

[30] Kyle Fahrbach, Isabella Sledge, Catherine Cella, Heather Linz, and Susan D. Ross. A comparison of the accuracy of two minimally invasive breast biopsy methods: a systematic literature review and meta-analysis. *Archives of Gynecology and Obstetrics*, 274(2):63–73, 2006.

[31] Florian Pohlig, Chlodwig Kirchhoff, Ulrich Lenze, Johannes Schauwecker, Rainer Burgkart, Hans Rechl, and Ruediger von Eisenhart-Rothe. Percutaneous core needle biopsy versus open biopsy in diagnostics of bone and soft tissue sarcoma: a retrospective study. *European journal of medical research*, 17(1):29–29, 2012.

[32] Gopal R. Vijayaraghavan, Sheehan David, Myriam Bermudez-Allende, and Hussain Sarwat. Imaging-guided parenchymal liver biopsy: How we do it. *Journal of clinical imaging science*, 1(1):30, 2011.

[33] Mahmoud B El-Tamer, B Marie Ward, Tracy Schifftner, Leigh Neumayer, Shukri Khuri, and William Henderson. Morbidity and mortality following breast cancer surgery in women: national benchmarks for standards of care. *Annals of surgery*, 245(5):665, 2007.

[34] Victor J. Zannis and Kristina M. Aliano. The evolving practice pattern of the breast surgeon with disappearance of open biopsy for nonpalpable lesions. *The American Journal of Surgery*, 176(6):525–528, 1998.

[35] Bruce R. Douglas, J. William Charboneau, and Carl C. Reading. Ultrasound-guided intervention: Expanding horizons. *Radiologic Clinics of North America*, 39(3):415 – 428, 2001.

[36] PNT Wells. Ultrasound imaging. *Physics in medicine and biology*, 51(13):R83, 2006.

[37] S Delorme, M Krix, and T Albrecht. Ultrasound contrast media–principles and clinical applications. *RöFo: Fortschritte auf dem Gebiete der Röntgenstrahlen und der Nuklearmedizin*, 178(2):155, 2006.

[38] Adrian MK Thomas, Arpan K Banerjee, and Uwe Busch. *Classic papers in modern diagnostic radiology*. Springer, 2005.

[39] J Thomas Payne. Ct radiation dose and image quality. *Radiologic clinics of North America*, 43(6):953–962, 2005.

[40] Jinlan Huang, John K Triedman, Nikolay V Vasilyev, Yoshihiro Suematsu, Robin O Cleveland, and Pierre E Dupont. Imaging artifacts of medical instruments in ultrasound-guided interventions. *Journal of Ultrasound in Medicine*, 26(10):1303–1322, 2007.

[41] JS Lewin, CA Petersilge, SF Hatem, JL Duerk, G Lenz, ME Clampitt, ML Williams, KR Kaczynski, CF Lanzieri, AL Wise, et al. Interactive mr imaging-guided biopsy and aspiration with a modified clinical c-arm system. *AJR. American journal of roentgenology*, 170(6):1593–1601, 1998.

[42] Stephen G Hushek, Alastair J Martin, Michael Steckner, Elyakim Bosak, Josef Debbins, and Walter Kucharzyk. Mr systems for mri-guided interventions. *Journal of Magnetic Resonance Imaging*, 27(2):253–266, 2008.

[43] Linda T Kohn, Janet M Corrigan, Molla S Donaldson, et al. *To err is human: building a safer health system*, volume 627. National Academies Press, 2000.

[44] J Jeffrey Carr, Paul F Hemler, Price W Halford, Rita I Freimanis, Robert H Choplin, and Michael YM Chen. Stereotactic localization of breast lesions: How it works and methods to improve accuracy1. *Radiographics*, 21(2):463–473, 2001.

[45] Peter L Roberson, Vrinda Narayana, Daniel L McShan, Raymond J Winfield, and P William McLaughlin. Source placement error for permanent implant of the prostate. *Medical physics*, 24(2):251–257, 1997.

[46] Sameer Nath, Zhe Chen, Ning Yue, Sharron Trumpore, and Richard Peschel. Dosimetric effects of needle divergence in prostate seed implant using 125i and 103pd radioactive seeds. *Medical physics*, 27(5):1058–1066, 2000.

[47] Heshmatollah S. Majidpour. Risk of radiation exposure during pcnl. *Urology journal*, 7(2):87–89, 2010.

[48] Tapani Koivukangas, Jani P. Katisko, and John P. Koivukangas. Technical accuracy of optical and the electromagnetic tracking systems. *SpringerPlus*, 2(1):1–7, 2013.

[49] A Beaulieu, T Shepard, and R Ellis. A process control system model for interactive image guided surgery. In *Systems Conference, 2008 2nd Annual IEEE*, pages 1–8. IEEE, 2008.

[50] P Grunert, K Darabi, J Espinosa, and R Filippi. Computer-aided navigation in neurosurgery. *Neurosurgical review*, 26(2):73–99, 2003.

[51] Jochen Krücker, Sheng Xu, Neil Glossop, Anand Viswanathan, Jörn Borgert, Heinrich Schulz, and Bradford J Wood. Electromagnetic tracking for thermal

ablation and biopsy guidance: clinical evaluation of spatial accuracy. *Journal of Vascular and Interventional Radiology*, 18(9):1141–1150, 2007.

[52] Liat Appelbaum, Jacob Sosna, Yizhak Nissenbaum, Alexander BBenshtein, and S Nahum Goldberg. New electromagnetic navigation system for ct-guided biopsy of small lesions. *Journal of Vascular and Interventional Radiology*, 21(2):S48–S49, 2010.

[53] Wolfgang Birkfellner, Franz Watzinger, Felix Wanschitz, Rolf Ewers, and Helmar Bergmann. Calibration of tracking systems in a surgical environment. *Medical Imaging, IEEE Transactions on*, 17(5):737–742, 1998.

[54] Adrian J Chung, Philip J Edwards, Fani Deligianni, and Guang-Zhong Yang. Freehand cocalibration of optical and electromagnetic trackers for navigated bronchoscopy. In *Medical Imaging and Augmented Reality*, pages 320–328. Springer, 2004.

[55] Kurt Schicho, Michael Figl, Markus Donat, Wolfgang Birkfellner, Rudolf Seemann, Arne Wagner, Helmar Bergmann, and Rolf Ewers. Stability of miniature electromagnetic tracking systems. *Physics in medicine and biology*, 50(9):2089–2098, 2005.

[56] Katisko Jani. *Intraoperative imaging guided delineation and location of regions of surgical interest feasibility study.* Ph.d. dissertation, University of Oulu, 2012.

[57] Mark Schneider and Charles Stevens. Development and testing of a new magnetic-tracking device for image guidance. volume 6509, 2007.

[58] Erkki Vahala, Mika Ylihautala, Juho Tuominen, Hagen Schiffbauer, Jani Katisko, Sanna Yrjn, Teuvo Vaara, Gsta Ehnholm, and John Koivukangas. Registration in interventional procedures with optical navigator. *Journal of Magnetic Resonance Imaging*, 13(1):93–98, 2001.

[59] DA Simon. Intra-operative position sensing and tracking devices. In *Proceedings of the first joint CVRMed/MRCAS Conference*, pages 62–64, 1997.

[60] Florian Kral, Elisabeth J. Puschban, Herbert Riechelmann, and Wolfgang Freysinger. Comparison of optical and electromagnetic tracking for navigated lateral skull base surgery. *The International Journal of Medical Robotics and Computer Assisted Surgery*, 9(2):247–252, 2013.

[61] Florian Kral, Elisabeth J. Puschban, Herbert Riechelmann, and Wolfgang Freysinger. Comparison of optical and electromagnetic tracking for navigated lateral skull base surgery. *Rhinology*, 49(3):364–368, 2011.

[62] Joachim Kettenbach, Gernot Kronreif, Michael Figl, Martin Frst, Wolfgang Birkfellner, Rudolf Hanel, Wolfgang Ptacek, and Helmar Bergmann. Robot-assisted biopsy using computed tomography-guidance: initial results from in vitro tests. *Investigative radiology*, 40(4):219–228, 2005.

[63] K. Cleary and C. Nguyen. State of the art in surgical robotics: clinical applications and technology challenges. *Computer aided surgery : official journal of the International Society for Computer Aided Surgery*, 6(6):312–328, 2001.

[64] R. H. Taylor and D. Stoianovici. Medical robotics in computer-integrated surgery. *IEEE Transactions on Robotics and Automation*, 19(5):765–781, 2003.

[65] Dogu Teber, Selcuk Guven, Tobias Simpfendrfer, Mathias Baumhauer, Esref O. Gven, Faruk Yencilek, Ali S. Gzen, and Jens Rassweiler. Augmented reality: A new tool to improve surgical accuracy during laparoscopic partial nephrectomy? preliminary in vitro and in vivo results. *European Urology*, 56(2):332–338, 2009.

[66] Frank Sauer, Ali Khamene, and Sebastian Vogt. An augmented reality navigation system with a single-camera tracker: System design and needle biopsy phantom trial. In *Medical Image Computing and Computer-Assisted InterventionMICCAI 2002*, pages 116–124. Springer, 2002.

[67] Wolfgang Birkfellner, Michael Figl, Klaus Huber, Franz Watzinger, Felix Wanschitz, Johann Hummel, Rudolf Hanel, Wolfgang Greimel, Peter Homolka, Rolf Ewers, et al. A head-mounted operating binocular for augmented reality visualization in medicine-design and initial evaluation. *Medical Imaging, IEEE Transactions on*, 21(8):991–997, 2002.

[68] Hong Hua, Axelle Girardot, Chunyu Gao, and Jannick P. Rolland. Engineering of head-mounted projective displays. *Applied Optics*, 39(22):3814, 2000.

[69] Yann Argotti, Larry Davis, Valerie Outters, and Jannick P. Rolland. Dynamic superimposition of synthetic objects on rigid and simple-deformable real objects. *Computers & Graphics*, 26(6):919–930, 2002.

[70] G Goebbels, K Troche, M Braun, A Ivanovic, A Grab, K von Löbtow, HF Zeilhofer, R Sader, F Thieringer, K Albrecht, et al. Development of an augmented reality system for intraoperative navigation in maxillo-facial surgery. *Proceedings AR/VR-Statustagung, Leipzig*, 2004.

[71] David Drascic and Paul Milgram. Positioning accuracy of a virtual stereographic pointer in a real stereoscopic video world. volume 1457, 2005.

[72] Soon-Yong Park and Go Gwang Park. Active calibration of camera-projector systems based on planar homography. In *Proceedings of the 2010 20th International Conference on Pattern Recognition*, ICPR '10, pages 320–323, Washington, DC, USA, 2010. IEEE Computer Society.

[73] WM Chang, N Amesur, A Zajko, and GD Stetten. Sonic flashlight: a new ultrasound display system that makes vascular access easier. In *Society of Interventional Radiology 29th Annual Scientific Meeting, Phoenix, AZ*, 2004.

[74] Gregory S. Fischer, Anton Deguet, Csaba Csoma, Russell H. Taylor, Laura Fayad, John A. Carrino, S. J. Zinreich, and Gabor Fichtinger. Mri image overlay: application to arthrography needle insertion. *Computer aided surgery : official journal of the International Society for Computer Aided Surgery*, 12(1):2–14, 2007.

[75] Siddharth Vikal, Paweena U-Thainual, John A. Carrino, Iulian Iordachita, Gregory S. Fischer, and Gabor Fichtinger. Perk station–percutaneous surgery training and performance measurement platform. *Computerized medical imaging and graphics : the official journal of the Computerized Medical Imaging Society*, 34(1):19–32, 2010.

[76] Paweena U-Thainual, Gregory S. Fischer, Iulian Iordachita, Siddharth Vikal, and Gabor Fichtinger. The perk station: Systems design for percutaneous intervention training suite. In *Proceedings of the 2008 IEEE International Conference on Robotics and Biomimetics*, ROBIO '09, pages 1693–1697, Washington,

DC, USA, 2009. IEEE Computer Society.

[77] Tamas Ungi, Caitlin T Yeo, U Paweena, Robert C McGraw, Gabor Fichtinger, et al. Augmented reality needle guidance improves facet joint injection training. In *SPIE Medical Imaging*, pages 79642E–79642E. International Society for Optics and Photonics, 2011.

[78] Sangyoon Lee, Gabor Fichtinger, and Gregory S. Chirikjian. Novel algorithms for robust registration of fiducials in ct and mri. In *Proceedings of the 4th International Conference on Medical Image Computing and Computer-Assisted Intervention*, MICCAI '01, pages 717–724, London, UK, UK, 2001. Springer-Verlag.

[79] Liakat A. Parapia. Trepanning or trephines: a history of bone marrow biopsy. *British Journal of Haematology*, 139(1):14–14, 2007.

[80] Mohammad Hau, Jeung Kim, Susan Kattapuram, Francis J. Hornicek, Andrew E. Rosenberg, Mark C. Gebhardt, and Henry J. Mankin. Accuracy of ct-guided biopsies in 359 patients with musculoskeletal lesions. *Skeletal Radiology*, 31(6):349–353, 2002.

[81] Kathryn K Bommer, Ibrahim Ramzy, and Dina Mody. Fine-needle aspiration biopsy in the diagnosis and management of bone lesions. *Cancer Cytopathology*, 81(3):148–156, 1997.

[82] Susan V Kattapuram and Daniel I Rosenthal. Percutaneous biopsy of skeletal lesions. *AJR. American journal of roentgenology*, 157(5):935–942, 1991.

[83] Hanh Khuu, Daniel Moore, Scott Young, Kenneth A. Jafe, and Gene P. Siegal. Examination of tumor and tumor-like conditions of bone. *Annals of Diagnostic Pathology*, 3(6):364–369, 1999.

[84] SG Leffler and FS Chew. Ct-guided percutaneous biopsy of sclerotic bone lesions: diagnostic yield and accuracy. *AJR. American journal of roentgenology*, 172(5):1389–1392, 1999.

[85] PM Logan, DG Connell, JX O'Connell, PL Munk, and DL Janzen. Image-guided percutaneous biopsy of musculoskeletal tumors: an algorithm for selection of specific biopsy techniques. *AJR. American journal of roentgenology*, 166(1):137–141, 1996.

[86] Apoorva Gogna, Wilfred CG Peh, and Peter L Munk. Image-guided musculoskeletal biopsy. *Radiologic Clinics of North America*, 46(3):455–473, 2008.

[87] M. Hutchinson. The burden of musculoskeletal diseases in the united states: Prevalance, societal and economic cost, 1st edition. *J Am Coll Surg*, 208(1):e5–e6, 2009.

[88] US Department of Health and Human Services. Summary health statistics for us adults: National health interview survey', vital and health statistics series. Series 10 (242), US Department of Health and Human Services, 2008.

[89] Paul W. Flint and Charles W. Cummings. *Cummings otolaryngology–head & neck surgery*. Mosby/Elsevier, Philadelphia, PA, 2010.

[90] Wendy R. Sackett, Bruce Barraclough, Tom S. Reeve, and Leigh W. Delbridge. Worldwide trends in the surgical treatment of primary hyperparathyroidism in

the era of minimally invasive parathyroidectomy. *Archives of surgery (Chicago, Ill. : 1960)*, 137(9):1055–1059, 2002.

[91] James A. Lee and William B. Inabnet. The surgeon's armamentarium to the surgical treatment of primary hyperparathyroidism. *Journal of Surgical Oncology*, 89(3):130–135, 2005.

[92] P Miccoli, P Berti, G Materazzi, and G Donatini. Minimally invasive video assisted parathyroidectomy (mivap). *European Journal of Surgical Oncology (EJSO)*, 29(2):188–190, 2003.

[93] Robert Udelsman. Six hundred fifty-six consecutive explorations for primary hyperparathyroidism. *Annals of surgery*, 235(5):665–672, 2002.

[94] Julie A. Sosa and Robert Udelsman. Minimally invasive parathyroidectomy. *Surgical Oncology*, 12(2):125–134, 2003.

[95] Nancy D. Perrier, Philip H. G. Ituarte, Eugene Morita, Timothy Hamill, Robert Gielow, Quan-Yang Duh, and Orlo H. Clark. Parathyroid surgery: separating promise from reality. *The Journal of clinical endocrinology and metabolism*, 87(3):1024–1029, 2002.

[96] Sanoop K. Zachariah. *Management of Primary Hyperparathyroidism: 'Past, Present and Future', Thyroid and Parathyroid Diseases - New Insights into Some Old and Some New Issues*, volume Chapter 11. INTECH, 2012.

[97] Gaurav Agarwal, Bruce H. Barraclough, Tom S. Reeve, and Leigh W. Delbridge. Minimally invasive parathyroidectomy using the focused lateral approach. ii. surgical technique. *ANZ Journal of Surgery*, 72(2):147–151, 2002.

[98] Gaurav Agarwal, Bruce H. Barraclough, Bruce G. Robinson, Tom S. Reeve, and Leigh W. Delbridge. Minimally invasive parathyroidectomy using the focused lateral approach. i. results of the first 100 consecutive cases. *ANZ Journal of Surgery*, 72(2):100–104, 2002.

[99] Orson W. Moe. Kidney stones: pathophysiology and medical management. *Lancet*, 367(9507):333–344, 2006.

[100] Charles Y. Pak. Kidney stones. *The Lancet*, 351(9118):1797–1801, 1998.

[101] J Michael Soucie, Michael J Thun, Ralph J Coates, William McClellan, and Harland Austin. Demographic and geographic variability of kidney stones in the united states. *Kidney international*, 46(3), 1994.

[102] Glenn M. Preminger, Dean G. Assimos, James E. Lingeman, Stephen Y. Nakada, Margaret S. Pearle, J Stuart Wolf, Jr, and AUA Nephrolithiasis Guideline Panel. Chapter 1: Aua guideline on management of staghorn calculi: diagnosis and treatment recommendations. *The Journal of urology*, 173(6):1991, 2005.

[103] Fabio C. Vicentini, Cristiano M. Gomes, Alexandre Danilovic, Elias A. C. Neto, Eduardo Mazzucchi, and Miguel Srougi. Percutaneous nephrolithotomy: Current concepts. *Indian journal of urology : IJU : journal of the Urological Society of India*, 25(1):4–10, 2009.

[104] Manjunath Anand, Tamas Ungi, Andras Lasso, Paweena U-Thainual, Jagadeesan Jayender, Jan Fritz, John A. Carrino, Ferenc A. Jolesz, and Gabor

Fichtinger. Workspace analysis and calibration method for mobile image overlay system used for image-guided interventions. In *The Hamlyn Symposium on Medical Robotics*, 2013.

[105] International Electrotechnical Commission. Determination of tensile safety factor - table 21 (section 9.8) - iec 60601 3rd edition.

[106] Manjunath Anand, Franklin King, Tamas Ungi, Andras Lasso, John Rudan, Jagadeesan Jayender, Jan Fritz, John A. Carrino, Ferenc A. Jolesz, and Gabor Fichtinger. Design and development of a mobile image overlay system for image-guided needle interventions. In *36th Annual International Conference of IEEE EMBS Chicago, IL, USA*, volume In-review, 2014.

[107] Food and Drug Administration. 21 cfr 860 - medical device classification procedures.

[108] Food and Drug Administration. 21 cfr 1040.10(b) - compliance guide for laser products.

[109] Clifford R. Weiss, David R. Marker, Gregory S. Fischer, Gabor Fichtinger, Antonio J. Machado, and John A. Carrino. Augmented reality visualization using image-overlay for mr-guided interventions: system description, feasibility, and initial evaluation in a spine phantom. *AJR. American journal of roentgenology*, 196(3):W305, 2011.

[110] Kevin A. Smith and John Carrino. Mri-guided interventions of the musculoskeletal system. *Journal of Magnetic Resonance Imaging*, 27(2):339–346, 2008.

[111] Leon Lenchik, Daniel J Dovgan, and Ruben Kier. Ct of the iliopsoas compartment: value in differentiating tumor, abscess, and hematoma. *AJR. American journal of roentgenology*, 162(1):83–86, 1994.

[112] JS Lewin, CA Petersilge, SF Hatem, JL Duerk, G Lenz, ME Clampitt, ML Williams, KR Kaczynski, CF Lanzieri, AL Wise, et al. Interactive mr imaging-guided biopsy and aspiration with a modified clinical c-arm system. *AJR. American journal of roentgenology*, 170(6):1593–1601, 1998.

[113] Jan Fritz, U Paweena, Tamas Ungi, Aaron J Flammang, Sudhir Kathuria, Gabor Fichtinger, Iulian I Iordachita, John A Carrino, et al. Mr-guided vertebroplasty with augmented reality image overlay navigation. *Cardiovascular and interventional radiology*, pages 1–8, 2014.

[114] Jinha Lee, Alex Olwal, Hiroshi Ishii, and Cati Boulanger. Spacetop: Integrating 2d and spatial 3d interactions in a see-through desktop environment. In *Proceedings of the SIGCHI Conference on Human Factors in Computing Systems*, CHI '13, pages 189–192, New York, NY, USA, 2013. ACM.

Appendix A

60-degree Design: Prototype Development

Different prototype versions developed for analyzing the optimal 60-degree mirror-monitor configuration resulting in workspace analysis and introduction of new 90-degree configuration.

Figure A.1: First version prototype

A.1 First version prototype

A clear transparent mirror was used to improve the object visibility when seen through mirror. Double reflected images appeared in the virtual image overlay plane and the

image quality was very poor under normal lighting conditions. The study further strengthens the benefit of using semi-transparent mirror or beamsplitter with single side reflection property.

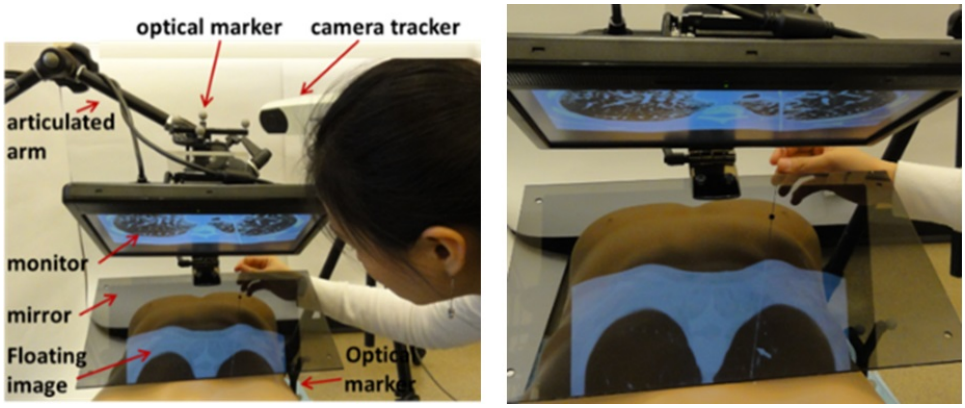

Figure A.2: Second version prototype

A.2 Second version prototype

A polycarbonate semi-transparent mirror used to overcome the double reflected image issue and improve the virtual image quality. The viewbox design was similar to the previous static systems [8, 84, 86]. An interference between mirror and patient observed while ensuring the visibility of complete depth of the virtual image overlay plane when seen through the mirror.

A.3 Third version prototype

Design was optimized to eliminate the interference between the mirror and the patient. However a compromise in the depth of virtual image overlay plane was required when seen through the mirror. This reduced viewing angle when seen through mirror adding challenges for virtual image overlay calibration using MicronTracker.

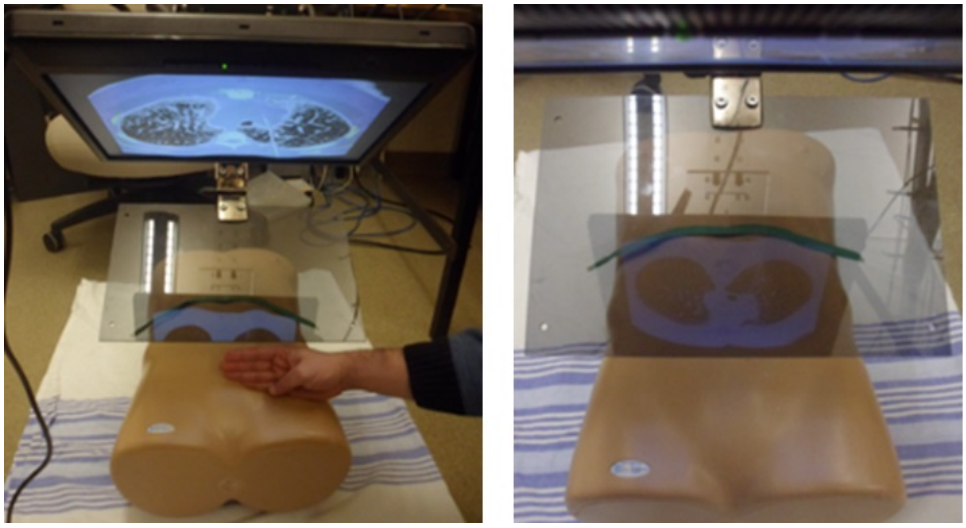

Figure A.3: Third version prototype

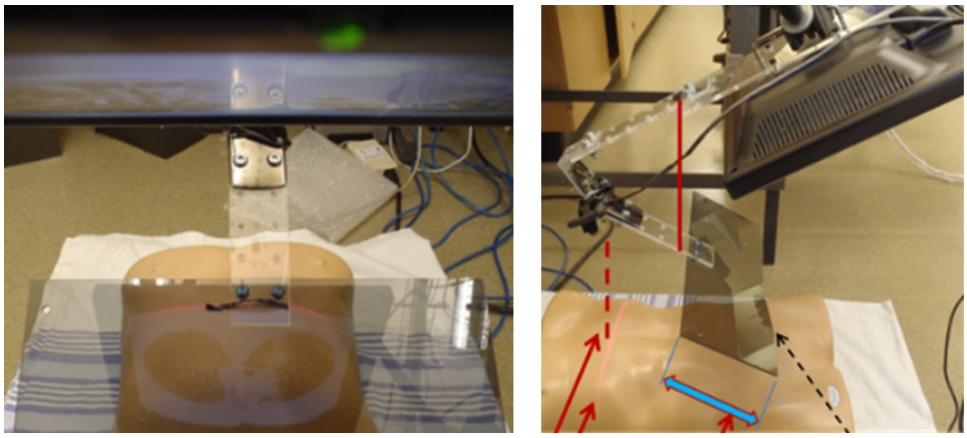

Figure A.4: Fourth version prototype

A.4 Fourth version prototype

The proposed design reduced the mirror length to increase the clearance above the patient. However this reduced the viewing angle of the virtual plane depth when seen through the mirror.

Appendix B

BOM - Adjustable Image Overlay System

The bill of material for the adjustable system and detailed prototype development (excluding the cost og labor for building) are shown below. All frame building parts were purchased from 80-20 Inc. *(www.80-20.net)* and the actual purchase costs are mentioned.

Table B.1: Prototype development Bill of Material (BOM)

80-20 Catalogue #	Component Description	Quantity	Price ($)
25-2525	25MM X 25MM T-SLOTTED PROFILE (L=6.62M)	24	49.0
40-4040	40MM X 40MM T-SLOTTED PROFILE (L=5.60M)	8	134.4
40-4080	40MM X 80MM T-SLOTTED PROFILE (L=4.75M)	6	199.5
25-3392	ANCHOR FASTENER BLACK W/M5 & STD T-NUT	4	12
75-3415	M6 X 25MM SHCS W/ ECONOMY T-NUT	1	0.48
25-3501	25 S LIVING HINGE BOLT ASSEMBLY	1	3.4
40-3368	40 S 90 DEG INSIDE CORNER CONNECTOR	2	12.6
75-3422	M8 X 16MM BHSCS W/ ECONOMY T-NUT	20	13.4
25-1961	25 S M6 X 1.0 ECONOMY T-NUT BRIGHT	30	8.1
25-1962	25 S M6 X 1.0 DOUBLE ECONOMY T-NUT BRIGHT	15	7.95
25-3266	12-24 X .375” SOCKET BUTTONHEAD THREAD BLK	10	2.1
40-3267	12-24 X .375” SOCKET BUTTONHEAD THREAD BLK	2	0.42
25-3501	25 S LIVING HINGE BOLT ASSEMBLY	1	3.4
75-3430	M8 X 20MM SHCS W/ECONOMY T - NUT	8	4.88

Continued on next page

Table B.1 – *Continued from previous page*

80-20 Catalogue #	Component Description	Quantity	Price ($)
25-3094	DOUBLE ANCHOR NUTS	4	21
25-1966	ROLL IN T-NUTS - 25 SERIES	20	21
11-6310	M6 X 10MM BHSCS BLACK	4	1.04
25-4150	25 S 4 HOLE 90degree joining plate	2	10.2
25-4172	25 S "COUNTERSINK" L PIVOT ARM	1	6.5
25-4136	25 S HOLE INSIDE GUSSET CORNER BRACKET	1	5.65
25-4132	25 S 4MM 2 HOLE INSIDE GUSSET CORNER BRACKET	1	3.95
65-4503	25 TO 40 S 2 HOLE INSIDE CORNER BRACKET	2	6.7
25-4172	25 S "COUNTERSINK" L PIVOT ARM	1	6.5
25-4118	25 S 3 HOLE JOINING STRIP	1	4.3
25-4107	25 S 2 HOLE JOINING STRIP	2	6.8
40-3368	40 S 90DEG INSIDE CORNER CONNECTOR	16	100.8
40-2135	40MM X 80MM BASE PLATE W/M12 TAIN CENTER	4	45.2
40-4367	40 S 4 HOLE JOINING PLATE	6	29.7
25-2496	SINGLE PANEL RETAINERS	4	15.8
25-4108	2 HOLE 3mm INSIDE CORNER BRACKET	3	8.25
25-2116	25 S RUBBER PANEL GASKET/ M	1	1.25
25-4181	25 S 0 DEGREE LIVING NUB	1	4.6
25-6425	w/ #25-7401	1	40.95
25-6426	w/ #25-7401	1	52.7
25-6850	25 S L-HANDLE LINEAR BEARING BRAKE	4	38.2
25-2015	25-2525 END CAP BLACK W/PUSH-INS	15	15.75
40-2045	40-4080 END CAP BLACK W/ PUSH-INS	2	3.2
12314	CA BLE MOUNT BLOCK 1/4TURN NYLON BLK SLOT 6	4	5.2
12316	CA BLE MOUNT BLOCK 1/4TURN NYLON BLK SLOT 6	10	14
25-2116	25 S RUBBER PANEL GASKET/ M	2	2.5
25-4184	25 S 90 DEGREE LIVING NUB	2	9.2
14011	PIVOT JOINT 25 TAB6 DIE CAST ZINC PC Al. COLOR	1	17.75
40-2030	40-4040 END CAP BLACK W/PUSH-INS	8	11.2
40-2849	40 SERIES RUBBER BUMPER	4	15.75
	PL1500M PLANAR MONITOR 15"	1	175
	LML <1mW, 650nm LINE LASER DIODE	1	25
	BRH LASER MOUNTING BRACKET 12mm 6	1	13.5
	SEMI-TRANSPARENT PC SHEET 1/8" Thick, 24" x 24"	1	29.22

Continued on next page

Table B.1 – *Continued from previous page*

80-20 Catalogue #	**Component Description**	**Quantity**	**Price ($)**
	LASER MOUNT 3D PRINTING	1	25
	CABLES AND ACCESSORIES	3	100*
	DESKTOP COMPUTER	1	1200*
	TOTAL COST ($)		**2735**

∗*approximate cost estimated, reused from lab resources for prototype building*

Appendix C

BOM - Mobile Image Overlay System

The bill of material for the mobile system and detailed prototype development (excluding the cost of labor for building) are shown below.

Table C.1: Prototype development Bill of Material (BOM

Component description	**Quantity**	**Price ($)**
GALAXY TABLET 10.1”	1	400
BEAMSPLITTER MIRROR	1	125
iDISPLAY APP	1	5
BRACKET & HOLDER- 3D PRINTING	3	75
LASER MOUNT - 3D PRINTING	1	25
HOST COMPUTER (LAPTOP)	1	1200*
3V PHOTO LITHIUM BATTERY	1	3*
2 WAY CONNECTOR SWITCH	1	3*
FASTENERS	1	10
CABLES AND ACCESSORIES	1	5*
TOTAL COST $		**1,851**

∗*approximate cost estimated, reused from lab resources for prototype building*